UNIONE EUROPEA
Fondo Sociale Europeo

Ministero dell'Istruzione, dell'Università e della Ricerca

PON RICERCA E INNOVAZIONE 2014 - 2020

UNIVERSITÀ DEGLI STUDI DI PALERMO

Dottorato di ricerca in
Scienze Fisiche e Chimiche
XXXIV Ciclo

Federico Bruno

Optical sensing of Pollutants by Fluorescent Carbon Nanodots

Tutor:
Prof. Simonpietro Agnello
Prof. Fabrizio Messina

Coordinatore:
Prof. Giuseppe Lazzara

Contents

Chapter 1

Introduction

1.1 Enviromental Pollution

In recent years, the issue of environmental pollution, caused mainly by human activity, has become increasingly pressing. This has had major repercussions in environmental, social and economic terms, in addition to the undisputed danger to human health, so much so that the member states of the UN have had to review their consumption and emissions of greenhouse gases [1, 2] with the discussion and introduction of the Kyoto Protocol, in order to achieve environmental sustainability that does not harm human health in any way. It is relevant to note that environmental pollution is now completely irreversible in many geographical areas, so much so that it is increasingly difficult to access drinkable water because of toxic industrial waste spills, or in some cases even the air is soaked in highly toxic substances. These are heavily borne some of the reasons for protecting the environment, given that the repercussions are borne exclusively by the living species on this planet, including man. But to make further illustrate the idea better we will now present some types of pollution and pollutants, in very general terms, to better understand the meaning of environmental pollution.

Natural greenhouse gases. Natural greenhouse gases include water vapour, carbon dioxide, methane, nitric oxide and ozone [3–6]. Certain human activities, however, increase the level of all these gases and release other exclusively anthropogenic greenhouse gases into the air [7–10].

Water vapour is present in the atmosphere as a result of evaporation from all water sources (seas, rivers, lakes, etc.) and as a product of various combustions. Carbon dioxide is released into the atmosphere mainly when solid waste, fossil fuels (oil, petrol, natural gas and coal) [11], wood and wood products are burned [12–14]. Methane is emitted during the production and transport of coal, natural gas and mineral oil and large methane emissions also occur as a result of the decomposition of organic matter

in landfills and the normal biological activity of higher organisms (mainly by the nearly 2 billion cattle on earth) [15–18]. Nitrous oxide is emitted during agricultural and industrial activities, as well as during the combustion of waste and fossil fuels [19–23]. Highly active greenhouse gases are gases that do not normally occur in nature, but are generated by various industrial processes, such as hydrofluorocarbons (HFCs), perfluorocarbons (PFCs) and sulphur hexafluoride (SF_6) [24–28]. The presence of a gas in the atmosphere over time is also called atmospheric half-life and represents the approximate amount of time it would take for the increase in concentration of a pollutant due to human activity to disappear and the concentration to return a natural level (either because the pollutant has been converted to another chemical, or because it has been captured by a natural deposit). This time depends on the sources of the pollutant, the deposits and the reactivity of the substance.

An increase in the Earth's temperature, also induced by pollutant gases, can cause a number of major environmental effects. Increased heat and thus evaporation from large reservoirs leads to a corresponding increase in the amount of water in the atmosphere and thus an increase in precipitation. Some researchers estimate that rainfall has increased by about one per cent on all continents in the last century. Areas at higher altitudes show larger increases, while precipitation has decreased in many tropical areas. In any case, there is an increase in the intensity of rainfall and more violent weather phenomena (such as storms and hurricanes) with a consequent increase in flooding and soil erosion [29–31]. Global warming is also leading to an overall decrease in ice areas. The large ice masses of Greenland and continental glaciers are receding significantly. Increased ocean volume due to higher temperatures and melting ice are also causing the average sea level to rise. Over the last hundred years it has risen by approximately 15-20 cm. In addition, in many tropical areas there is already a reduction in soil moisture leading to a decrease in agricultural yields; many areas, also in Europe, are at risk of desertification. All these effects are already scientifically evident from the many data obtained on this subject, and it is assumed that the current situation will worsen if greenhouse gas concentrations increase. It should be noted that global warming would continue for centuries even if greenhouse gas concentrations in the atmosphere were stabilised: given the masses involved, the responses of the Earth's climate to changes in the composition of the atmosphere are rather slow [32–34].

Air and Industrial pollution. Atmospheric pollution, as mentioned above, has increased due to aggressive urban and industrial activity, thus creating a major problem in terms of pollutant emissions, and the presence of compounds in the atmosphere that disproportionately increase the greenhouse effect creates major damage to human health and the environment [35–37]. However, European legislation is enabling a reduction in emissions and a better, albeit slow, conversion of industrial sites to reduce the amount of harmful substances released into the environment as those shown in Figure (1.1).

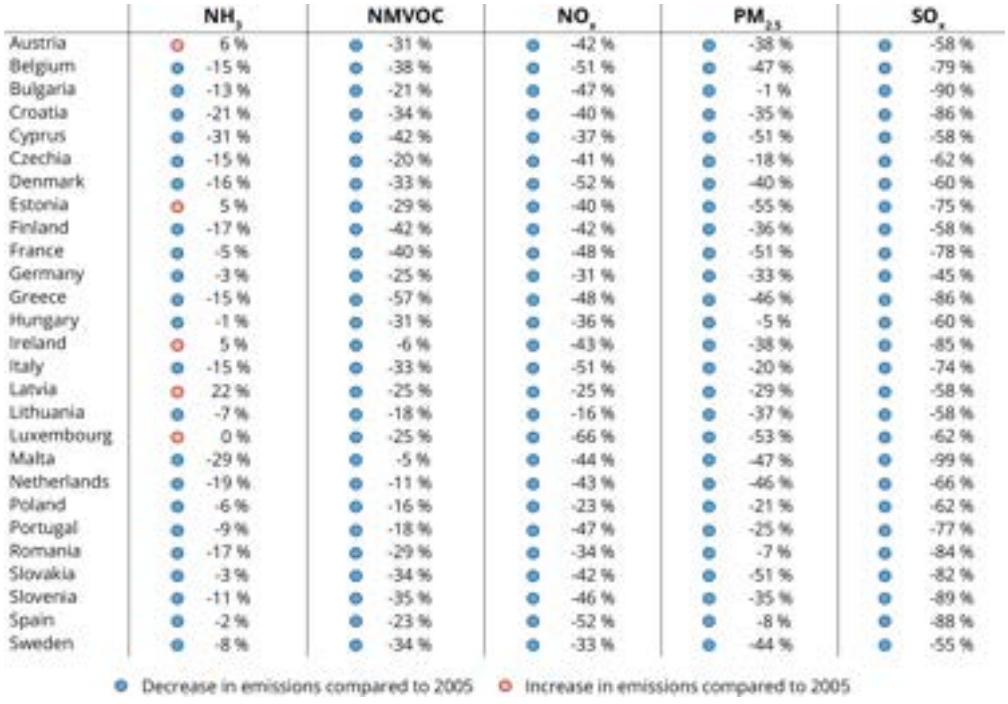

	NH_3	NMVOC	NO_x	$PM_{2.5}$	SO_x
Austria	6 %	-31 %	-42 %	-38 %	-58 %
Belgium	-15 %	-38 %	-51 %	-47 %	-79 %
Bulgaria	-13 %	-21 %	-47 %	-1 %	-90 %
Croatia	-21 %	-34 %	-40 %	-35 %	-86 %
Cyprus	-31 %	-42 %	-37 %	-51 %	-58 %
Czechia	-15 %	-20 %	-41 %	-18 %	-62 %
Denmark	-16 %	-33 %	-52 %	-40 %	-60 %
Estonia	5 %	-29 %	-40 %	-55 %	-75 %
Finland	-17 %	-42 %	-42 %	-36 %	-58 %
France	-5 %	-40 %	-48 %	-51 %	-78 %
Germany	-3 %	-25 %	-31 %	-33 %	-45 %
Greece	-15 %	-57 %	-48 %	-46 %	-86 %
Hungary	-1 %	-31 %	-36 %	-5 %	-60 %
Ireland	5 %	-6 %	-43 %	-38 %	-85 %
Italy	-15 %	-33 %	-51 %	-20 %	-74 %
Latvia	22 %	-25 %	-25 %	-29 %	-58 %
Lithuania	-7 %	-18 %	-16 %	-37 %	-58 %
Luxembourg	0 %	-25 %	-66 %	-53 %	-62 %
Malta	-29 %	-5 %	-44 %	-47 %	-99 %
Netherlands	-19 %	-11 %	-43 %	-46 %	-66 %
Poland	-6 %	-16 %	-23 %	-21 %	-62 %
Portugal	-9 %	-18 %	-47 %	-25 %	-77 %
Romania	-17 %	-29 %	-34 %	-7 %	-84 %
Slovakia	-3 %	-34 %	-42 %	-51 %	-82 %
Slovenia	-11 %	-35 %	-46 %	-35 %	-89 %
Spain	-2 %	-23 %	-52 %	-8 %	-88 %
Sweden	-8 %	-34 %	-33 %	-44 %	-55 %

Figure 1.1: Reduction of the percentages of atmospheric pollutants in European countries

It is therefore fair to give an overview of the major environmental pollutants and what effects they have on human health.

CO. Carbon monoxide is a colourless, odourless, non-flammable, and very toxic gas. It is formed during the combustion of organic substances, when they are incomplete due to lack of air (i.e. lack of oxygen). Natural and anthropogenic emissions are now of the same order of magnitude. Carbon monoxide is extremely prevalent, especially in urban areas, due to pollution from vehicle exhausts [38–41]. The main natural emissions are due to forest fires, volcanic eruptions, emissions from oceans and marshes and oxidation of methane and hydrocarbons in general emitted naturally into the atmosphere. The main source of man-made emissions is the use of fossil fuels for motor vehicle combustion engines and industrial activities. The amount of carbon monoxide emitted by combustion processes in motor vehicles is about 10 times greater than that of other pollutants. The highest concentrations in the exhaust gases occur when the engine is idling; at higher engine speeds CO production is much lower. This is why CO concentrations can be particularly high in urban areas with slow-moving traffic and frequent stops at traffic lights [42–46]. Diesel engines operate with greater quantities of air, ensuring more complete combustion and emitting less CO than petrol engines on the other hand, they emit more particulates, but above all, this particulate matter contains heavy metals released by car catalytic converters, which when released into the environment cause a series of problems such as the pollution of surface water and land, including agricultural land. In recent years, the amount of CO emitted from car exhausts has decreased due to improved engine efficiency, mandatory emission controls and the increasing use of catalytic converters [47–50]. Among the industrial processes that cause significant CO emissions into the atmosphere, the main ones are emissions from steel plants, where coke is used to reduce ferrous material, or in conversions, where oxygen is used to oxidise the carbon in pig iron to convert it to steel or to lower the carbon content [51,52]. Other sources are the petrochemical industries, which produce the synthesis gas (a mixture of CO and hydrogen) used in the production of important synthetic chemical compounds, and oil refineries. CO remains in the atmosphere for about 3-4 months and is removed through oxidation reactions to carbon dioxide or through photochemical reactions involving methane and OH-radicals. Because of its low reactivity it is often used as a tracer of the time course of pollutants at ground level.

Particulate Matter. The terms particulate matter and suspended particles refer to all solid or liquid particles, smaller than 100 μm in size and usually indistinguishable to the naked eye, dispersed in the atmosphere, such as soot, dust, ash, pollen, etc [53, 54]. Depending on the nature and size of the particles we can distinguish aerosols, made up of solid or liquid particles suspended in the air and with a diameter of less than 1 μm; mists, given by droplets with a diameter of less than 2 μm; fumes, made up of

solid particles with a diameter of less than 1 μm and usually released by chemical and metallurgical processes; smoke, consisting of solid particles usually less than 2 μ m in diameter and carried by gas mixtures; dust (true dust), consisting of solid particles between 0.25 and 500 μm in diameter; sand, consisting of solid particles over 500 μm in diameter [55–58]. Primary particles are those that are emitted as such from natural and man-made sources, while secondary particles originate from a series of chemical and physical reactions in the atmosphere. Fine particles are those with a diameter of less than 2.5 μm, the others are called coarse. PM10 dust is particulate matter with a diameter of less than 10 μm, while PM2.5, which accounts for about 60% of PM10, is particulate matter with a diameter of less than 2.5 μ [59–61]. Inhalable dust is dust that can penetrate the upper respiratory tract (from the nose to the larynx). Thoracic dust is dust that can reach the lungs. Breathable dust, on the other hand, can penetrate the lower respiratory tract (from the trachea to the pulmonary alveoli) [62–64]. Dust originates from both natural and anthropogenic sources. Fine dust originates mainly from combustion processes and gas reaction products; the coarse fraction of dust generally originates from mechanical processes. The main natural sources of primary particulate matter are volcanic eruptions, forest fires, erosion and rock disintegration. Anthropogenic particulate matter, on the other hand, is due to: the use of fossil fuels (domestic heating, thermal power stations, etc.); vehicle emissions; tyre, brake and road surface wear; and various industrial processes (foundries, mines).

Effects on humans: Apart from their toxicity, the particles that can have undesirable effects on humans are mainly those of smaller size, as particles larger than 15 μ m are generally stopped by nose during the breathing process. Due to their particular surface structure, particles can also adsorb carcinogenic chemicals from the air; by drawing them into the respiratory tract and prolonging their residence time, they exacerbate their effects. Smaller particles penetrate the respiratory system at various depths and can take long periods of time to be removed, making them the most dangerous. These dusts aggravate respiratory diseases.

Effects on the environment: The effects of particulate matter on climate and materials are quite obvious. Particulate matter from smoke and fumes causes a decrease in atmospheric visibility; at the same time it also decreases brightness by absorbing or reflecting sunlight. Particulate matter also damages electrical and electronic circuits, soils buildings and artwork, and reduces the durability of textiles.

Polycyclic Aromatic Hydrocarbons. The term PAH stands for Polycyclic Aromatic Hydrocarbons, a large class of organic compounds that are all structurally characterised by the presence of two or more condensed aromatic rings [65–67]. The simplest PAH from a structural point of view is naphthalene, a two-ring compound which, as an airborne pollutant, is mostly found in gaseous form at room temperature [68–70]. PAHs consisting of three to five rings can be present either as a gas or as particulate matter,

while those with five or more rings tend to occur mostly in solid form. They are formed during incomplete combustion of organic products such as coal, oil, gas or waste; many are used for research and some are artificially synthesised; some are used in the production of dyes, plastics, pesticides and medicines [71–76]. They are usually never found in the air as single compounds, but in mixtures where many dozens of different PAHs are present, and in proportions that can vary greatly in some cases. The fact that exposure occurs to a mixture of compounds, the composition of which is not constant, makes it difficult to attribute health consequences to the presence of a specific polycyclic aromatic hydrocarbon. Although the study of these mixtures is particularly complicated, it has been shown that exposure to PAH mixtures leads to an increase in the occurrence of cancer, especially in the presence of benzo(a)pyrene (the only PAH that has been studied in depth so far) [77–79]. Natural pollutant sources can be particularly important: Polycyclic Aromatic Hydrocarbons are released into the air during volcanic eruptions and as a result of forest fires; a small amount is produced by certain species of bacteria and fungi. Human activities are also very significant sources, as PAHs are formed in all processes involving the incomplete combustion of carbon-based materials such as coal, oil, wood and gas. As a guide, the more smoke produced during combustion, the more PAHs are released into the air. The use of various fuels also produces a considerable amount of pollutants. Relatively high amounts of PAH can be found in food as a result of various cooking methods, especially barbecuing and smoking [80–84]. The main industrial sources of PAH include raw metal processors, oil refineries, coke plants, paper, chemicals and plastics industries. Waste incinerators and toxic depots can also be major sources. Polycyclic aromatic hydrocarbons in the air can generally degrade by reacting with sunlight and other chemical compounds within a few days or weeks. Higher mass PAHs adhere to airborne particulate matter and sooner or later settle on the ground. Because of their relative stability, PAHs can also be found over long distances in remote locations far from their production areas. However, PAHs are present in the atmosphere at relatively low concentrations compared to many other pollutants [71, 85–90].

Effects on humans: Once in the body, PAHs spread rapidly due to their fat-solubility, which makes them able to cross cell membranes and penetrate and deposit in fatty tissues. Target organs include the kidneys and liver [91–93]. However, metabolism is quite rapid and within a few days PAH are eliminated via urine and faeces. The main health effect associated with exposure is certainly cancer [94–96].

Heavy Metals Another source of pollution caused by industrial activity and the catalytic converter of cars is the disproportionate increase of heavy metals in the atomosphere. The chemical industry's main customers are the chemical industry itself, the manufacturing industry, particularly the rubber and plastics industry, the service industry and end consumers [97–101]. Among the heavy metals most toxic to human health and the environment are Cadmium (Cd), Lead (Pb) and Mercury (Hg). Cadmium

is mainly used in heavy industry for batteries and the paint industry [102–104], For mercury, a main route of emission into the atmosphere is through, its previous use in thermometers and dental applications in the form of amalgam [105–108]. Finally, lead, also a very dangerous heavy metal, was formerly used in the petroleum industry as an anti-knock agent for petrol. Therefore, the use of these metals, which have now been replaced by other less toxic or even non-toxic metals, has caused damage to the environment and human health, especially due to the incorrect way in which this type of waste is disposed [109–112]. Fortunately, European laws have now regulated the quantities of these metals that can be consumed by humans and their use in heavy industries. However, it is important to give some thought to each metal and its degree of toxicity.

- Mercury, causes physiological stress, tremors and damage to the central nervous system
- Cadmium, is the most toxic of the elements, as even in very low concentrations it causes damage to the kidneys, bones, liver and blood.
- Lead causes damage to the nervous system, kidneys and reproductive system.

After an overview of environmental pollution in general, we can now move on to the real aim of this thesis, which is pollution in food, which will be discussed in the next section, trying not only to understand what the main pollutants are, but also how the presence of these can be determined by sensing.

1.2 Pollution in Food

The main causes of pollutants in food are due to acid rain that settles on the soil, making it rich in harmful chemical substances that are absorbed by plants and grazed by animals [113–115]. However, the presence of other activities such as agriculture also causes other possibly harmful substances such as pesticides and pesticide derivatives to enter the soil through irrigation water [116–118]. However, the European community by the regulations created by European Food Safety Authority (EFSA), in addition to giving an overview of the amount of chemicals used per country, has created a regulation on food, creating a protocol of legal limits of toxic substances assimilated by humans, such as heavy metals and pesticides [119–121]. On the one hand, the massive use of pesticides, especially in agriculture, improves the growth of plants, which are not attacked by pathogens, but on the other hand, the excessive and continuous use of pesticides allows the active ingredients to penetrate into fruit and vegetables, which are then ingested by humans. However, even in this case there is a Community law limiting the use of certain families of pesticides and in some cases banning them permanently Figure (1.2).

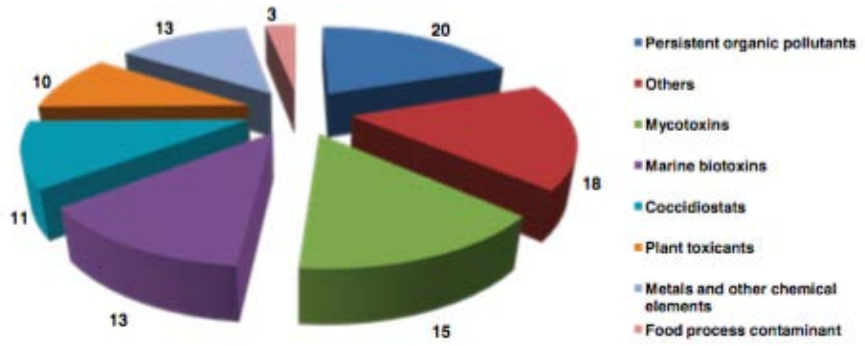

Figure 1.2: Overview of risk assessments provided by the CONTAM Panel between 2003 and 2012, (adapted from [120])

Nevertheless, European or Italian legislation does not recognise the term pesticide; on the contrary, it precisely defines the meaning of biocide, plant protection product and pest control product against crop diseases. Pesticide risk assessment aims to determine whether these products, when properly used, do not produce, directly or indirectly, adverse effects on human or animal health (e.g. through drinking water, food or feed) and do not compromise groundwater quality. In addition, environmental risk assessment aims to assess the impact that these products, if used correctly, could have on non-target organisms. This activity is mainly carried out by EFSA, which, in 2008, established a new Pesticides Steering Committee, composed of representatives from EFSA, the European Commission and Member States. This body was given specific responsibility to manage and plan the risk assessment of pesticides in general and to consider ways to further reduce their impact in view of an ever-increasing use and the changing regulatory environment.

Pesticides. From the point of view of definition, the term 'pesticides', often used as a synonym for plant protection products, refers to chemicals used, primarily, in agriculture to protect crops in order to prevent and/or imitate damage caused to crops by diseases and pests.

The term pesticide, often used instead of plant protection product, refers to all products intended to combat organisms that live at the expense of plant species, such as plants or fruit, or that damage it in some way [122–125]. These products are generally used in agriculture, although considerable progress has also been made in the field of domestic hygiene [126–132]. The synthesis of substances capable of fighting all forms of pests has led to real progress for mankind: the problems of malnutrition in entire regions have been solved, the average life span of entire populations has increased, thanks also to the control and prevention of serious epidemics that have been

achieved with the massive use of these products, and the quality of life of farmers has improved considerably [133–136]. In addition to the positive aspects, today the irrational use of plant protection products leads us to face serious problems which will gradually become clearer as we read these pages; for example, one of these concerns the destruction, alongside the harmful species, of useful insects and organisms (pollinators) which causes ecological imbalances which are sometimes unpredictable in their extent [137–139]. Pesticides are generally classified both by their chemical characteristics and by the object of their action. Historically, pesticides originated around the 1940s, the first being dichlorodiphenyltrichloroethane, better known as DDT, in those years, the presence and massive production of this molecule, led to a whole series of improvements in the agricultural sector. However, DDT and its derivatives were banned in the 1980s because of their high degree of toxicity to humans, and then replaced by synthetic pesticides, which greatly reduce the degree of toxicity to human health. Among the main classes of pesticides are various compounds with different chemical properties:

- Organochlorines
- Organophosphates
- Carbammates

Organochlorines I The typical structure of an organochlorine pesticide shows in Figure (1.3), where there are multiple aromatic groups, which are highly dangerous to humans due to the ease of interaction with DNA and other enzymes, to which chlorine atoms are directly linked [140–143].

Organochlorine pesticides have a broad spectrum of action on target organisms, they have a low acute toxicity for humans, while their chronic toxicity is quite high [144–146]. They are extremely stable to the action of various chemical, physical and biological agents (acids, bases, air, water, light, heat, etc.), which is why they are very persistent in the environment, thanks also to their low vapour pressure at room temperature, which limits losses through evaporation. Because of their apolarity they are practically insoluble in water, with the exception of lindane; being fat-soluble they accumulate in the fat, the liver and the brain of organisms. The chronic toxicological risks to humans from the use of organochlorine pesticides are not fully known. Experimental data show that they interfere with the enzymatic functions of cells, inhibit ATPase, which is important in the body's energy balance, alter the metabolism of carbon hydrates, stimulate liver enzymes and accelerate the liver's metabolic rate. One of the most significant consequences is the rapid degradation of steroid hormones on which reproductive capacity depends. DDT has also been found to have mutagenic properties, so its use in Italy was restricted by Ministerial Decree of 31 July 1973. It also appears to have carcinogenic action.

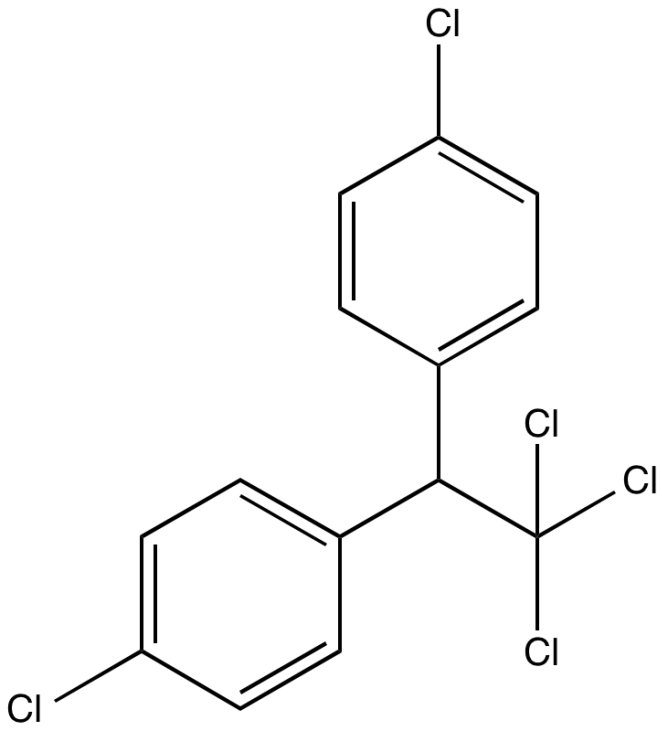

Figure 1.3: Typical aromatic structure of pesticides, this picture shows the progenitor of pesticides, DDT.

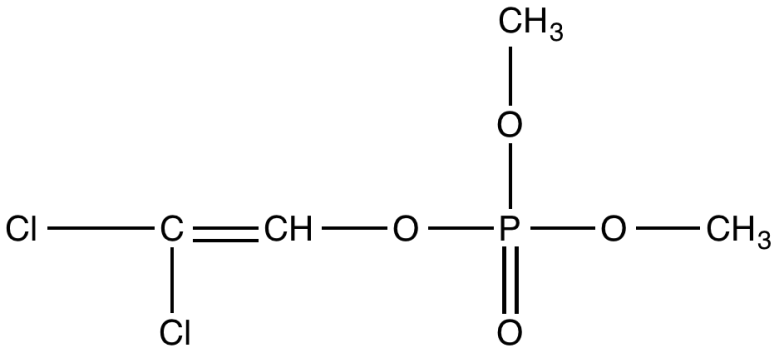

Figure 1.4: Chemical structure of dichlorvos, types of organophosphate pesticide used extensively in agriculture

Organophosphates The discovery of the biological activity of this class of substances dates back to 1932, although they began to be used a few years later, when the use of many organochlorine pesticides was banned because of their toxicity, persistence and bioaccumulation in the environment [147–150]. Chemically, they can be formally regarded as phosphoric acid esters, in which the central pentavalent phosphorus atom is linked by a double bond to an oxygen or sulphur atom, to two methoxyl or ethoxyl groups by single bonds, and finally to an R group, by an oxygen or sulphur atom by a single bond. An example of an organophosphate is dichlorvos, which is used in various crops against the larvae of minnows, aphids, mealybugs, on which it acts by asphyxiation and contact; it is also used as an acaricide insecticide to control silage cereals Figure (1.4).

Most phosphates have insecticidal properties, but there are also fungicides, herbicides and plant growth regulators falling in this family. They are volatile, soluble in water and organic solvents and not very persistent, especially in acidic solutions [151,152]. In general, phosphorus pesticides are less toxic to humans, domestic animals and aquatic organisms than organochlorine pesticides, although toxicity varies greatly from compound to compound. Among the plant protection products currently used in agriculture, phosphorates are the ones that persist the least in the environment, since in many cases they are inactivated through rapid hydrolytic metabolism, but sometimes produce substances of greater toxicity. The efficiency and speed of degradation in the environment depend on various factors: climatic conditions, the type of soil, the pH of the medium, the presence of particular micro-organisms, the presence of particulate material, the association with other active ingredients or co-formulants, etc. For example, organic soils are able to retain them more than sandy and mineral soils. In the soil, phosphorus pesticides can easily be degraded chemically or by micro-organisms. Their tendency to be adsorbed by soil particles limits their mobility in the environment, even though they are more water-soluble than organochlorines. The chemical and physical characteristics

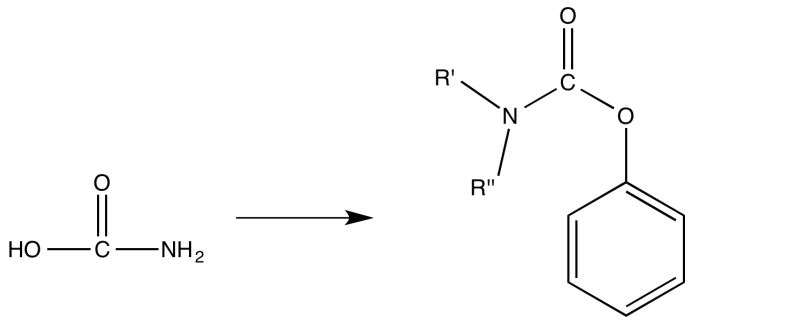

Carbamic Acid Carbamate R', R''= Alkyl, H

Figure 1.5: Carbamic acid and its derivative, widely used in intensive agriculture

of organophosphorus pesticides justify the fact that, in general, once used in agriculture, they are rarely found in groundwater [153–156]. Hydrolysis studies have shown that phosphorus derivatives are more labile than chlorinated derivatives, but in river waters the rate of degradation, under particular environmental conditions, could be slow enough to constitute a potential pollution hazard. These considerations, together with their wide use in agriculture, their high toxicity to aquatic organisms, and the possible effects of long-term exposure on organisms, should lead environmental controllers to carry out periodic monitoring of aquatic systems (including sediments). In aquatic environments, in addition to the active substances, degradation products can be found, often consisting of phenols and/or thiophenols. Phenolic compounds in chlorinated water produce chlorinated compounds which impair the organoleptic characteristics (odour) and the quality of the drinking water [157, 158]. When analysing pesticide residues in food, it is therefore necessary to take into account the metabolites that may be present. Insecticides belonging to this class of substances exert their action through the ability of the central phosphorus atom to phosphorylate the active site of the enzyme cholinesterase (ChE), which is a central constituent of the nervous system of both insects and higher animals.

Carbamates Although the biological action of carbamates was already known in 1929, their use in agriculture, as insecticides, began in 1951 but remained scarce until the 1970s. Chemically, they can be formally regarded as derivatives of carbamic acid Figure (1.5):

Carbamic acid, and the corresponding sulphurates, do not exist in the free state as they decompose easily, but their salts and the N-methyl and NN-dimethylcarbamic esters are stable and used as pesticides. [159–162] Ammonium carbamate has been used together with aluminium phosphide in commercial products against rodents and insects, while the esters constitute the majority of all carbamate pesticides. Two examples of carbamates are carbaryl and propoxur Figure (1.6)

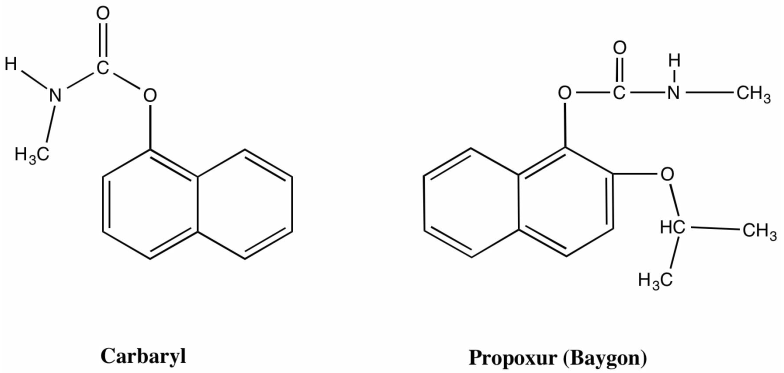

Carbaryl **Propoxur (Baygon)**

Figure 1.6: Carbamic acid and its derivative, widely used in intensive agriculture

In general, carbamic acid derivatives are used as insecticides, while thiocarbamic and dithiocarbamic acid derivatives are used as herbicides and fungicides respectively. Pure carbamates are colourless, crystalline solids with high thermal stability due to their high melting point and low vapour pressure. They may be slightly coloured and semi-solid; the presence of particular impurities affects their stability. They are fairly soluble in water, which is why they cannot accumulate in biological tissues, and are easily transported by water [163, 164]. An absolutely positive note about plant protection products such as carbamates, they allow low toxicity to humans, thanks also to their easy degradation so that half-life times are very low compared to other derivatives that have been treated previously.

Food contamination by pesticides . The rate of degradation of an active ingredient is extremely variable and is decisive in determining the safety interval, i.e. the time between the last treatment and harvest. The persistence of pesticides also depends on the type of plant treated, e.g. for some vegetables, the descending order of persistence is as follows: lettuce, green beans, tomato, courgette, aubergine. By determining the concentrations of residues in the plants, immediately after treatment and after intervals of time, it is possible to trace the decay curve, until it is ascertained that the residues have been reduced to negligible quantities from a toxicological point of view. Once the theoretical toxicological limit, i.e. the amount of residue that can be ingested daily, is known, ruling out with certainty any risk of harmfulness, and comparing this limit with the decay curve, it is possible to identify the deficiency time, i.e. the minimum time required for residues to be reduced to quantities below the tolerance limit. However, it is advisable to limit oneself to lower quantities in order to avoid the presence of foreign substances in the food. The tolerance limit is the legal limit and generally lies between the zero value and the toxicological limit value.

National and EU legislation on the subject is constantly evolving, as regulations often take into account the production evolution of new active ingredients, analytical and

toxicological data found in the literature, and the increased sensitivity of instruments. Italian legislation on plant protection products regulates production, trade and sale, and monitors environmental and food contamination resulting from the use of these products. For example, Article 5 of Law 283 of 30 April 1962 prohibits the possession, trade and use of foodstuffs containing residues of toxic products used during cultivation and storage. Article 6 establishes, partially amended by Article 441 of the Law of 26.2.63, that plant protection products are subject to the authorisation of the Ministry of Health for control and registration as medical devices, i.e. subject to the same discipline as medicines. More recent provisions are to be found in Presidential Decree No 1255 of 3 June 1968 and No 223 of 24 May 1988, which transpose the EEC directives on the classification, packaging and labelling of plant protection products. An ordinance of 18.7.90 lists the permitted pesticides and foodstuffs in which residues may be found, maximum quantities and safety intervals. Many countries have adopted specific regulations governing the operation and financing of organic farming. The EEC issued a law regulating the "organic production method" in 1991. Acute-oral toxicity is taken into account for the classification of pesticides by Italian legislation:

- Class I All those products containing an active substance with an Lethal Death 50 (LD_{50}) below 50 to 50 mg/Kg, which may entail a risk of fatal intoxication by ingestion, inhalation, and skin contact with humans;

- Class II All those health care products that have an active substance of LD_{50} between 50 and 500 mg/Kg and that involve risks of serious intoxication by ingestion, inhalation, and skin contact;

- Class III All those medical devices that have an LD_{50} greater than 500 mg/Kg and that are dangerous if swallowed, inhaled or if they come into contact with the skin;

- Class IV Medical devices whose handling and normal use can only lead to negligible risks.

In addition, the legal limits are set by the annual EFSA reports in accordance with Regulation (EC) No 396/2005, which sets parameters for monitoring pesticide residues in food, using the parameter 'maximum residue levels' or briefly 'MRLs', which allows the determination of one or more residues and thus the continuous monitoring of food. EU-harmonised MRLs are set for more than 500 pesticides covering 370 food products/food groups. A default MRL of 0.01 mg/kg is applicable for pesticides not explicitly mentioned in the MRL legislation. Regulation (EC) No 396/2005 imposes on Member States the obligation to carry out controls to ensure that food placed on the market is compliant with the legal limits.

Heavy metals The term heavy metal refers to all metallic chemical elements that have a relatively high density, based on their atomic weight as well as other special characteristics. They are toxic already in low concentrations. Generally in the group of heavy metals are considered Ag, Ba, Cd, Co, Mn, Hg, Mo, Ni, Pb, Cu, Sn, Tl, Ti, V, Zn and some metalloids such as As, Sb, Bi and Se [165–169]. Some human activities cause the mobilisation of naturally occurring metals in the ecosystem, causing them to accumulate in the biosphere and enter the food chain, with serious damage to humans and animals. The most common sources are paints and other finishing products, combustion of PVC plastics, cigarette smoke, car exhaust, household dust - where smog is deposited - batteries and mercury thermometers. Heavy metals can enter water supplies from consumer or industrial waste, or even from acid rain that penetrates soils and carries heavy metals into streams, lakes, rivers and groundwater. Among environmental contaminants, heavy metals play a major role as they are concentrated along the food chain and metal contamination can be caused by their presence in food containers. The most dangerous metals are Hg, Pb, Cd.

Mercury Traces of mercury have been found in the seabed adjacent to large petrochemical plants. The contamination is due to waste water from the old mercury cells of the chlor-alkali process. The mercury in the water is ingested by plankton and moves up the food chain becoming more and more concentrated [170]. Fish at the top of the food pyramid can have a concentration of 3000 to 27000 times higher than the water in which they live. Most of the mercury we ingest comes from fish, especially from large predators such as tuna, swordfish, dogfish, eel, pike, etc. Usually the most contaminated fish contain 0.1-0.3 ppm (parts per million) of mercury [171], but those living in highly contaminated waters (e.g. the Rhine in Germany) can be as high as 2 ppm. In humans, further concentration occurs, and when the mercury in the brain exceeds certain values, neurological problems occur due to bioaccumulation [172–174]. Sources of pollution are all activities in which metal or some of its organic or inorganic derivatives are used. Waste from chemical and dental laboratories, together with batteries, broken thermometers, products used in agriculture and industry, mining and industry, mining waste, and the burning of solid waste all contribute to the spread of mercury in the environment, although in isolation they have insignificant contributions. The number of publications on mercury pollution and studies on the biogeochemical cycle of mercury have increased considerably with time. Biogeochemical cycle have increased considerably since the outbreak of Minemata disease, a disease of the nervous disease, which affected the population of the coastal area around Minemata Bay in Japan, most of them poor fishermen [175–178]. Between 1953 and 1960 more than 100 cases of mercury poisoning occurred of which 43 were fatal, and 19 cases of births of children with birth defects among those who had consumed fish products caught in the bay, where very high concentrations of mercury (5-20 ppm) were found. Mercury, in the form of the

Hg^{2+} ion, was continually dumped into the bay by an industry using it as a catalyst for the production of polyvinyl chloride. It has been found that although mercury is not an essential element for the body, it easily accumulates in living tissue. In addition to the oral route, the uptake of a metal into the body, and of mercury in particular, can also occur via other routes. In particular, can also be absorbed through inhalation or can be absorbed through the skin even if intact. Mercury, whether of natural or anthropogenic origin, diffuses into the environment through the waters of rivers, lakes and oceans and, to a lesser extent, through the atmosphere.

Cadmium Cadmium can have three oxidation states +2, +1 and 0, but under natural conditions it is mainly present in the Cd(II) state. The Cd^{2+} ion is characterised by its strong tendency to form both inorganic and organic complexes, and even under natural conditions, metallorganic Cd compounds can form. Cd has very low average concentrations in the earth's crust (0.2 ppm); oceanic waters contain only 0.05 ppb and pristine continental waters generally have concentrations below 0.1 ppb [179–181]. The geochemical mobility of cadmium is low; cadmium in solution is generally adsorbed on the solid phases (minerals, suspended particles) with which natural waters come into contact. A large proportion of anthropogenic Cd is released to the environment via the atmosphere. This is due to the high volatility of metallic Cd (melting point = 321°C; boiling point = 765°C) and many of its compounds. It is used in the electroplating industry, in the production of pigments, alloys, batteries, semiconductors, stabilisers, plastics, some pesticides [182–186]. Diethyl cadmium is used in the production of tetraethyl lead. Small amounts of cadmium can be released to drinking water from plastic pipes. Like other toxic elements (Hg, As) Cd can give rise to accumulation processes and tends to be progressively enriched along the food chain. It is easily absorbed by the digestive system and lungs [187, 188]. While there are cases of serious health effects known to result from excessive exposure to cadmium in industries and when harvesting rice grown in polluted soil and water, there are no known cases of chronic toxicity to humans using drinking water with abnormal cadmium concentrations [189–191]. Due to the high toxicity of Cd and its compounds, current legislation provides for very low limits in drinking water and wastewater, 5 μ g/l and 20 μ g/l respectively [192, 193].

Lead Lead is present in the galena ore, which is the main source of supply for mining the metal. Lead can have oxidation states +4, +2 and 0, but in nature only the +2 state is of practical importance. Pb has an amphoteric behaviour, giving rise in strongly basic media to anions of the type Pb(II), to anions of the type $HPbO_2^-$ and PbO_2^{2-}

Pb^{2+} ion has a marked tendency to form complexes with all the most abundant inorganic anions in natural waters (chlorides, bicarbonates, carbonides, sulphates). Pb forms a large number of insoluble salts with constituents normally present in appreciable concentrations in natural waters (sulphates, carbonates, phosphates, etc.). Even

under natural conditions, Pb can form metal-organic compounds (e.g. Pb alkyls), which have a high vapour pressure even at room temperature. Pb in solution shows a marked tendency to be adsorbed by solid substances such as clays and organic substances. Under reducing conditions Pb sulphide is formed with extremely low solubility.

Pb is a highly toxic element, which is why the legislator has set very low limits for both wastewater and drinking water (0.2 mg/L and 50 μ g/L respectively) [194, 195]. This element, like other toxic elements (e.g. Hg and As), can undergo a progressive enrichment along the food chain. The circulation of Pb in nature has been completely disrupted by environmental contamination processes, and its global geochemical cycle is influenced more by human activity than by natural processes. The toxicity of lead to animals and humans depends on the amount adsorbed by soft tissue and not on the amount in blood or bone. The risk of lead poisoning is greatest in calcium-deficient individuals and in children. Inorganic lead can enter the body through two routes: oral and inhalation. Negligible amounts of lead can be absorbed through the skin, which is permeable to tetramethyl and tetraethyl lead [196–198]. Out of the dietary intake of lead, only a fraction of less than 10% is absorbed by adults, whereas for children the fraction can reach 50%. Absorption occurs in the small intestine and depends on a number of factors such as age, gastric acidity, diet; high dietary intakes of calcium, iron and phosphorus reduce lead absorption, probably due to competing reactions or formation of poorly soluble compounds (e.g. phosphorus may result in the formation of poorly soluble lead phosphate) [199–201].

Food contamination by Heavy Metals. Metals such as cadmium, lead and mercury are naturally occurring chemical compounds. They can be present in various concentrations in the environment, for example in soil, water and the atmosphere. But metals can also be present in food as residues, being already in the environment as a result of human activities such as livestock farming, industry and car exhaust, or due to contamination during food processing and storage. Humans can therefore be exposed to these metals through the environment or by ingesting contaminated food or water, and their accumulation in the human body can cause harmful effects over time.

These metals are the subject of attention by international authorities such as the World Health Organisation (WHO) and the European Food Safety Authority (EFSA), which have assessed the risks to human health from their dietary intake [202, 203]. The Istituto Superiore di Sanità (ISS) has also carried out food exposure studies on the Italian population [204].

With the exception of smokers, the main source of exposure to cadmium, stresses the Istituto Superiore di Sanità, is the diet. The main foods responsible are: cereals, vegetables, potatoes, crustaceans and molluscs.

Mercury, on the other hand, is mainly linked to certain types of fish: in this regard, the European Food Safety Authority calls for reducing consumption [205], especially

during pregnancy and early childhood, of large predators such as swordfish, tuna and pike, and replacing it with other fish, such as blue fish or sea bream, which contain much lower concentrations of methylmercury [206]. With regard to lead, according to EFSA regulations and guidelines, this metal is found in various forms of speciation in foodstuffs, especially in vegetables, as many irrigation waters contain discrete levels of lead in both inorganic and organic forms. The EFSA therefore proposes a relative reduction in plant foods, especially for pregnant women and children, especially in certain areas of the EU and in products imported from non-European countries. However, in addition to an overview of the type of pollutants in food, it is also important to be able to determine these types of analytes in time with advanced techniques, so the next section will discuss some techniques for the determination of pollutants and what are the emerging materials to determine these pollutants in the shortest possible time.

1.2.1 Techniques for determining pollutants in food

Residues of heavy metals and pesticides in food, as mentioned above, are very dangerous to human health, so the quality of food control has increased and the physical and chemical techniques for determining them are increasingly precise. Among the techniques we can include high performance liquid chromatography (HPLC), gas chromatography (GC), mass spectrometry, can also be use hyphenated techniques, HPLC-MS, GC-MS. Other techniques used especially for metals inductively coupled plasma source mass spectrometry (ICP-MS) [207]; inductively coupled plasma source atomic emission spectrometry (ICP-AES). Mass spectrometry is a highly sensitive analysis technique, capable of determining various inorganic, metallic and non-metallic substances, with detection limits in the order of ppt (ng/l). This proven versatility has allowed its use to be extended to numerous scientific disciplines, considering the need for an instrument capable of providing accurate data on trace and ultra-trace element concentrations in different matrices. The ICP-MS uses a plasma torch, a quadrupole as a filter and a detector for final counting, which can be either analogue or digital. Although this type of instrumentation is highly accurate, there are still some interference problems which, if not detected and eliminated immediately, can lead to a loss of data, or hinder the accuracy of the analysis. The biggest interference problem is with isotopes of different elements that have the same atomic number, and therefore could be detected as one element. In the work of *Shana et Al*, ICP-MS was used to determine the quantity of metals in food matrices, specifically green and black olives. The data obtained showed that in addition to the classic content of metals found naturally in olives, such as Mg^{2+}, which is the most abundant, there were also significant traces of Co, Pb, Cr, Cd, which are among the most toxic heavy metals. According to the authors, however, despite the presence of the ten heavy metals examined, the levels within safety limits. Another example of the determination of residues of pollutants in food is the analysis proposed by *Hercegovà et Al.*, who show a series of separation and analysis

techniques for the determination of pesticides in baby food.The principle is to prepare the sample and separate the pollutants by liquid chromatography, extraction being performed by (liquid extraction, solid-phase extraction (SPE), dispersive SPE (DSPE), microextraction procedures, matrix solid-phase dispersion (MSPD) and supercritical fluid extraction (SFE), techniques suitable for extracting the active ingredients. Then, after sample preparation, different techniques such as HPLC and GC are used to determine the amount of residues, using mass spectrometer (MS) as a detector, this work shows that pesticides in children's food do not exceed the limit of quantification, LOQ, dictated by EU regulations [208]. Another work proposing analyses on heavy metal residues and pesticides was proposed by *Naccari et Al.*, analysed Sicilian honeys to assess the presence of certain pollutants [209]. The analysis process is divided into two parts: one part of the honey is intended for heavy metal analysis, by digesting the honey in concentrated HNO_3, while the other part is intended for pesticides. For heavy metals detection, after digestion in mineral acid, graphite furnace atomic absorption spectrometry is used as the analysis technique, using an atomic absorption spectrophotometer equipped with single element hollow cathode lamps, with the purpose of detecting lead and cadmium. For pesticides, sample preparation consists of extraction by SPE (solid-phase extraction), and after extracting the pesticides with an eluent phase using acetonitrile, the samples were placed in vials for analysis by gas chromatograph coupled to mass spectrometry. The authors conclude their analysis by stating that in several Sicilian honeys, the Pb content is ten times higher than the Cd content, in some cases exceeding the legal limits imposed by the EFSA, which is very worrying given that the risk of bioaccumulation in the human organism is very high, while pesticides are totally absent from the honeys. With regard to mercury, *Dezfouli et Al.* succeeded in determining mercury residues in tuna from the Persian Gulf using two analytical techniques, being able to distinguish between inorganic and organic mercury. Using Flame Atomic Absorption Spectrometer (FAAS), they determined the total mercury, without being able to distinguish from organic mercury. However by GC-MS, the authors were able to determine the amount of organic mercury, in the form of methyl mercury. The results show that the amount of mercury in the tuna fish is very high and above legal limits, so the authors say that the trend of growth of this highly toxic metal in fish is unfortunately set to increase [210]. From these techniques used to determine pollutants in food, it can be seen that there is a growing need in the scientific community to safeguard human health and bring food to the table that is safer and contains as few pollutants as possible.

However, in addition to the classic analysis techniques for determining pollutants such as heavy metals and pesticides, there are a number of nanomaterials in the literature that attempt to overcome this problem and increase sensitivity and selectivity towards these markers. One example is the work of Neupane et Al. who use highly fluorescent peptides to determine mercury, in the form of different salts, using fluorescence [211], to be exact, the emissive property of peptides is exploited, which when excited at an

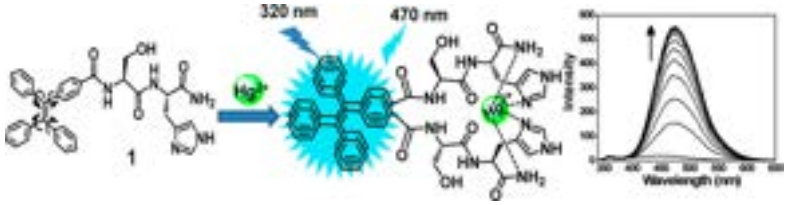

Figure 1.7: A fluorescent peptidyl chemosensor for the detection of heavy metal ions in aqueous solution as well as in cells was synthesized on the basis of the peptide receptor for the metal ions using an aggregation-induced emission fluorophore. (adapted form [211])

appropriate wavelength show an increase in luminescence intensity as the concentration of mercury increases. The figure 1.7 shows the hypothetical mechanism that exploits the fluorescence enanchement of peptides, where the nitrogen groups of this peptide bind mercury with a coordination bond, and the effect of this bond is to increase the luminescence property of the peptide.

Again trying to use materials with a low environmental impact, *Morton et Al.*, after functionalising a carbon nanotube electrode with L-cysteine, used voltammetry to exploit the redox potential of heavy metals in solution. The mechanism is quite simple, but very effective, i.e. in a solution containing the electrode properly functionalised with L-cysteine, a salt of a heavy metal is dissolved and by applying a potential difference the positive ion is bound to the ligand present in the electrode, producing no more current, which is another method for sensing heavy metals in solution [212].

In addition to heavy metals, as we have already seen for other nanomaterials, the literature has also focused on the determination of pesticides and phytopharmaceuticals in general, which, as mentioned above, are very dangerous to human health. One way of pesticide determination was carried out by *Yang et Al.* The authors developed a smart adsorbent capable of effectively detecting and removing toxic organophosphorus pesticides which is based on MOF, Fe3O4@SiO2@UiO-67, the application of this composite nanomaterial served for simultaneous selective recognition, detection and removal of glyphosate by exploiting all chemical and physical properties of the constituent materials. The prepared smart adsorbent contains Zr-OH groups with high affinity for phosphate groups, endowing it with selective recognition and enhanced adsorption capacity for glyphosate. Exploiting the optical properties of the composite material, the combination with glyphosate leads to changes in the fluorescence intensity of the smart adsorbent, and the incorporation of silica prevents electron transfer between UiO-67 and the magnetic core, which can lead to the identification of the adsorbate and its concentration, and achieve a lower detection limit. By optimising the analysis conditions, the nanomaterial shows excellent detection and adsorption performance, being able to adsorb very high concentrations of analyte (256.54 mg g^{-1}) [213]. All this indicates

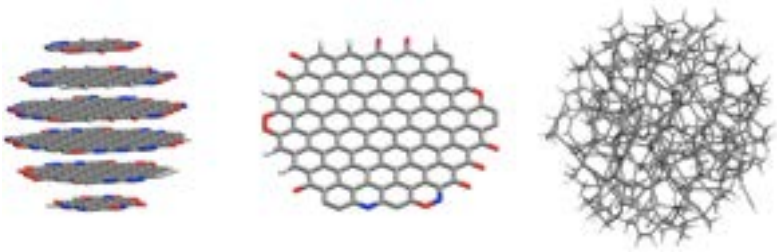

Figure 1.8: CDs can have crystalline or amorphous structure (adapted from [214])

that MOF-based smart adsorbents are promising for synchronous adsorption/detection and removal of pesticides, presenting a viable option for water quality monitoring and wastewater treatment. However, the methods of analysis we have seen have undoubted advantages such as high reproducibility of analysis on different food matrices, but also very low limits of determination that can reach ppb, but they have the major disadvantage of being very expensive and difficult to exploit outside an analysis laboratory. For this reason, in this thesis work, we have proposed an alternative way of determining heavy metals and pesticides in food, namely to exploit the emission properties of carbon nanoparticles (CDs), which will be discussed in the following section.

1.3 Carbon nanodots

In the last decade, the scientific community has dedicated itself to researching carbon-based nanomaterials for a variety of uses, examples of which include various carbon nanoforms such as graphene, carbon nanotubes and fullerenes. However, a new form of nanosized carbon has appeared in the last decade which has been attracting an increasing interest in fundamental and applied science: carbon nanodots. This class of new nanomaterials includes several types of nanoparticles, with sizes in the range of 1-10 nm, with different crystal structures such as graphenic, amorphous and polymeric Figure (1.8).

The interest in this new nanomaterial is mainly due to its remarkable optical properties, such as strong absorption and bright fluorescence transitions, which show up over a wide range from the UV to the visible [214–216]. Another important feature is undoubtedly the ease with which it can be prepared and synthesised, as well as its remarkable response in terms of electronic and optical properties to the external environment and its wide range of applications in various fields such as optoelectronics, bioimaging, catalysis, drug delivery and sensing [217–219]. In this thesis work, we have focused on exploiting the optical and surface properties of CDs for the sensing of heavy metals and pesticides in food, as these are very important pollutants that endanger human health. Therefore, the main goal is to develop the use of fluorescent CDs as probes to allow the

timely detection of these pollutants by fluorescence measurements.

1.3.1 Synthesis

The two most common synthetic approaches for the preparation and synthesis of CDs are top-down and bottom-up. The two synthesis methods differ in the types of precursors used: in the case of top-down synthesis, extended carbon precursors such as graphite, carbon nanotubes and fullerene are used. Starting from these precursors, several synthesis routes can be followed, such as arc discharge, laser ablation, electrochemical route and chemical oxidation, all of which result in highly surface-functionalised carbon nanoparticles (CDs) with very variable optical and structural properties. Bottom-up synthesis, on the other hand, involves the carbonisation or pyrolysis of molecular precursors such as citric acid and urea. The main difference, especially from the point of view of the surface, is that the samples prepared by this synthetic method are already full of functional groups derived from the functional groups present in the precursors. The carbonisation processes from molecular precursors tend to be solvothermal synthesis, microwave synthesis and autoclave pyrolysis. These synthetic approaches make it possible to construct different CDs with different chemical, optical, structural and morphological properties, so that CDs can be used in different fields of application. Some of the main synthetic approaches are schematized Figure (1.9) and are summarized in the following.

Laser Ablation. Laser ablation was the first top-down approach for the preparation of carbon nanodots (CDs). This technique consists of irradiating an extended solid carbonaceous precursor with a pulsed laser in order to fragment the extended carbon network to eventually form carbon nanoparticles [220]. One of the first works carried out using laser ablation was carried out by irradiating graphite with a laser, obtaining fairly small (around 5 nm) but non-luminescent aggregates. Only after chemical treatment in an acid solution was it possible to identify the presence of highly luminescent nanoparticles in these aggregates, with a high variety of functional groups and chromophores present on the surface. This technique was then used again by several papers [220–222] and became one of the standard ways to produce CDs. For example, in the work of *Goncalves et Al.*, where the synthesis is carried out using a fairly large carbon target immersed in an aqueous solution and irradiated with a pulsed laser at 248 nm, obtaining carbon aggregates that were then activated in an acid environment and then subsequently functionalized by reacting with NH_2-polyethylene$-$glycol(PEG_{200}) and N$-$acetyl$-$l$-$cysteine(NAC). At the end of the functionalization process highly fluorescent carbon nanoparticles were obtained [221].

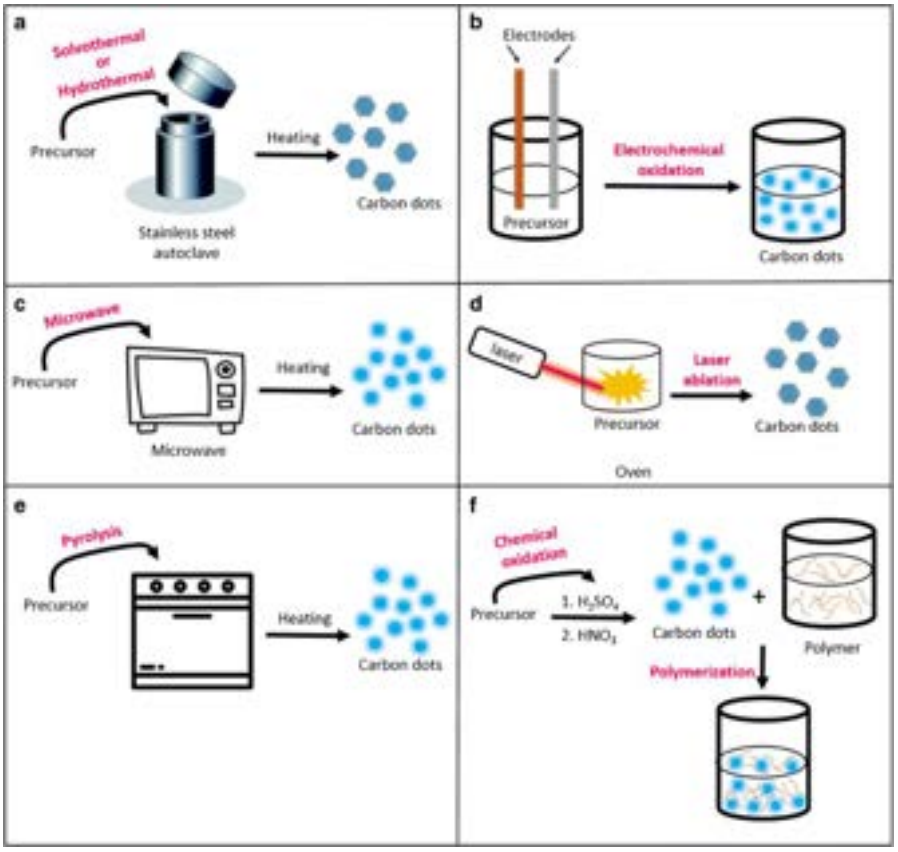

Figure 1.9: a) Solvothermal or hydrothermal synthesis conducted in an autoclave with molecular precursors; b) Electrochemical synthesis using the electrical properties of extended precursors, such as graphite; c) Microwave synthesis from molecular precursors; d) Laser ablation of extended precursors to form CDs; e) Pyrolysis synthesis using molecular precursors in the absence of solvents; f) Chemical oxidation synthesis using extended precursors and reacted with mineral acids or acid mixtures; g) Synthesis of molecular precursors using the use of solvents to form CDs.

Chemical Oxidation. The synthetic process consists in the oxidation of carbonaceous material such as graphite, carbon nanotubes and fullerene with an acid mixture, generally H_2SO_4andHNO_3, which allows both the fragmentation of the carbon network due to sulphuric acid and the formation of carboxyl and hydroxyl groups due to the oxidation of the surface by nitric acid. At the end of the reactive process, highly surface functionalised nanoparticles are formed with optical properties that were not present in the precursors. As in the case of *Yang et Al.* that used various extended carbon systems such as carbon nanotubes as precursors, which are placed in a Teflon container and digested with a sulphur-nitric mixture, resulting in highly luminescent carbon nanoparticles used for photocatalytic purposes.

Electrochemical synthesis. Electrochemical synthesis is a another typical top-down approach for the synthesis of CDs. This reaction, which can be defined as a redox reaction, uses a potential difference applied to two graphite electrodes with an electrolyte solution, leading to the formation of CDs from the chemical oxidation of the electrodes to improve the synthetic process in the work of *Li et Al.* the best condition found consists in an alkaline alcohol environment favouring the oxidation-reduction process on one of the electrodes enabling the formation of CDs. This type of synthetic approach was already common for the synthesis of carbon nanotubes [223].

Hydrothermal or Solvothermal. One of the main bottom-up synthesis methods is solvothermal synthesis, in which the molecular precursors are solubilised in a suitable solvent and burnt at temperatures of over 180^o. The reaction is generally carried out in an autoclave or in microwave, i.e. a closed, high-pressure system without the possibility of heat dispersion, which results in homogeneous heating of the reaction environment and a better reaction yield. An example is the reaction between citric acid and urea, where the precursors are solubilised in water, placed in an autoclave and burnt at a temperature of 200^o, at the end of the reaction there is a black powder in the autoclave. In the work of *Arcudi et Al.*, several bottom-up syntheses are presented using a plethora of synthetic precursors. For example, citric acid pyrolysed at 180^o for 150 minutes resulted in CDs that are particularly carboxylated and have peculiar optical properties of absorption, emission and quantum yield. The same work also reported the reaction between arginine and ethylenediamine in water, whereby the resulting material, in contrast to the previous reaction, not only has different optical properties, but also a different surface where in this case nitrogen-containing groups are mostly found. Solvothermal syntheses therefore have the great advantage of being able to construct different CDs with different optical, structural, morphological and surface properties [222]. Generally speaking, doping refers to the introduction into the crystal lattice of an atomic species alien to those forming it. These impurities, depending on whether they carry valence electrons in defect or in excess, are called acceptors or donors respectively. The effect

of the addition of these atoms is to introduce a new energy level into the band-gap of the doped species. Although the exact position of the new level depends on the reciprocal interaction between the specific impurity and the crystal lattice, what typically occurs is a modification of the absorption and luminescence properties, literature data also show that the role of nitrogen as a dopant in the core or surface increases the QY of the nanoparticle.

Purification method Another very important point is certainly purification, i.e. being able to properly separate CDs from chromophores formed as sub-reaction products or unreacted starting chromophores. The importance of purifying the CDs is due to the fact that the chromophores created during the reactive process often disturb the optical properties of the CDs, as well as sometimes having very similar optical properties, so purifying the sample enables the nanoparticles to be precisely isolated. In addition, purification allows separation according to the structure of the CDs. among other things, it is known in the literature that the most difficult samples to separate are bottom-up samples, which, compared to top-down samples, show more reaction by-products that have optical properties similar to CDs, so it is important to be able to separate and purify the CDs resulting from this type of synthesis as well as possible. [224] The most common processes for purifying and separating CDs include dialysis, size-exclusion chromatography and HPLC. Dialysis allows the removal of molecular traces known as reaction by-products. In this procedure the CDs sample is first solubilised in distilled water and then placed inside the dialysis membrane with known pore size values, from which the reaction by-products come out and the CDs sample remains inside the membrane to be characterised. SEC, on the other hand, consists in separating the CDs resulting from the synthesis according to their size. The operation is divided into two phases, a stationary phase consisting of a maltodextrose resin, known as Sephadex, which is inserted into the column and activated with a suitable mixture of solvents, and the mobile phase, in which the sample is inserted into the column and separated according to size, which makes it possible to obtain a homogeneous subset of the nanoparticles with different optical and structural properties. Finally, HPLC, an anagram of high-performance liquid chromatography, allows the separation, like SEC, of CDs into optically active fractions, which enables to obtain a plethora of CDs with different surface groups and structures.

1.3.2 Structure and Optical Properties

The most fascinating feature of CDs is certainly their luminescence, although the fundamental mechanisms responsible for it are not still very clear in the literature. However, the optical properties of this nanomaterial are intrinsically due to its core and surface properties. Depending on the synthesis route, core can have crystalline or amorphous structures, so it is correct to speak of three different families of carbon nanodots, namely

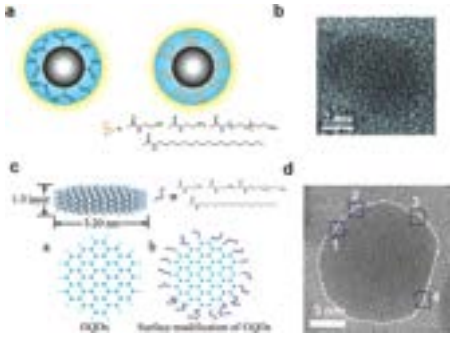

Figure 1.10: Graphene and Carbon quantum dots example and HRTEM image (adapted from [225]

the GQDs, graphene quantum dots, the CQDs, carbon quantum dots and CDs carbon dots. The main difference is that GQDs are a few sp2-hybridized carbon layers and tend to be flat, CQDs are spherical with a well-defined crystal structure and a single carbon hybridisation in addition to having a spherical shape, and CDs are amorphous nanoparticles with a carbon core where both hybridisations coexist, i.e. sp^2 and sp^3 Figure (1.10)

The different hybridisation of the carbonaceous core, and the overall morphology, therefore makes it possible to identify different sizes of nanoparticles, but as mentioned above, everything also depends on the synthetic precursors. For example, with regard to graphene quantum dots, the dimensions easily vary from 5 to 20 nm, due to the presence of starting materials such as graphite or carbon nanotubes that have a carbon network of the sp^2 . However, the opposite can be said for CDs, since the starting materials are mainly small molecules such as the aforementioned citric acid and urea, this creates a more disordered network and not very precise from a carbonaceous core point of view, so CDs are mainly derived from bottom-up synthesis. The properties of cores are mainly studied with fairly precise techniques such as Transmission electron microscopy (TEM), Raman spectroscopy and atomic force microscopy (AFM). TEM gives important information about the structural properties of carbon nanoparticles, and this technique, when combined with AFM, allows the core property and the size of the carbon nanoparticles to be identified, so these techniques combined can give important information about the structure and morphology of CDs. In regard to Raman spectroscopy, the information provided relates to the crystalline structure, and therefore, from the presence of the typical bands of carbon materials, i.e. D and G, it is possible to identify the presence of a graphitic, graphenic, diamond-like and amorphous core, depending on the ratio between the I_D and I_G intensities. This additional information therefore makes it possible to complete the structural overview of CDs, identifying precisely certain properties of structure and size. An example is provided by the work of Mewada et al, who show a series of core characterisations to understand the crystal structure of CDs as in Fig-

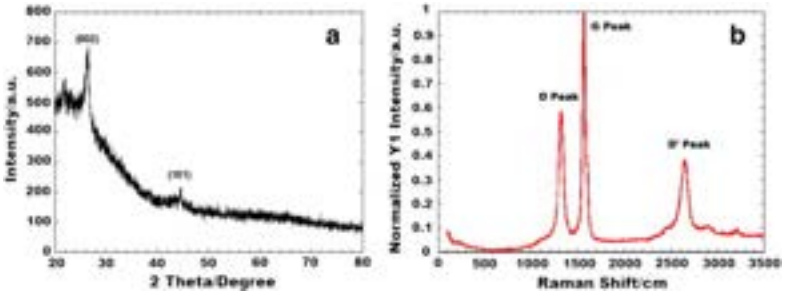

Figure 1.11: XRD and Raman spectra of carbon nano dots (adapted from [225]

ure (1.11), which allow to identify the crystalline structure of CDs. For example, XRD shows peaks that are directly compatibile with a graphitic crystal structure, also confirmed by Raman spectra. Sharp and intense Raman peak of G band observed at 1578 cm^{-1} feeble peak of D band at 1331 cm^{-1}. An additional peak at 2654 cm^{-1} explains the sp^2 hybridization pattern. It is the 2nd order two phonon process but sometimes clearly seen in Raman spectra. A ratio of intensities of I_D/I_G was calculated to be 0.59 which denotes the sp^2 or sp^3 character of the nanomaterial.

In addition to the important core properties, the surface characteristics, i.e. the functional groups present on the CDs, such as carboxyl groups, containing COOH and COOR, amino groups, NHx, and aromatic groups, are of fundamental importance. The presence of these groups is due to the method of synthesis, i.e. the CDs with more functional groups tend to be those synthesised by the bottom-up method, because the presence of functional groups already present in the precursors makes it possible to have a richer and more varied surface. However, it is also possible to passivate the surface post-synthesis, by inserting chemical groups on the surface in order to add them to the existing ones or to replace them, which makes it possible to change not only the surface properties, but also the luminescence properties, since the absorption and luminescence feature depend in a dual way on both the surface structure and the core structure. The post-synthesis passivation or functionalisation process is mainly carried out on top-down synthesised nanoparticles, because there is greater surface homogeneity, which makes the process of inserting new chemical groups easier. An example is the work of *Kwon et Al.* the solvothermal synthesis of citric acid, and then functionalise them with aromatic groups, in this case anilines [225] Figure (1.12), replacing with other chemical groups such as nitrogen, oxygen and sulphur, which makes it possible to add chemical groups on the surface to change the optical properties of the nanoparticles, As shown in Figure (1.12), the authors characterise the functionalised CDs with TEM to understand the core properties, but also with XPS and FT-IR to identify the surface properties, but above all to understand whether the reaction is successful by looking at the change in typical peaks with FT-IR.

The importance of being able to correctly synthesise and functionalise CDs, allows

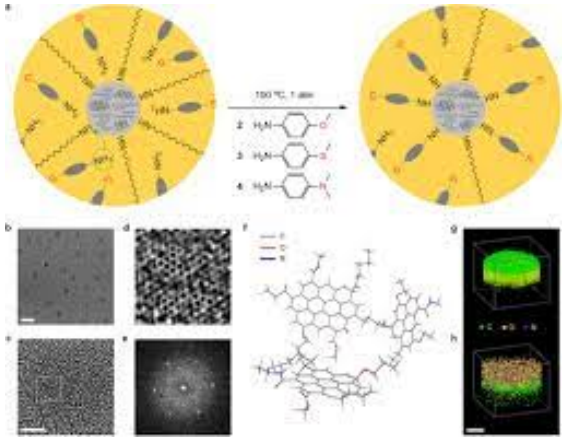

Figure 1.12: Synthesis Process and caractherization of CDs produced by Bottom-up approach (adapted from [225])

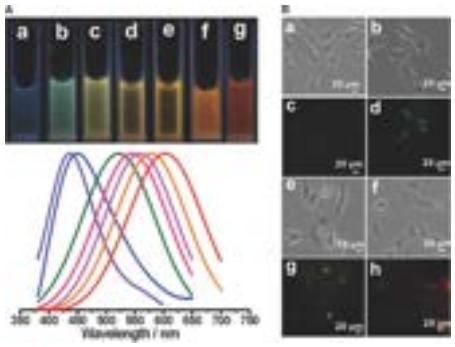

Figure 1.13: CDs emission spectra and Tunability process (adapted from)

all those optical characteristics such as absorption and fluorescence to be controlled. The phenomenon of photoluminescence is undoubtedly the most peculiar and fascinating one, but it is also very debated in the literature, since it is still not clear whether the emission process depends on the core or on the surface or on a combination of the two effects.

Anyway, CD fluorescence shows some very interesting features such as tunability, ease of response to the external environment, which makes them good candidates for various applications. The presence of a large absorption range across the UV-Vis spectrum allows CDs to be excited at different wavelengths, showing fluorescence bands that shift according to the wavelength of excitation. This makes it possible to have CDs with various emission colours from blue to red; in the Figure (1.13) in the work of *Bao et Al.*, the dependence of the emission wavelength on changing the excitation wavelength can be seen.

However, carbon nanoparticles do show very active optical behaviour, but with dif-

ferent quantum yields (QY), the differences are mainly due to the different synthetic pathways Bottom-up and Top-Down, which show slightly different optical behaviours. Bottom-up synthesized CDs tend to show higher QYs, probably due to their more molecular than nanoparticle-like behaviour, given the presence of highly conjugated aromatic π-chemical groups, the fluorescence of these CDs is more molecular-like, which increases luminescence and thus QY, in contrast to top-down CDs that show behaviour more similar to the starting precursor material such as graphene or carbon nanotubes, as for example in the work of *Wang et Al.* both systems are compared and after the same purification processes the quantum yield of the two systems differs, evidencing that the bottom-up sample after purification decreases its QY due to the loss during dialysis of the small chromophores that give the nanomaterial its molecular behaviour [226].

Another important aspect of CD fluorescence is the response to the external environment, for example CDs are very sensitive to the solvent in which they are dispersed, but also to certain compounds, such as the transion metals that extinguish the fluorescence intensity of CDs. The best quenchers are e.g. Hg^{+2}, Cu^{+2}, Fe^{+3} as for example in the work of *Meng et Al.*, in which after synthesising CDs by a bottom-up route the quenching of CDs by such metals is used for heavy metal sensing. As mentioned above, in addition to interactions with heavy metals, CDs are very sensitive to pH, i.e. their luminescence properties change depending on whether the system in which they are immersed is acidic, basic or neutral. In the work of *Marin et Al.* [227] the response of CD luminescence to pH is used for biological purposes. In particular, the authors note that changing the concentration of hydrogen ions leads to cellular disruption, which they determined by using the luminescence properties of CDs as probes in a confocal fluorescence spectroscopy, so being able to detect the electron-transfer process between organelles and CDs in a variable pH environment. The versatile optical properties directly linked to the core and surface structure, the sensitivity to the external environment, tunability across the UV-Vis range, biocompatibility and ease of synthesis make carbon nanoparticles excellent candidates for a multitude of application fields.

1.3.3 Emission Mechanism

One of the questions still being debated in the scientific community is certainly the CDs emission mechanism, since it represents the most marked property of this new nanomaterial. In this respect, models attempting to explain CD fluorescence can be generally classified in two process one that argues that the emission mechanism depends on the core and therefore from the size of the nanoparticle and the other in which it is proposed that the emission mechanism occurs in electronic states located on the surface of the dot. Some of the first works on CDs initially investigated the effect of the size of the CDs, hypotesizing that the emission could be interpreted as a sort of quantum confinement effect that is dependent on the size of the nanoparticle. This can be proved

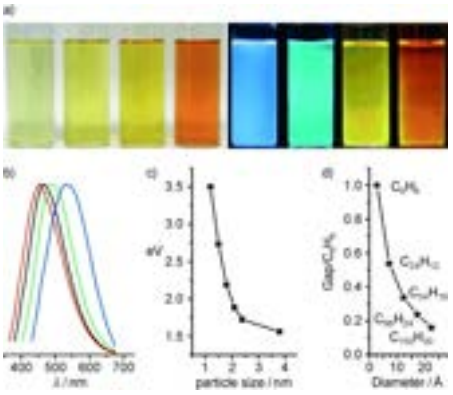

Figure 1.14: CDs emission by size depnding (adapted from [223])

by trying to extract and separate CDs using purification methods such as size-exclusion chromatography, which separates the nanoparticles by size and thus explains how the optical properties are directly dependent on the size of the nanoparticles. In doing so, *Li et Al.* were able to demonstrate that the luminescence of CDs was size-dependent by studying the energy separation of the HOMO and LUMO frontier molecular orbitals of all the fractions collected during the purification process. As the absorption and emission spectra changed as shown in Figure (1.14), but the surface of the CDs, which had been characterised by FT-IR spectroscopy, did not, this is the first evidence that the size of the nanoparticle influences the emission mechanism through the core state [223].

Another study carried out by *Ye et Al.*, using top-down synthesis, proposes a further mechanism based on the size of the carbon nanoparticle, the authors suggest that the emission mechanism is related to two phenomena, namely excitation in the core of the nanoparticle and radiative recombination on the surface of the CDs, which is ultimately responsible of the emission property, proposing a highly localised emission mechanism on the surface, also due to the chemical groups present, which can act as additional chromophores [228]. Besides, according to the authors, the size dependence helps to understand the tunability process, so much so as to demonstrate how two nanoparticles from the same synthesis but of different sizes (from 2.96 nm to 2.30 nm), show different optical behaviour, so that the emission wavelength blue shifted from 500 to 460 nm; this emission phenomenon suggests that CDs are indeed quantum dots, given their behaviour very similar to classic semiconducting metallic dots. In conclusion, the authors argue that the correlation between size and different optical properties may be due to further processes that, for example, establish a correlation between size and surface structure, which is probably also involved in the emission mechanism.

Another process that is also much debated in the literature involves the surface state of CDs, where it is hypothesised that the mechanism of excitation and subsequent emission depends solely on the surface of the CD or, even better, on the chemical groups

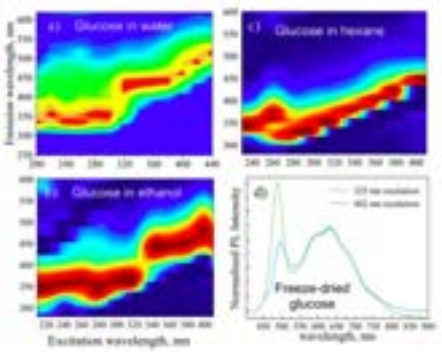

Figure 1.15: PL maps glucose CNDs in water (a, relative polarity 1); ethanol (b, relative polarity 0.654) and in hexane (c, relative polarity 0.009). Normalized PL data of freeze-dried glucose sample with two excitation wavelengths (325 nm and 442 nm) are also shown (d), (adapted from [230])

present, which act as chromophores exclusively responsible of the emission. It is mainly assumed that surface-dependent luminescence phenomena are dependent on the synthesis techniques, with bottom-up syntheses being the most likely to yield CDs characterized by a surface-related emission, the reason being that the molecular precursors used for this synthesis contain functional groups that dope the surface and make the dot very luminescent during the synthesis process.

Furthermore, it has been proposed that molecular side-products of the synthesis can be adsorbed on CD surfaces and contribute to their fluorescence. In the work of *Das et Al.*, they argue that the possibility of having a plethora of different chromophores on the surface enables the fluorescence mechanism. To prove this model, the authors oxidise and reduce the surface of the dots obtained by a bottom-up approach and they find that a change of the chemical groups present on the surface leads to different responses despite the crystalline core remaining unchanged [229].

Another way to address the emission mechanism of CDs is to study the interaction between CDs and the external environment, as in the case of Papaioannou et Al, who after synthesising CDs with a bottom-up method and characterising them structurally, study interactions with different solvents, This study proposes an emission mechanism that is strongly dependent on the chemical groups present on the surface in the presence of different solvents, two polar (water and ethanol) and one apolar (hexane) [230], and it is shown that the increasing polarity of the solvent influences the emission given the easy interaction between solvent and surface, as shown in Figure (1.15)

As we have seen so far, there is a large debate on the possible fundamental mechanisms responsible of CD fluorescence, and it is very likely that CDs with different structures obtained by different synthetic approaches emit thourgh different mechanisms. Anyway, from a practical point of view, the fascinating fluorescence properties

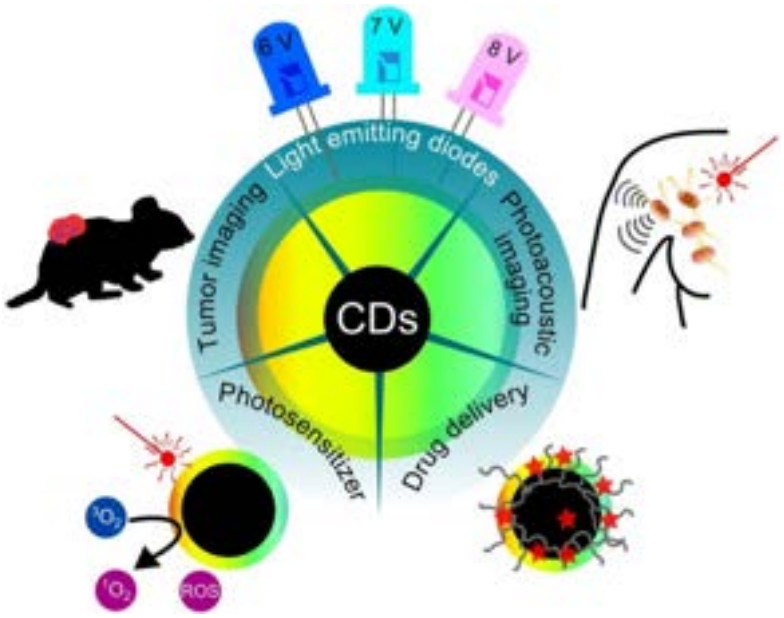

Figure 1.16: Applications field for CDs nanoparticle (adapted from [231])

of CDs combined with their strong response to the environment make them useful for several technological applications, which are being intensely explored by many research groups, and are described in the next paragraphs.

1.3.4 Application

CDs, can be broadly described as an optically active carbon-based nanomaterial with characteristics similar to semiconducting quantum dots, with the advantage of being a much less toxic material, so much so that they can be used in a series of application fields, such as bioimaging or in the biomedical field in general for drug delivery, which can be inoculated through carbon nanoparticles, or as optoelectronic devices , based on their strong tendency of behaving as electron donors, or in catalysis, given the presence of chemical groups that can be easily photoactivated to improve the yields of reactions [231]. Last but not least, an important field of application of CDs which is of particular importance in this thesis is nanosensing, given the ease of interaction with heavy metals. Some of these applications shown in Figure (1.16) will be discussed in more detail in the next few paragraphs.

Biomedical. Beside their optical properties, another important characteristic of CDs is undoubtedly their biocompatibility, so that in recent years there has been much discussion in the literature about the application of these carbon nanoparticles in the biological and medical fields, thanks to their low impact on human health, so much so that they

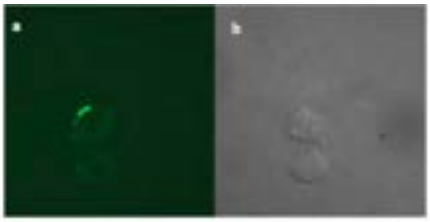

Figure 1.17: Fluorescence images of 16HBE cells incubated for 24 h with the CDs (adapted from [232])

are candidates as materials of the future for bioimaging given their luminescence properties, but also as drug transporters and even as possible drugs in their own right. A first example is bioimaging, as exemplified by the work *Chen et Al.* which uses CDs for biomaging in vitro of bronchial tissue cells after an incubation time of 24 hours, the cell is viewed by fluorescence microscopy and the stability of the cell with CDs allows for potential application in vivo [232].

Another application of CDs in the nanomedical field is that of drug delivery, i.e. the CDs are loaded with the active ingredient by means of a coupling reaction, but when they reach the active site of interest, the CDs slowly release the drug. An example is given by the work of *Tang et Al.* who, after passivating with PEG [233], bind the drug Doxorubicin to the surface of the CDs and then carry out release tests by means of FRET.

Photocatalysis. In addition to applications in the biological field, given the very pronounced optical and reactive properties of CDs, they have many applications in the field of catalysis, more specifically photocatalysis. The principle of photocatalysis exploits the interaction between sunlight and generally a metal or metal oxide, such as TiO_2, which can be defined as the photocatalyst par excellence. For example. the work of *Ji et Al* it presents TiO_2 nanoparticles that are photo-activated for the degradation of polycyclic aromatic hydrocarbons [234] which are very dangerous for the environment as well as being one of the main sources of air pollution caused by the combustion of fossil fuels. However, metal oxide photocatalysts contain elements from the periodic table that tend to be toxic to human health, which is why the scientific community tends to look for metal-free materials, such as CDs. Given the high sensitivity of CDs to light radiation in UV-Vis, this property makes CDs prime candidates to achieve metal-free photocatalysis, e.g. in the work of *Song et Al.*, boron-doped CDs are used in conjunction with graphitic carbon nitride ($g-C_3N_4$) to efficiently break down and degrade organic pollutants [235]. Thus, the authors were able to construct a heterojunction between CDs and $g-C_3N_4$, demonstrating a catalytic efficiency comparable to that in the presence of transition metals.

Nanosensing. In the literature, the use of carbon nanoparticles varies widely, but recently there has been a massive use for nanosensing, in which carbon nanoparticles act mainly as a highly sensitive chemical sensor to a whole range of molecular and ionic compounds [236], thanks also to the presence of a surface highly rich in chemical groups that allow better interaction with the analytes of interest. Thus, CDs can act as non-selective but highly sensitive chemical sensors due to post-synthesis with certain chemical groups relevant to the highly selective recognition of certain chemical compounds. Several works in the literature have pursued the selective sensing of heavy metals such as Hg^{2+}, Pb^{2+} and other heavy metals that are particularly polluting and very dangerous to human health, and the versatility of the functional groups allow a high selectivity towards these pollutants. CDs detect other dangerous environmental pollutants, such as polycyclic aromatic compounds and pesticides, both of which have very similar mechanisms of interaction that will be explained later in this section. As far as heavy metals are concerned, the interaction with the highly functionalised surface of CDs tends to take place through luminescence quenching, i.e. the selective switching off of radiative channels that allow the dot to luminescence. For example, in the work of *Wang et Al.*, the quenching of the luminescence of CDs prepared via bottom-up methods is reported. The authors also explain the mechanism of interaction between the surface of the dot and the metal in question, which in this case is mercury Figure (1.18), as being the result of photoinduced electron transfer from CDs to the ion.

The process that occurs is given by the collision of the mercury ion with the surface of the CDs, leading to the formation of a coordination compound made possible by the presence of functional groups containing nitrogen, which have a particular predisposition to bind in an exclusive way the mercury. Morover another mechanism of action is due to electrostatic interaction between the positively-charged ion and the negatively charged CD surface [237].

In addition to the multiple selectivity towards transition metals, in recent years in the literature various attempts to use CDs to detect pesticides and other molecules have been reported. The interaction process between aromatic molecules and CDs in this case predict that no bonds are formed with the surface, bonds that allow the fluorescence radiative channels to be switched off, but the attachment of the aromatic molecule to the CD surface occurs through weak-type interactions, such as for example the hydrogen bond or intercalation p-p stacking, a process that occurs quite easily if the pesticide is aromatic and the CDs has a graphenic or graphitic structure, where the π-orbitals of the two systems interpenetrate to form fairly stable intermolecular interactions, capable of turning off the radiative channels of the CDs. An example is the work done by *Muckoya et Al.* able to determine a family of pesticides using liquid chromatography extraction coupled with mass spectrometry, managing to determine the concentrations of pesticides, in this case the family of parabens, coming from waste water [238]. In this case the authors exploit the chemical properties of the CDs and not the optical

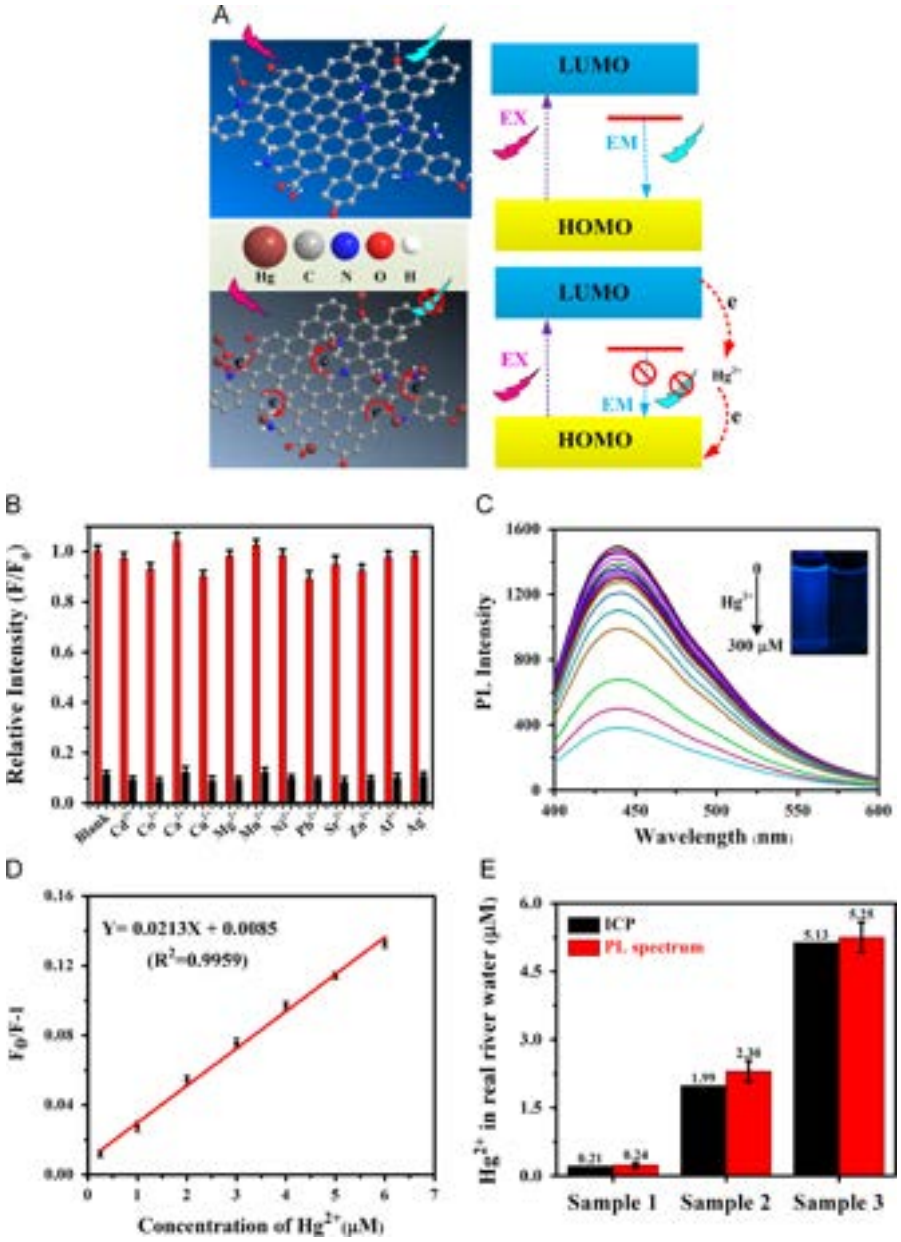

Figure 1.18: Mercury ion sensing based on PL spectrum. (A) The proposed PL quenching mechanism for N-doped CNDs/Hg^{2+} system; (B) the relative fluorescence intensities (F/F_0) of N-doped CNDs in the presence of metal ions (300 μM), and following treatment of the mixture solution with 300.0 μM Hg^{2+}; (C) representative PL emission with increasing Hg^{2+} concentrations (0-300 μM), the inset displays photographs with Hg^{2+} concentrations of 0 and 300 μM; (D) the dependence of (F_0/F)-1 on concentrations of Hg^{2+}; (E) Hg^{2+} concentration in river water measured by PL spectrum (red) and using ICP-AES (black). (adapted from [237])

ones, this demonstrates a remarkable ductility of the CDs. Another way to use CDs for pesticide determination is to utilise their emissive properties. In the work of *Li et Al.* [239] a bioplatform is created to monitor and determine organophosphorus pesticides which is designed through dual-mode (fluorometric and colorimetric) channels based on acetylcholinesterase (AChE)-controlled quenching of fluorescent carbon dots (CDs). By exploiting quenching by a target molecule TNBA which is able to function as a powerful absorber the fluorescence of CDs was quenched through a dynamic quenching process. It was also found that by the presence of organophosphorus pesticides, the enzymatic activity of acetylcholine is inhibited, leading to the recovery of the fluorescence signal. The experiment provided good sensitivity for the rapid detection of paraoxon (model analyte) with a detection limit of 0.4 ng/mL^{-1}. Therefore, by exploiting the excellent optical property of CDs and the specificity of the enzyme, the dual output platform may potentially be a promising candidate for the detection of organophosphorus pesticides [239].

1.4 Aim of Project

The research project aims to create optical sensors of polluting substances using the photoemission of Carbon Dots (CDs) as a sensitive element. CDs are a recently discovered family of carbon-based nanomaterials, at the center of considerable research interest due to their peculiar optical emission properties, usable in multiple applications, for example in optoelectronics and biotechnology. It is known in particular that CDs are particularly suitable for use in nanosensing, because their fluorescence is extremely sensitive to the environment and to interactions with surrounding molecules and ions. In general, the use of nanomaterials as sensors has a number of potential advantages over traditional detection methods, such as, for example, the high active surface, high selectivity and sensitivity. Among the many nanomaterials with this functionality, CDs are of particular interest because, unlike many other nanosystems, they appear to be fundamentally non-toxic, eliminating the concern that currently limits the advancement of many nanotechnologies. Furthermore, CDs can be produced at very low cost, with simple and sustainable procedures, and also from waste materials, which makes them very suitable for environmentally friendly commercial exploitation. Due to this combination of properties, the study of nanosensors based on CDs is now a very competitive sector. The project intends to develop CDs-based sensors for two classes of analytes of great environmental importance: heavy metals and pesticides. The detection of metals in water, or of pesticide and herbicide residues in food products, are problems of considerable social and industrial importance due to the toxicity and the absorption of these substances by consumers. There is already several evidences that CDs can be used by metal ion sensors (Pb^{2+}, Cd^{2+}, Hg^{2+}) and some recent examples of how CDs can be engineered so that their fluorescence reveals some common pesticides and herbi-

cides (e.g. organophosphates or triazines). However, more research is needed to bring these applications to full fruition. In fact, the interaction processes between CDs and the surrounding environment are still poorly understood, as are the mechanisms responsible for their fluorescence. The research activities proposed here aim at a much deeper understanding of the photo-physics of CDs interacting with the surrounding environment, allowing to optimize their use in sensors and to obtain low-cost devices to detect different types of metals and / or pesticides.

Chapter 2

Theory and basic concepts related to sensing

In this chapter, the physical phenomena necessary to describe the scientific aspects explained in the previous chapter will be addressed and described from a purely theoretical point of view.

2.1 Optical Absorption and Emission

Optical spectroscopy is the study of the absorption and emission of light by atoms, molecules, or larger assemblies. The absorption or emission processes are related to a rearrangement of the electrons in the system. To a first approximation, the rearrangements usually correspond to an electron being transferred from one orbital to another, and a transition will be described in terms of those orbitals. The wavelengths or frequencies of transitions help identify atoms and molecules and give information about their energy levels and hence their electronic structure and bonding. Intensities of absorption or emission give information about the nature of the electronic states and help to determine concentrations of species.

Absorption spectroscopy is a common and well developed technique for studying electronic transitions between the ground state and excited states of atoms or molecules. A beam of light passes through a sample, and the amount of light that is absorbed during the passage is measured as a function of the wavelength or frequency of the light. The absorption is measured by comparing the intensity, I, of light leaving the sample with the intensity, I_0, entering the sample. The transmittance, T, is defined as the ratio:

$$T = \frac{I}{I_0} \tag{2.1}$$

It is often quoted as a percentage. In measuring the spectra of gases or solutions

contained in cells, I_0 is usually taken to be the light intensity passing through an empty cell or a cell of pure solvent. This corrects well for reflection at the surfaces, absorption by the solvent or light scattering, which are not usually the quantities of interest [240, 241]. It is usually convenient to work with the decadic absorbance, A(OD), defined by:

$$OD(\lambda) = \log \frac{I_0}{I} = -\log T \tag{2.2}$$

From the equation we can then derive the Lambert-Beer limit law which thus makes explicit the quantities from which the absorbance depends on

$$OD(\lambda) = \epsilon c B \tag{2.3}$$

Where ϵ is the molar extinction coefficient which is directly proportional to the cross section, c is the concetration of the compound absorbing the photon energy and B is the optical path. The electronic absorption spectrum of a compound is usually shown as a plot of ϵ versus wavelength or frequency.

To understand emission spectroscopy of molecules and/or their photochemistry it is essential to have a picture of the radiative and non-radiative processes among the electronic states. Most stable molecules other than transition metal complexes have all their electrons paired in the ground electronic state, making it a singlet state. To illustrate the processes that occur between absorption and subsequent emission, it is useful to introduce Jablonski diagrams; an example is shown in Figure 2.1. Singlet states are designated by the letter S and numbered in order of increasing energy. The ground state is called S_0. Excited singlet states have configurations in which an electron has been promoted from one of the filled orbitals to one of the empty orbitals of the molecule. Such configurations with two singly occupied molecular orbitals will give rise to triplet states as well as singlet states. A triplet state results when one of the electrons changes its spin so that the two electrons have parallel spin. Each excited singlet state will have its corresponding triplet state. Because the electron–electron repulsion is less effective in the triplet state, it will normally be lower in energy than the corresponding singlet state. After an absorption process the electron, promoted to a given excited state, usually comes back to the ground state emitting a photon of energy equal to the energy separation of the electronic levels. Those listed and shown here are only some of the processes involving electronic states, another important process being fluorescence quenching [240, 242].

The emission process is characterized by a typical permanence time, named lifetime. Typical singlet lifetimes are measured in nanoseconds while triplet lifetimes of organic molecules in rigid solutions are usually measured in milliseconds or even seconds. In liquid media where diffusion is rapid the triplet states are usually quenched, often by the nearly ubiqitous molecular oxygen. Because of that, phosphorescence is seldom observed in liquid solutions. In the spectroscopy of molecules having a singlet ground

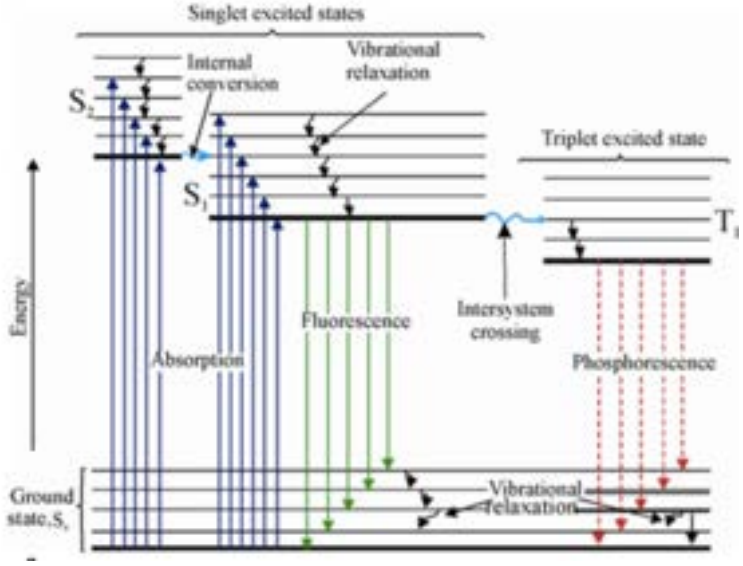

Figure 2.1: Jablonski diagram; the most common processes that matter undergoes when interacting with radiation are presented, namely absorption, fluorescence and phosphorescence. The diagram shows the electronic ground state S_0, the excited singlet states $S_{1,2}$ and a triplet state T_1. Horizontal lines represent the vibrational energy levels related to each electronic state.

state the term fluorescence is now usually used to refer to emission from an excited singlet state and phosphorescence to emission from a triplet state, regardless of the actual lifetimes. If a light beam is used to excite one of the higher singlet states, say S_2, a very rapid relaxation occurs to S_1, the lowest excited singlet state. This non-radiative process just converts the difference in energy into heat in the surroundings. A radiationless transition between states of the same multiplicity is called internal conversion. Relaxation between states of the same multiplicity and not too far apart in energy is usually much faster than radiative decay, so fluorescence is seen only from the S_1 state. These radiationless processes in large molecules are the analogue of the perturbations observed in small molecules. They are caused by small terms in the Hamiltonian such as spin–orbital coupling or Born–Oppenheimer breakdown, which mix electronic states. The density of vibrational levels of large molecules can be very high and these interactions favour irreversible transitions to lower states. Once the excited molecule reaches the S_1 state it can decay by emitting fluorescence or it can undergo a further radiationless transition to a triplet state. A radiationless transition between states of different multiplicity is called intersystem crossing. This is a spin-forbidden process. It is not as fast as internal conversion and often has a rate comparable to the radiative rate, so some S_1 molecules fluoresce and others produce triplet states. There may also be further internal conversion from S_1 to the ground state, though it is not easy to determine the extent to which that occurs. Photochemical reactions or energy transfer may also occur from S_1 [242, 243].

2.2 Lifetime and Quantum Yield

Lifetime and quantum yield, are other important intrinsic characteristics of chromophores, and are directly related to each other. When we speak of QY, we mean the ratio between the number of photons emitted and the number of photons absorbed. In general, species with higher quantum yields show more intense emission and the QY can also be defined as the fraction of excited molecules that return from the excited state to the fundamental state by emitting a photon. The QY is given by the relationship between Γ, which is defined as the radiative decay rate of a molecule and k_{nr}, which is the non-radiative decay rate; this relationship gives the QY value of a fluorescent system by the following equation:

$$QY = \frac{\Gamma}{\Gamma + k_{nr}} \tag{2.4}$$

Among other things, when the quantum yield is equal to or at least close to 1, it means that the dissipative processes dependent on k_{nr}, are negligible and therefore $\Gamma \gg k_{nr}$. Given the dependence of these two quantities, Γ and k_{nr}, one can also calculate the

fluorescence lifetime, which gives information about the time the fluorophore lives in the excited state, so the lifetime τ is given by

$$\tau = \frac{1}{\Gamma + k_{nr}} \tag{2.5}$$

However, the process causing the depopulation of the excited state is still random, so the all excited fluorophores do not decay with a time precisely equal to τ, but the lifetime should rather be seen as the average of the decays of all fluorophores, which as mentioned above occur randomly. Although there are various processes that depopulate the excited state, a simple general model is as follows: suppose at time t the excited state is composed of a population n(t). Having already introduced the radiative and non-radiative transition rates, it is possible to express the population variation per unit time by the following equation when the system has been excited and is then let to relax

$$\frac{dn(t)}{dt} = -(\Gamma + k_{nr})nt \tag{2.6}$$

therefore , assuming a population n(0) at t=0s that is the time when the excitation source is removed,

$$n(t) = n(0)^{-(\Gamma + k_{nr})(t)} \tag{2.7}$$

From here we then obtain the exponential decay regulating the depopulation of the excited state, and considering that the intensity I emitted per unit time is proportional to the population change per unit time, we can also write:

$$I(t) = I(0)e^{-\frac{t}{\tau}} \tag{2.8}$$

However, single exponential decay is not the only possible law describing how a fluorophore undergoes depopulation of the excited state. In fact, some fluorophores can display two components in that decay with very similar lifetimes. In this case it is appropriate to describe this phenomenon with a double exponential as follows:

$$I(t) = I(A)e^{-\frac{t}{\tau_A}} + I(B)e^{-\frac{t}{\tau_B}} \tag{2.9}$$

where I(A) and I(B) are the respective emission intensities of the two variants of the fluorophores characterized by two different lifetimes τ_A and τ_B, so the emission intensity varies over time as a linear combination of two exponential decays. Another type of decay, observed in time-resolved spectroscopy, is the stretched exponential:

$$I(t) = I(0)e^{(-\frac{t}{\tau})^{\beta}} \tag{2.10}$$

This decay law is characteristic of highly disordered system, and can be taken as a phenomenological way of representing a broad distribution of lifetimes. The parameter

β is related to the distribution of lifetimes; for β = 1 we return to the case of simple exponential decay. The smaller this parameter, the wider the lifetime distribution of the emissive species.

2.3 Quenching

Fluorescence quenching refers to all those processes that cause a decrease in emission intensity and in some cases a complete removal of the fluorescence. The dynamics involved in quenching the fluorescence are given by the reaction between a fluorophore [F] and a quencher [Q], in which energy is transferred from the fluorophore to the quencher. This type of process makes it possible to switch off the fluorophore's radiative channels, but the process is not always irreversible, so that there are two different types of quenching, namely dynamic or collisional quenching and static quenching. Collisional, or dynamic, quenching occurs when the fluorophore is returned to the ground state due to a collision following a diffusional encounter with other molecular species present in solution; this collision must also occur during the lifetime of the excited state [242]. Typically, this process does not lead to alterations in the emissive species, the fluorophore can still carry out absorption although decay through radiative channels is prevented by the quencher, which interacts with the fluorophore before emission occurs. When a reaction occurs between a chromophore and a quencher, in the case of static quenching, we have the formation of a quencher-fluorophore complex which is no longer emissive. Typically a change in the absorption spectrum can be observed. In some cases, the new species is no longer able to absorb the energy by electronic transition. In other cases, absorption is still possible but the new species is affected by strong non-radiative decay processes that completely prevent fluorescence.

We can therefore study quenching processes not only by observing the disappearance of emissive properties, such as fluorescence, but also how other parameters such as the absorption spectrum and how the fluorescence lifetime varies, thus being able to obtain information on the type of quenching in question and differentiate between them.

Dynamic Quenching. Dynamic quenching results in a decrease in fluorescence due to collisions of the excited fluorophore with other molecules (quenchers) and subsequent non-radiative decay. Among other things, dynamic quenching is described by the Stern-Volmer equation:

$$\frac{I_0}{I} = 1 + k_q \tau_0 [Q] = 1 + k_D [Q] \tag{2.11}$$

where I_0 and I represent the emission intensity in the absence and presence of the quencher, the product between the proportionality constant k_q and [Q], the concentration of quenchers, indicates the rate at which the excitation is dissipated due to dynamic

quenching processes and finally τ_0 is the lifetime in the absence of the quencher, while k_D which is the Stern-Volmer constant for the dynamic quenching mechanism, encloses k_q and τ_0. Data on quenching processes are often created by comparing I_0/I as a function of [Q] since the expected trend is linear. Such graphs are called Stern-Volmer graphs and their importance lies in the fact that simply by analysing the slope of the line represented, information on the process can be obtained.

Considering now the ratio between the two lifetimes τ_0/ τ:

$$\frac{\tau_0}{\tau} = \frac{\Gamma + k_q[Q]}{\Gamma} = 1 + k_q\tau_0[Q] \tag{2.12}$$

it can be seen from the equation that a typical feature of dynamic quenching is characterized by equal decrease of emission intensity and lifetime as can be seen from the identity:

$$\frac{I_0}{I} = \frac{\tau_0}{\tau} \tag{2.13}$$

The fact that the fluorescence lifetime and intensity decrease at the same time means that the quencher is able to selectively switch off those radiative channels, thereby changing the fluorophore's properties of remaining in the excited state.

Static Quenching. As far as static quenching is concerned, however, the interaction process is slightly different. A fluorophore interacts with a quencher, which switches off those radiative channels in the excited state, forming a a non-fluorescent complex. This type of quenching is controlled by the equilibrium constant of the complex formation:

$$K_s = \frac{[F-Q]}{[F][Q]} \tag{2.14}$$

Where [F-Q], [F] and [Q], are the concentrations of the fluorophore-quencher complex, the free fluorophore and the free quencher. The total concentration of the fluorophore that has been quenched or not by the quencher [F_0] can also be identified from the mass balance as follows:

$$F_0 = [F-Q] + [F] \tag{2.15}$$

by substituting and solving the previous equation:

$$K_s = \frac{[F_0] - [F]}{[F][Q]} = \frac{[F_0]}{[F][Q]} - \frac{1}{[Q]} \tag{2.16}$$

As in the case of dynamic quenching, the concentration of the fluorophores can be substituted by the intensity emitted in the presence and absence of a quencher.

$$K_s = \frac{[I_0]}{I[Q]} - \frac{1}{[Q]}; \frac{I_0}{I} = 1 + K_s[Q] \tag{2.17}$$

The equation obtained to describe static quenching processes linearly relates the quantity I_0/I to the concentration of the quencher [Q]. The resulting dependence is identical to that obtained for dynamic quenching processes, but in this case the K_s constant appearing in equation 2.17 represents a chemical equilibrium constant, rather than the product of a diffusion constant and the lifetime, as found before. However, given the similarity between the two types of quenching from a graphical point of view, we cannot discriminate between the two processes by only using steady-state fluorescence analysing only the decrease in fluorescence intensity.Nevertheless, one technique that allows the two types of process to be discriminated is time-resolved fluorescence, as we have seen dynamic quenching depends on the τ lifetime in the excited state. When dynamic quenching is present, the excited state has an extremely short lifetime due to new, very efficient non-radiative decay channels. In the static quenching, at variance, it can therefore be said that the mechanism removes part of the fluorophores by making them non-fluorescent: the lifetime of the remaining fraction, however, remains unchanged and we can write:

$$\frac{\tau_0}{\tau} = 1 \tag{2.18}$$

As already said, in case of dynamic processes this same quantity is instead proportional to the concentration [Q] of the quencher. Therefore, by using time-resolved measurements to check for changes in the decay lifetimes, one can discriminate static from dynamic quenching and it is possible to be certain about the type of process at play for a given system.

2.3.1 Quenching Mechanism

In the previous paragraph we have seen the types of quenching, i.e. static and dynamic, but in this section we will look at a number of phenomena that can cause fluorescence quenching. The most important prerequisite is that the quencher in certain concentrations is close enough to the fluorophore to be quenched, so the distance between a fluorophore in the excited state and the quencher must be such that there can be an exchange of energy and the fluorophore is quenched and then returns to the ground state by relaxing through non-radiative channels. Three main types of processes are typically involved in quenching, namely Resonance Energy Transfer (RET), Intersystem Crossing, Photoinduced Electron Transfer (PET).

Resonance Energy Transfer RET occurs when there is an overlap between the emission spectrum of a fluorophore, known as the donor, and the absorption spectrum of

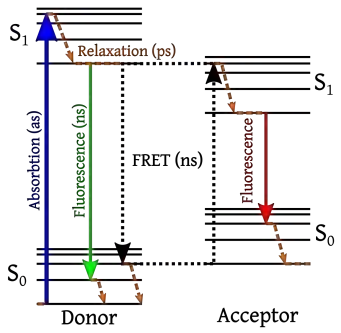

Figure 2.2: FRET scheme

another species present in solution, known as the acceptor. The donor fluorophore absorbs electromagnetic radiation and then goes into an excited state. When the RET process occurs, the donor returns to the ground state while the acceptor is simultaneously excited. At this point, if the acceptor is fluorescent, the return to the ground state can be mediated by emission; on the contrary, dissipation occurs in the form of heat and fluorescence quenching occurs. The phenomenon is not mediated by photons, but rather the coupling between donor and acceptor is due to dipole-dipole interactions, which makes possible an interaction on a spatial scale of the order of nm, the longest among the processes mentioned here Figure 2.2.

Intersystem Crossing Intersystem crossing is a non-radiative transition between two vibrational levels of the same energy belonging to electronic states of different multiplicities. For example, an excited molecule in the 0 vibrational level of the S_1 state can move to the iso- energetic vibrational level of the T_1 triplet state; then vibrational relaxation brings it into the lowest vibrational level of T_1, Figure 2.3. Intersystem crossing may be fast enough (10^{-7}–10^{-9} s) to compete with other pathways of de-excitation from S_1 (fluorescence and internal conversion S_1 -> S_0). Crossing between states of different multiplicity is in principle forbidden, but spin–orbit coupling (i.e. coupling between the orbital magnetic moment and the spin magnetic moment) can be large enough to make it possible. The probability of intersystem crossing depends on the singlet and triplet states involved. If the transition S_0 -> T_1 is of n -> π type for instance, intersystem crossing is often efficient. It should also be noted that the presence of heavy atoms (i.e. whose atomic number is large, for example Br, Pb) increases spin–orbit coupling and thus favors intersystem crossing since the systems undergoes a transition from S_1 to T_1, no fluorescence is possible, and phosphorescence from T_1 is typically quenched by collisions with ubiquitous molecular oxygen.

Photoinduced Electron Transfer Photoinduced electron transfer (PET) is often responsible for fluorescence quenching. This process is involved in many organic photo-

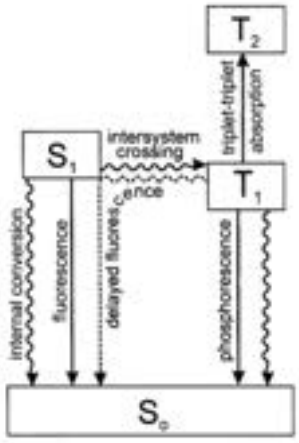

Figure 2.3: IC scheme

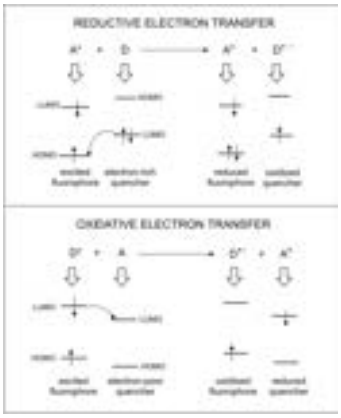

Figure 2.4: PET scheme

chemical reactions. It plays a major role in photosynthesis and in artificial systems for the conversion of solar energy based on photoinduced charge separation. PET causes fluorescence quenching because it removes from the fluorophore either the electron or the hole, therefore preventing the possibility of radiative recombination. In general, the transfer effect is only transient, and the system returns to the ground state via channels involving the return of the electron to the donor via non-radiative channels, Figure 2.4.

It should be noted that electron transfer can take place in both directions and the fluorophore can act as both donor and acceptor. What occurs is that the direction of the transfer is governed by the redox potentials of the ground and excited states. An interesting aspect of PET is that many metal ions are well known to behave as efficient electron acceptors (e.g. Hg, Cu, Ag...), and therefore as efficient fluorescent quenchers. This is the fundamental mechanism which typically lies at the basis of metal fluorescent

sensors already mentioned in section 1.3.4, where the interaction process between CDs and heavy metals is reported.

Chapter 3

Experimental Set-ups

In this section, I will describe all the instrumental apparatuses used during this thesis work, in order to better characterise CDs, so as to understand their optical, structural and morphological properties.

3.1 Parr Reactor

The Parr reactor was used to synthesise some of the CDs that will be discussed in this thesis. The reactor consists of a stainless steel vessel which is inserted into a heating chamber which is in turn connected to an electronic controller that enables the vessel to be heated to the required reaction temperature. Working at fairly high pressures the vessel is sealed in order to avoid gas leakage and comprises a pressure transducer which allows the pressure to be monitored during the reactive process, next to the pressure gauge there are two gas valves which are used to insert the gas for the reaction in the vessel and then must remain closed to increase the pressure inside the reaction chamber. The reaction process consists of setting a temperature ramp through which the reactor reaches the target temperature for the reaction. After that, the reactor maintains a constant temperature for a specified amount of time and finally goes back to room temperature. The synthetic processes for CDs were carried out in a Parr 4651 reactor. The synthesis conditions were optimised by adding an aqueous solution of the reagents used to prepare the CDs to the steel vessel, reaching a temperature of 190 degrees Celsius and a pressure of 14 bar, for a reaction time of 3 hours.

3.2 Spectrofluorometer

Emission and excitation spectra were obtained using the JASCO FP-6500 fluorometer. The related block diagram is shown in Figure 3.1.

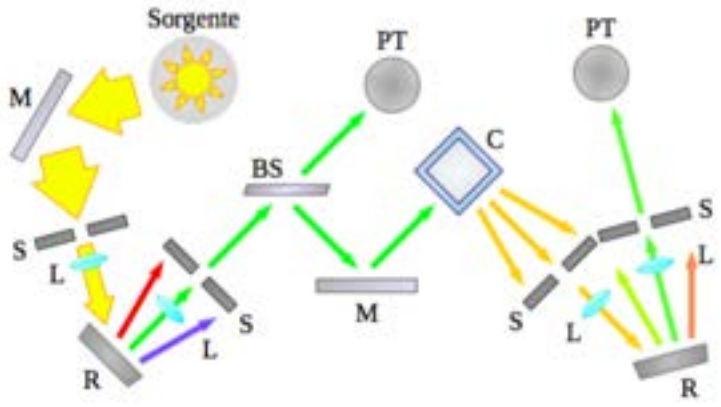

Figure 3.1: Block diagram of JASCO FP-6500 spectrofluorometer. **M**: mirror; **S**: slit; **L**: lens; **R**: grating; **BS**: beam splitter; **PT**: photomultiplier tube; **C**: sample chamber.

The light radiation is generated by a xenon lamp capable of emitting a continuous spectrum in the range of 220 - 750 nm. This is separated into its components, after the beam size has been reduced by an initial slit and collimated with a lens it is directed to a dispersion grating. The latter, controlled by a microprocessor linked to a motor, enables the excitation wavelength to be selected. This selection process is carried out by means of a second lens and slit; the latter, depending on the chosen aperture, allows the passage of radiation of a chosen λ, within a certain bandwidth. The beam is then separated on two different paths by a beam splitter; a first portion is sent to a photomultiplier tube, whose output signal is processed by the data recording software in order to eliminate random fluctuations in lamp intensity. The second part of the monochromatic radiation is directed to the sample. The sample will absorb part of the radiation and consequently emit an emission signal in an isotropic way, as discussed in Section 2.1. In order to minimise the part of the recorded radiation coming from the excitation lamp, since only the signal coming from the sample is to be analysed, the emitted fluorescence is taken by means of a slit at an angle of 90° to the excitation beam direction, again as shown in Figure 3.1. The emitted beam, after being collimated, is divided into its components by a second radiation grating; again, the angle of incidence of the radiation on it is controlled by a motor. The emission wavelength is then selected by means of a final slit, the opening of which makes it possible to decide the desired emission bandwidth. The monochromatic beam is finally recorded by a second photomultiplier tube. The instrument operates in two different modes, emission (PL) and excitation (PLE). In PL mode, the sample is excited by radiation of a fixed wavelength and its full emission spectrum is recorded. In PLE mode, the observed emission λ_{em} is selected by software and the corresponding intensity is recorded as the excitation wavelength λ_{exc} changes. It is also possible to change various parameters; in addition to the already mentioned

λ_{em} and λ_{exc}, which should be set as mentioned depending on the working mode. In particular it is possible to select the recorded wavelength range, the scanning speed (SS), the integration time (RT) and the apertures of the emission and excitation slits, linked to the respective bandwidths (BW_{em} and BW_{exc}). Finally, it is possible to choose the gain of the photomultipliers.

The recorded spectra convey information about the transitions between the energy levels of the studied sample. However, the data must be corrected before they can be analysed; the shape of the source emission spectrum influences, in particular, what is observed in a PLE spectrum. This is due to the fact that the number of photons emitted by the sample depend on how many have been absorbed and therefore, even before that, on how many have been emitted by the lamp. In addition, the PL spectra should be corrected for the instrumental response of the photomultiplier and the grating used to scatter the emission. Nonetheless for the comparison between spectra of a given sample as a function of a specific treatment, as those reported in this thesis work, there is no need for correction because relative changes are of relevance.

3.3 Spectrophotometer

The absorption spectra were recorded in aqueous solution with a Star Line ULS2048CL-EVO single-beam optical fiber spectrophotometer (Avantes, Apeldoorn, The Netherlands) equipped with dual halogen-deuterium light source) with a spectral range of 200–1200 nm.

3.4 Time resolved Spectrometer

Time-resolved fluorescence measurements were conducted using the following set-up which is divided into three parts: the excitation system, the monochromator and the detector, the block diagram is shown in Figure 3.2

Radiation is generated by an Nd:YAG solid-state laser. The active medium, a yttrium-aluminium garnet doped with Nd^{3+} ions, is pumped through a flash lamp. Thanks to Q-Switching, a system that allows the quality factor Q of the cavity containing the active medium to be varied, the laser is able to emit pulses of 5 ns duration at a variable frequency of 1 - 10 Hz; a frequency of 10 Hz was used in the experimental measurements. The laser radiation is generated in the IR, at 1064 nm, but by means of a system of non-linear crystals it is possible to vary the output wavelength: the beam is first directed towards a crystal capable of generating the second harmonic (SGH) and then towards a second crystal capable of generating the third harmonic (TGH). The radiation, which now has a wavelength of 355 nm, finally reaches a further non-linear system, the so-called OPO - Optical Parametric Oscillator. This consists of a resonant cavity con-

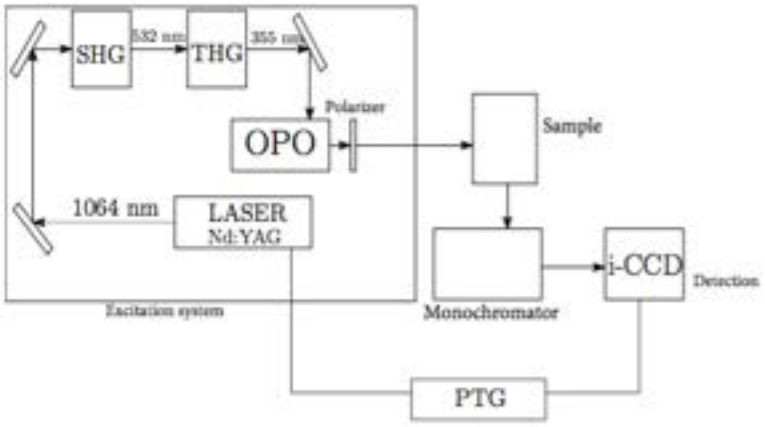

Figure 3.2: Experimental set-up used for time-resolved fluorescence measurements

taining a birefringent non-linear crystal which, when pumped by laser radiation, is able to generate tunable radiation. In particular, a beam with a chosen wavelength between 410 and 2400 nm can be generated. The parametric crystal, more precisely, is able to generate two beams, called signal and idler. Given ω_p, ω_s and ω_i as the frequencies of the pump, signal and idler beams respectively, it can be shown that the conditions to be met in order to generate the beams are as follows:

$$\begin{cases} \omega_p = \omega_s + \omega_i \\ \vec{k_p} = \vec{k_s} + \vec{k_i} \Rightarrow n_p\omega_p = n_s\omega_s + n_i\omega_i \end{cases} . \tag{3.1}$$

These are called phase matching conditions, k and n refer to the wavenumber and refractive index, respectively, of the non-linear medium at the given frequency. In order to obtain the desired wavelength radiation, the properties of birefringent crystals are exploited: in these, the refractive index n depends on the direction of polarisation of the light passing through it. Consequently, by simply rotating the crystal it is possible to satisfy the phase matching conditions, selecting the signal and idler frequencies in a continuous manner. In particular, the signal beam can have λ_s = 410-710 nm while the idler beam has λ_i = 710 - 2400 nm. Since signal and idler have perpendicular polarisation, filter can be used to choose which beam to output. When the radiation excites the sample, its emission, after passing through an adjustable aperture slit, is collected by a lens and directed onto a grating that disperses its components. Strictly speaking, three different gratings can be selected, characterised by different λ_{blaze} and lines/mm. In the course of the work, a grating with λ_{blaze} = 300 nm and 150 lines/mm was used. This has a spectral resolution of 20 nm/mm, so that by setting the slit aperture to 250 μ m during each measurement, the lambda resolution is 5 nm. The signal dispersed in its components is detected by an intensified CCD. This detector acquires images at precise delays with respect to the excitation pulse in reaction to the trigger signal sent

by the laser via the PTG - Programmable Timing Generator. Thanks to this system, it is possible to obtain the kinetics of sample emission. The use of a CCD makes it possible to obtain the entire luminescence spectrum in a single acquisition and thus record the corresponding decay traces. In addition, thanks to the intensification system, it is possible to obtain data with an excellent signal-to-noise ratio despite the fact that the number of photons emitted during a single acquisition is relatively small.

The working principle of the intensified CCD can be described as follows. The radiation from the monochromator, dispersed in its components, arrives at the detector through the input window and strikes a photocathode. This converts the photons into electrons, which are accelerated by the potential difference in the system towards the Micro Channel Plate (MCP). This is the device that intensifies the image by a cascade process; when the walls of the numerous micro-channels that make up the MCP are hit by an electron from the photocathode, they produce a quantity of electrons proportional to the potential difference at their ends. The flow of electrons from the MCP then hits a fluorescent phosphor screen, which is able to convert them all back into photons, in greater numbers than those that initially entered through the input window. At this point, the radiation is directed to the acquisition surface, a normal CCD, via a bundle of optical fibres.

The time interval during which the signal is to be acquired is regulated by the switching on and off of the potential difference between the photocathode and the MCP, which is connected as previously mentioned to the PTG. The decay trace is reconstructed by putting together the signals acquired at various delays from the excitation of the sample. Most of the operations of the acquisition system can be controlled by software. In particular, it is possible to select the delay from the trigger pulse at which to start acquiring, the time at which to end the acquisition and the width of the single interval, which then acts as a time resolution. In addition, it is possible to adjust the gain of the detector and the number of acquisitions to be accumulated on the CCD, or on the memory of the computer to which it is connected, before recording the signal; these parameters make it possible to improve the signal to noise ratio of the kinetics observed.

3.5 Raman Spectrometer

Raman spectra were acquired by a LabRam HR Evolution microRaman spectrometer (Horiba, Kyoto, Japan), under a 325 nm excitation wavelength. The laser power was reduced to avoid any sample degradation. Measurements were acquired with integration times of 5–10 s, averaging 10 spectra, and several independent measurements (typically 5) were acquired per sample in different positions to enhance the statistical significance of the sampling procedure. The Raman signal was dispersed on a grating with 600 lines/mm, calibrated by using the Raman line of a silicon substrate. In these conditions, we obtained a spectral resolution of 2 cm^{-1}. The samples were prepared by depositing a

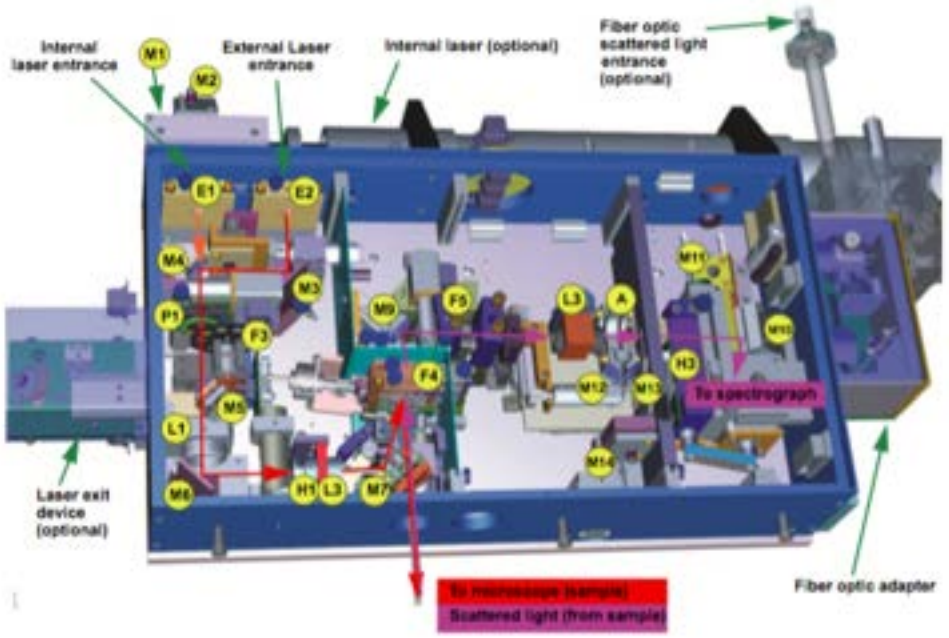

Figure 3.3: Experimental set-up used for Raman scattering measurements

drop of CDs solution on a silica or on a silicon slide.

The LabRAM HR Evolution is an integrated Raman system. The microscope is coupled confocally to a 800mm focal length spectrograph equipped with two switchable gratings shown in Figure 3.3

The system includes an internal HeNe 17 mW laser (optional) is mounted on the back of the instrument: it supplies a vertically polarized 633 nm excitation wavelength. 2 laser entrances can be used: E1 for internal laser and E2 for external lasers in our case the 325 nm laser. Using an external bench with commutation devices, it becomes possible to use many other lasers. The external laser beam is introduced to the main path via the E2 input and the removable mirrors M3 and M4. The internal laser beam is directed by the two mirrors M1 and M2 (M1 is located below the M2) in order to go through the polarizer P1 and the laser intensity absorption filter F3. This 6-filter wheel, driven by the software, is dedicated to absorb laser intensity: there are 9 different positions ND neutral filters with the optical densities 100%, 50%, 25%, 10%, 5%, 3%, 1%, 0.1% and 0.01%. Then, the L1 lens focuses the laser beam on the pinhole H1. The resulting laser image is focused by the lens L3 via the mirror M7 on the F4 notch filter with an appropriate angle in order to be completely reflected towards the sample. This filter is used to purify the plasma lines of the laser. An appropriate notch filter is necessary for every exciting line of a laser.

The pinhole H1 is conjugated with the spot on the sample and is used as a reference for alignment. It is replaced with a field lens when working in laser scanning image

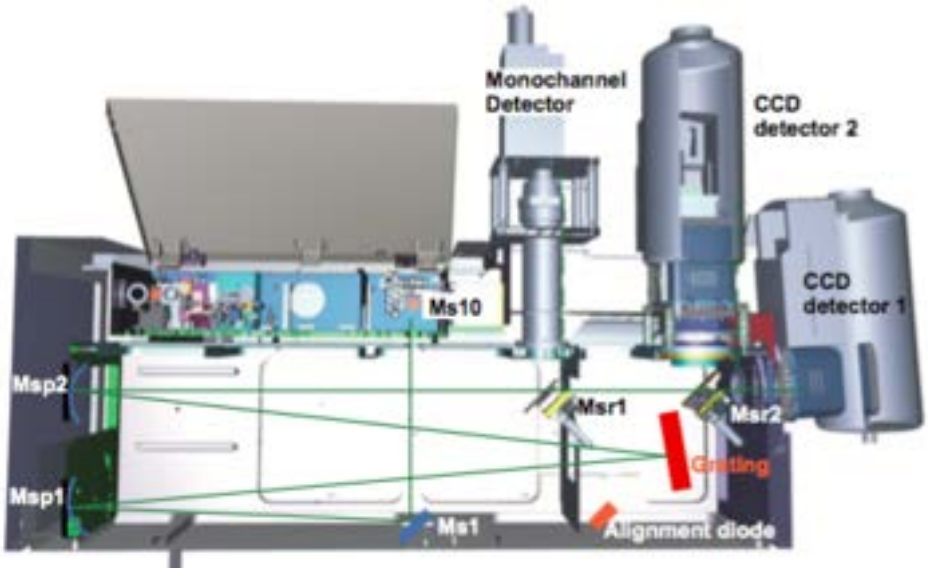

Figure 3.4: Raman Spectrograph optic path

mode. A lens L2, (not shown) put at the exit "to microscope", produces a parallel beam that is focused on the sample by the infinite-optics microscope objective. The Raman collected by the microscope objective in back scattering configuration follows the same way back. The Raman beam passes through the notch filter. L2 reforms the image of the laser spot on the sample onto a confocal hole H2. An additional polarizer filter or a second filter (for higher suppression of the exciting line) can be inserted on the F5 position.

A shutter is placed just behind the entrance slit H3 of the spectrograph, in Figure 3.4. The mirror M10 sends the Raman scattering to the spectrograph.

The LabRAM HR Evolution spectrograph is a symmetric Czerny Turner which is optimized for flat field and for minimum optical aberrations.

The diverging beam coming from the slits is reflected by the mirror M10 and then by Ms1 and becomes parallel after the spherical mirror Msp1 (800 mm focal length). The mirror Msp1 reflects the parallel beam onto the grating. The diffracted first order is collected by the spherical mirror Msp2 (800 mm focal length) and focused onto the CCD detector 1, or CCD Detector 2 or Monochannel Detector via the retractable mirrors Msr1 and Msr2.

3.6 FT-IR and ATR Spectrometer

ATR spectra were acquired on a Platinum ATR spectrometer (Bruker, Billerica, MA, USA) equipped with a single-reflection diamond crystal. Measurements were carried

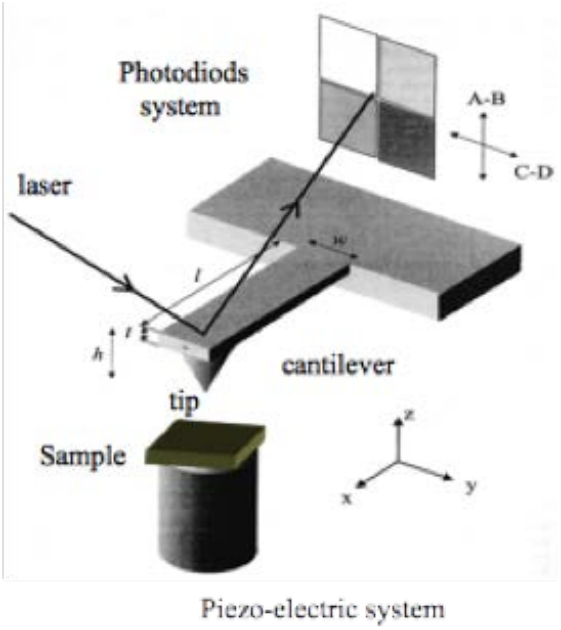

Figure 3.5: AFM schematic draft

out at room temperature by depositing a drop of concentrated CD solution in water on the sample holder of the instrument, and letting the solvent dry out before acquiring spectra in the 200–4000 cm^{-1} spectral region. Each measurement was acquired with an integration time of 5–10 s. Measurements were repeated a few times and averaged to further increase the signal-to-noise ratio. FT-IR measurements were carried out with a FT/IR 7600–JASCO spectrometer (JASCO Corporation, Tokyo, Japan) in an inert nitrogen atmosphere, depositing CDs droplets on a silica support evaporated for 2 h, before conducting the acquisition of spectra in the range 1000–4000 cm^{-1}.

3.7 Atomic Force Microscopy (AFM)

Atomic force microscopy (AFM) enables surface morphology, roughness and Z-axis dimension determination to be studied with nano-metric resolution. The type of technique focuses on the repulsive and attractive interactions that can occur between the probe and the surface of the nanomaterial being considered, the interactions depending on the distance between the probe and the surface. Figure 3.5 shows a pictorial representation of the AFM and its operating principle.

In a very simplified description a precise morphological study consists of the probe (tip) approaching the surface of the sample and beginning to flex as if it were a spring when it touches the surface, then scanning the entire surface enables to obtain a mor-

phological profile of the sample.

Atomic force microscopy (AFM) images were acquired on a sample obtained by depositing a drop of an aqueous solution of CDs on a mica substrate having sub-nanometer surface roughness. After drying in a vacuum environment for 2 h, AFM measurements were performed at room temperature in tapping mode by using FastScan Bio and FastScan A probes (Bruker) with a tip radius approximately equal to 5 nm, equipped with a closed-loop piezoscanner (maximum xy range = 34 μ m and maximum z range = 3.6 μ m) and a four-segment photodetector for cantilever deflection monitoring. The scanner was calibrated by using a 1 μ m x 1 μ m reference grid. The nominal resonant frequency and spring constant of the probe were 1400 KHz and 18 N/m, respectively. AFM images were obtained with a tip velocity of 20 μ m/s and a target amplitude of about 15 nm. The pixel resolution was fixed at about 1000 x 1000 points. Each sample was typically characterized by acquiring five images obtained in different points.

Chapter 4

Synthesis and characterization of Carbon dots

This chapter will discuss the results obtained during this thesis work, in regard to the synthesis and characterization of the CDs used in sensing applications. The results are organized into three parts.

- Synthesis and Optical characterization of CDs obtained by a Bottom up approach;
- Synthesis and Optical characterization of CDs obtained by a Top Down approach;
- Structural and morphological properties of carbon dots.

4.1 Synthesis by a bottom up approach

This section will describe the different bottom-up syntheses that have been carried out to construct fluorescent carbon nanoparticles. The syntheses carried out include solvothermal and pyrolysis.

The bottom-up syntheses were conducted using two different approaches, the first being a pyrolytic synthesis conducted in a Parr reactor. The second is a solvothermal syntheses, that was conducted by heating the reaction mixture contained in an open 250 mL reaction flask, while being agitated by a magnetic stirrer.

The bottom-up approach consists of the reaction of burning small molecules for a certain length of time [222, 244]; which ultimately enables the synthesis of CDs. In this thesis, several such syntheses were carried out using small molecular precursors. The first synthesis described is that between citric acid and urea, i.e. a tricarboxylic acid and and an amide, respectively. Notably, the use of urea as one of the precursors allows to have nitrogen doping both at the surface and in the bulk phase of the CDs. The reaction consists of solubilising 500 mg of citric acid (2.6 mM) and 500 mg of urea (8.3 mM)

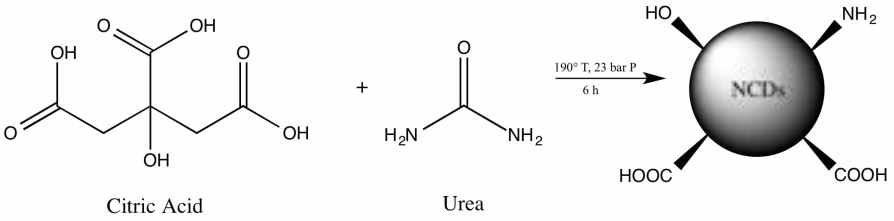

Figure 4.1: Reaction meachnism between Citric acid and urea, enabling the carbonaceous precursors to be efficiently carbonised into NCDs (see text).

in 20 mL of distilled water. The stoichiometric ratio adopted, i.e. approximately 1:3, allows for a high degree of doping given by the nitrogen from the urea. After the two compounds have solubilised well, they are transferred to a Parr reactor to begin pyrolytic decomposition shown in Figure 4.1.

The reaction is carried out at a temperature of 190°C and a pressure of 23 bars, keeping the system under these conditions for 6 hours. At the end of the reaction, a black powder is obtained, which is called NCDs, which was subsequently purified by size-exclusion chromatography using Sephadex G25 as the stationary phase. To this aim, Sephadex was first activated in water to create a gel, and then packed in a 30-cm long column with a diameter of 23 mm. Successively, the raw product of the synthesis was processed through the column using water as an eluent. This purification procedure was chosen to eliminate by-products of the pyrolysis reaction, such as small molecular impurities. The fractions were finally lyophilised and characterised by optical, structural and morphological techniques.

Another synthesis carried out in the same way, i.e. in a Parr reactor, is that between citric acid and o-phenylenediamine. The important difference with the previous one is that the molecular precursor containing nitrogen is aromatic, so during the reactive process one may expect the formation of a well-defined crystalline structure and not an amorphous one such as might be expected from the previous one. The compounds were solubilised (3 mM citric acid and 9 mM o-phenylenediamine) in 20 mL distilled water, after which they were placed in the Parr reactor, but this time at a slightly higher temperature of 200 °C to improve the pyrolytic process and reduce the presence of aromatic reaction by-products [245].

At the end of the reaction (Figure 4.2), a black powder deposited in the vessel, that was named PCDs, which is subsequently purified by size-exclusion chromatography, again using Sephadex G25 as the stationary phase.

Another route of synthesis has been tried with highly aromatic molecules such as xanthenes, which are well-known fluorescent dyes, but these syntheses are aimed at obtaining carbon nanoparticles not necessarily displaying the same optical properties of the starting precursors. In this case, we used a solvothermal route instead of a pyrolitic approach. The xanthenes considered for the solvothermal syntheses include fluorescein,

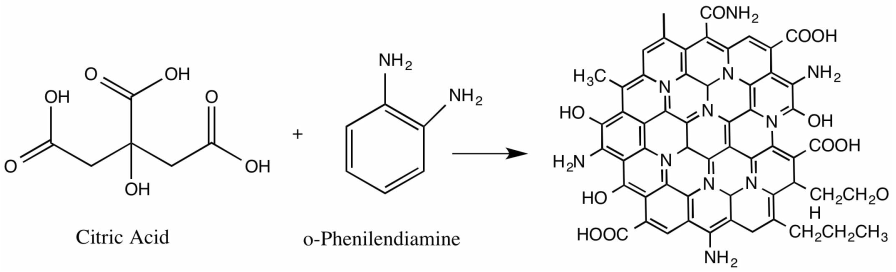

Figure 4.2: Reaction meachnism of PCDs, synthesized from Citric acid and o-phenylenediamine in the same molar ratio

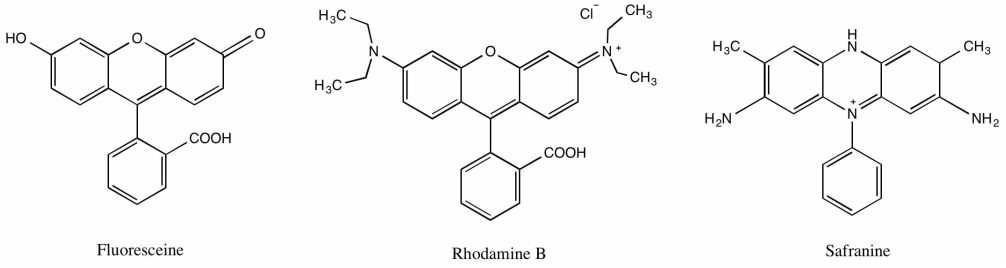

Figure 4.3: Different structures of xanthene precursors, from left to right: fluorescein, rhodamine B and safranin. All aromatic fluorescent dyes with strong fluorescent properties.

rhodamine B and safranine (figure 4.3), all three of which were reacted with the same amount of citric acid [244].

The first reaction conducted between fluorescein (2 mM) and citric acid (1 mM) in a stoichiometric ratio of 2:1 was carried out by solubilising the reagents in a solution of distilled water in a reaction flask under constant stirring. After solubilisation of the reagents, the flask was placed on a heating plate bringing the solution to the boiling point and maintaining the reaction for 3 hours. At the end of the reaction there is a black precipitate with a colloidal consistency accompanied by a strong sweetish odour (Figure 4.4).

The compound was first filtered and then purified in two steps, the first being size-exclusion chromatography again using the Sephadex G25, after which the best fraction was dialyzed for 72 h in distilled water in 0.5-1 kDa dialysis tubes to obtain FDots.

The other reaction using a xanthene as a precursor is that between rhodamine B and citric acid see in Figure 4.4, under the same stoichiometric conditions as the previous one, i.e. 2:1, the excess of rhodamine B is an attempt to have CDs with emissive properties similar to those of rhodamine and therefore to have CDs that cover a wide range of emission, possibly up to the near infrared.

The reaction also consists of mixing and solubilising the starting reagents in a 250

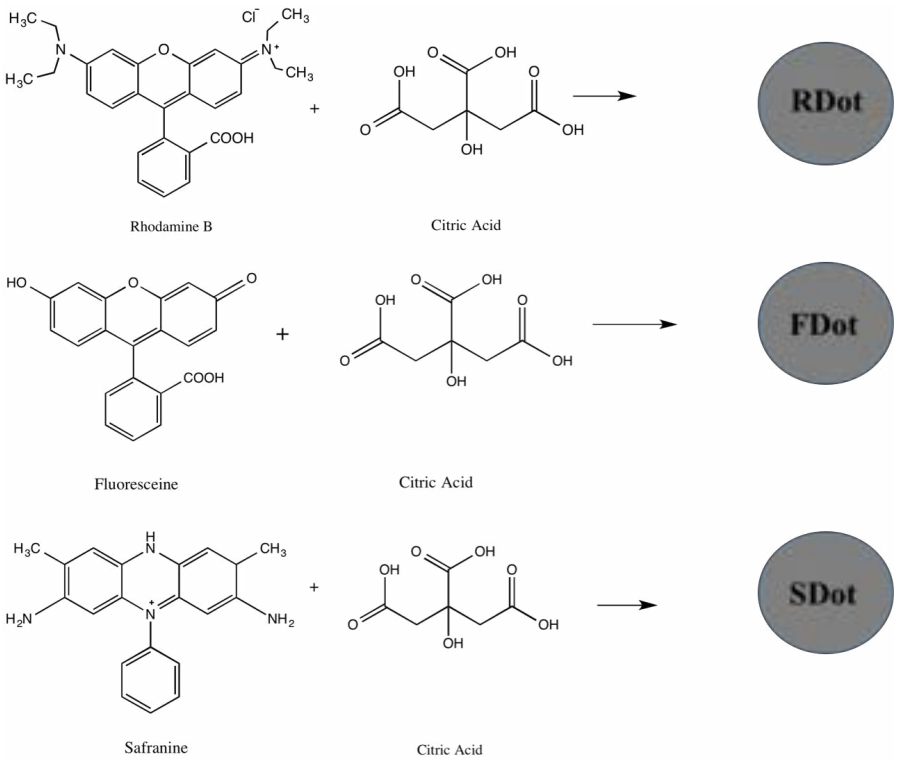

Figure 4.4: Reactive pattern of fluorescent dyes with citric acid to form RDot, FDot and SDot

mL reaction flask which is kept under constant stirring for a few minutes, after which the reaction flask is brought to a temperature of 170°C and left on a heating plate for approximately 3 hours. At the end of the reaction, a black suspension is formed, RDot, which is subsequently filtered and then centrifuged to remove unreacted parts and finally purified on a chromatographic column using size-exclusion chromatography, again using Sephadex G25 as the stationary phase. After purification, the sample is characterised optically and structurally.

Finally, the last reaction is between safranin and citric acid (Figure 4.4). In this case too, the synthesis is carried out under the same conditions as in the previous cases, i.e. by heating the substances previously solubilised in 25 mL of distilled water. As soon as the system reaches a temperature of 170°C, the reaction is left on the plate for 3 hours.

Also, in this case a black powder can be seen as a precipitate at the end of the reaction, namely SDot, which is first cleaned and filtered, after the filtration process the resulting CDs solution is purified first by size-exclusion chromatography and then in dialysis to eliminate other traces of unreacted precursors.

All resulting compounds were characterised by optical techniques such as UV-Vis absorption, fluorescence and time-resolved spectroscopy in order to assess the optical properties of the prepared CDs. In addition, the CDs were characterised structurally and morphologically by Raman spectroscopy, infrared spectroscopy (ATR; FT-IR) and atomic force microscopy (AFM). These techniques provide important information on the optical properties the surface structure and size of the nanoparticles. The absorption and emission spectra of carbon nanodots synthesised by solvothermal process are shown in figure 4.5. The NCDs and PCDs spectra (in violet and red) show fairly structured bands in the UV due to the n->π^* transitions. However, in the area around 400 nm, both spectra show a hint at a broad band, more clearly visibile in the PCDs sample, which implies a molecular component on the surface of the nanoparticle. The spectrum of PcDs (in red), on the other hand, should be analysed on its own, as it has fairly structured bands throughout the spectrum, typical of molecular components that make the spectrum structured. For this reason, even in the literature, this CDs is defined more as a polymer than a carbon nanoparticle with its own crystalline structure. The spectrum shows a prominent band in the UV at 270 nm, again due to n-> π^* transitions and a fairly strong band around 410 nm, suggesting a chromophore attached to the surface.

Emission spectra were also recorded for all samples and 440 nm was chosen as the excitation wavelength. The emission spectra show similar reported in Figure 4.5 characteristics, i.e. quite asymmetric bands, which are typical of carbon nanoparticles, but the emission maxima are slightly different, perhaps due to the fact that different chromophores are present on the surface with their emissive activity in different areas of the visible spectrum. To be precise, the emission maxima for the nanoparticles are 515 nm for NCDs and 530 nm for PCDs, respectively. Finally, the quantum yield was calculated for all samples using fluorescein as a reference. The quantum yields are 46%

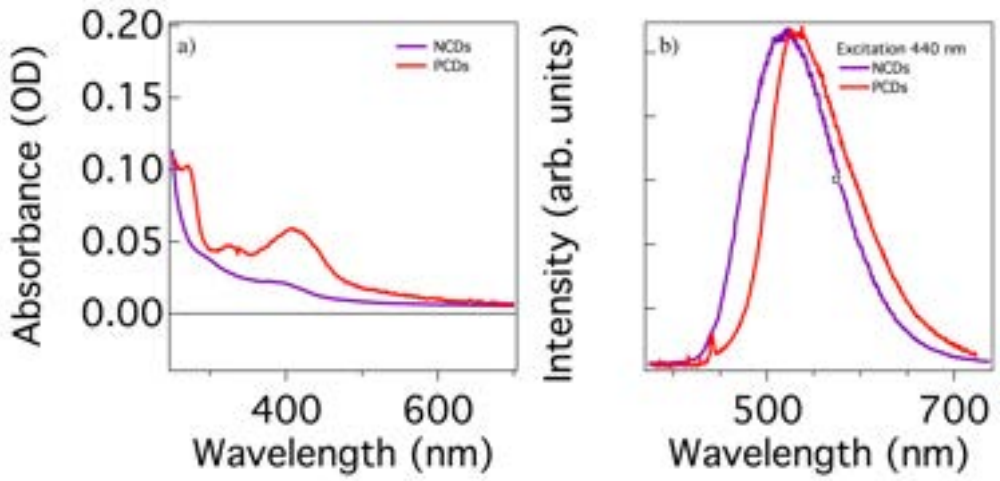

Figure 4.5: a) Absorption spectra of the samples prepared using the Parr reactor, NCDs-Parr (purple-line), PCDs (red-line) (blue-line), there are clear differences in the spectra showing different bands. b) Emission spectra recorded using an excitation wavelength of 440 nm, the bands are broad and unstructured, as typically observed for CDs.

for NCDs and 62% for PCDs, respectively. An important aspect to understand whether carbon nanaparticles have actually been synthesized is the optical study of tunability, i.e. the displacement of the emission peak as a function of the excitation wavelength [244], In this respect, we observed that, in NCDs (Figure 4.6) the peak continuously shifted from 490 to 530 nm when excitation changed from 410 nm to 510 nm, with negligible changes of shape, confirming the typical optical response of carbon dots .

The same optical characterisation was carried out on nanoparticles synthesised from xanthenes. The extended aromatic structure of xanthenes makes them a potentially interesting precursor to produce CDs with a well-defined aromatic cystalline structure. Besides, such a structure may also favour certain types of interactions with analytes for a sensing application, such as for instance pi-pi stacking to pesticides. In regard to the fluorescent response, depending on the degree of decomposition of the original dyes, in principle these dots may or may not display optical properties that are related to those of the original precursors. The optical absorption spectra of these dots are reported in figure 4.7. The SDot (in purple) has a broad band around 350 nm, that extends to visible. Interestingly, there is no absorption band of safranin around 520 nm, suggesting that the precursor is completely decomposed during the synthesis. As regards FDot and RDot, the carbon nanoparticle synthesised from fluorescein, the spectrum shows an absorption that can be defined as quasi-continuum, with a very broad band that covers the entire UV spectrum with a tail down to 380 nm. Given the absence of the optical properties of the starting material, fluorescein and rhodamine, respectively, the thermal decomposition of

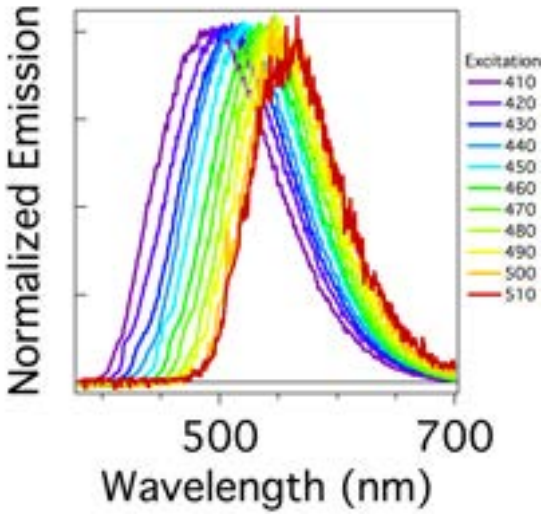

Figure 4.6: NCDs emission tunability normalized to the maximum as observed exciting the sample in the range 410–510 nm.

these products can be said to be complete.

The emission spectra were all recorded using an excitation wavelength of 350 nm, as all samples prepared from xanthenes show optical activity in the UV. The spectra in Figure 4.7 show remarkable similarities, i.e. all three samples have very broad bands typical of carbon nanoparticles, thus suggesting the absence of the initial chromophores, which do not show any optical activity in the range considered. To be more precise, it can be seen that the emission peaks are slightly different, i.e. the maximum for SDot is at 415 nm, the FDot at 420 nm slightly shifted away and finally the RDot at 430 nm. Therefore, these small spectral differences make it possible to differentiate between samples assuming the presence of quite different chromophores on the surface, despite the lack of any obvious similarity of these chomophores to the starting precursors.

To complete the optical characterisation, time-resolved spectroscopy analyses were carried out on all samples synthesised using the bottom-up method, in order to understand possible structural differences between carbon nanoparticles from their emission lifetimes.

Measurements made with time-resolved spectroscopy highlight different optical properties that are not always appreciable in steady state spectroscopy. The samples that have been characterised are all CDs from xanthenes and the two samples prepared in Parr reactor, NCDs and PCDs. The lifetimes, shown in Figure 4.8, were acquired using 440 nm as the excitation wavelength, it can be seen that the NCDs sample displayed a single-exponential kinetics with a lifetime of τ = 7.3 $\pm$ 0.2 ns. As far as PCDs are concerned, despite the fact that the steady state absorption measurement suggest

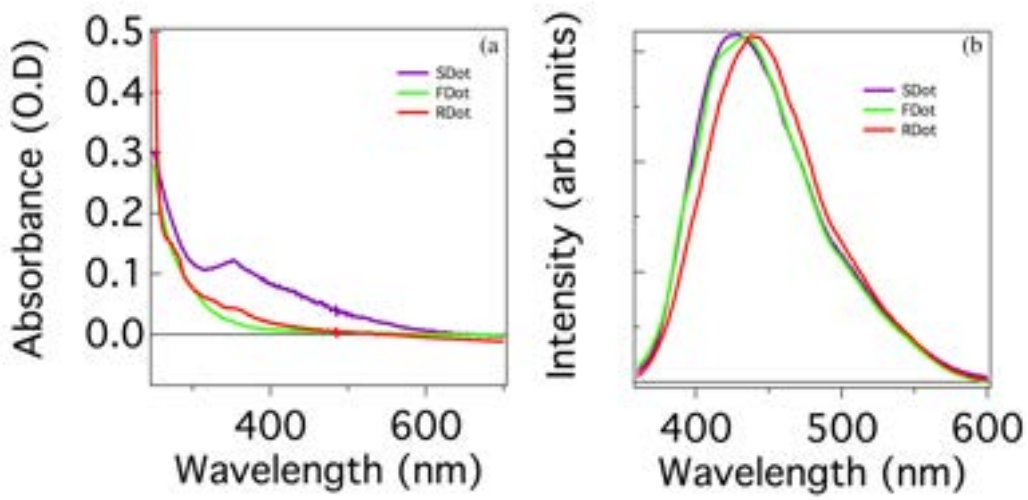

Figure 4.7: a) Absorption spectra of samples prepared using xanthenes as precursors, the spectra are very different from each other and do not have any spectral characteristics of the initial samples, SDot (purple-line), RDot (red-line) and FDot (green-line). b) Emission spectra were recorded using an excitation wavelength of 350 nm, showing broad bands with small differences of the emission peaks.

a simple and quasi-molecular behaviour, it can be seen from the time-resolved measurement that a double exponential is present, therefore applying the following equation, $I(t) = A_1 e^{(-\frac{t-t_0}{\tau_1})} + A_2 e^{(-\frac{t-t_0}{\tau_2})}$, fluorescence decay times are τ_1 =2.9 $\pm$ 0.2 ns and τ_2 =8.1 $\pm$ 0.2 ns. For samples with xanthene precursors, however, the lifetimes are quite different and also reflect the heterogeneity seen especially during absorption measurements. In this case, the samples under investigation show double-exponential decays in two cases, RDot and SDot, and a single-exponential behaviour in another case, FDot. As mentioned above the lifetimes are respectively τ_1 =1.6 $\pm$ 0.2 ns and τ_2 =5.2 $\pm$ 0.2 ns for RDot, τ_1 =3.5 $\pm$ 0.3 ns and τ_2 =9.8 $\pm$ 0.2 ns for SDot and τ =3.2 $\pm$ 0.4 ns for FDot. These measurements with very different decay times imply that the chromophores present on the surface of these nanoparticles are varied and above all different. Therefore, after a thorough optical characterisation of the CDs using different techniques, it can be stated that the CDs are all different from an optical point of view, but with similarities, i.e. they all have very pronounced emission bands and some absorption spectra show molecular-like behaviour, highlighted by well-defined absorption features emerging over the broad background, while time-resolved fluorescence measurements show the differences in the chromophores present on the CDs. After the synthesis and characterisation of bottom-up samples, a similar study will be carried out in the next section, but exclusively on the preparation and characterisation of top-down samples, so as to have a complete overview of the optical properties of this emerging nanomaterial

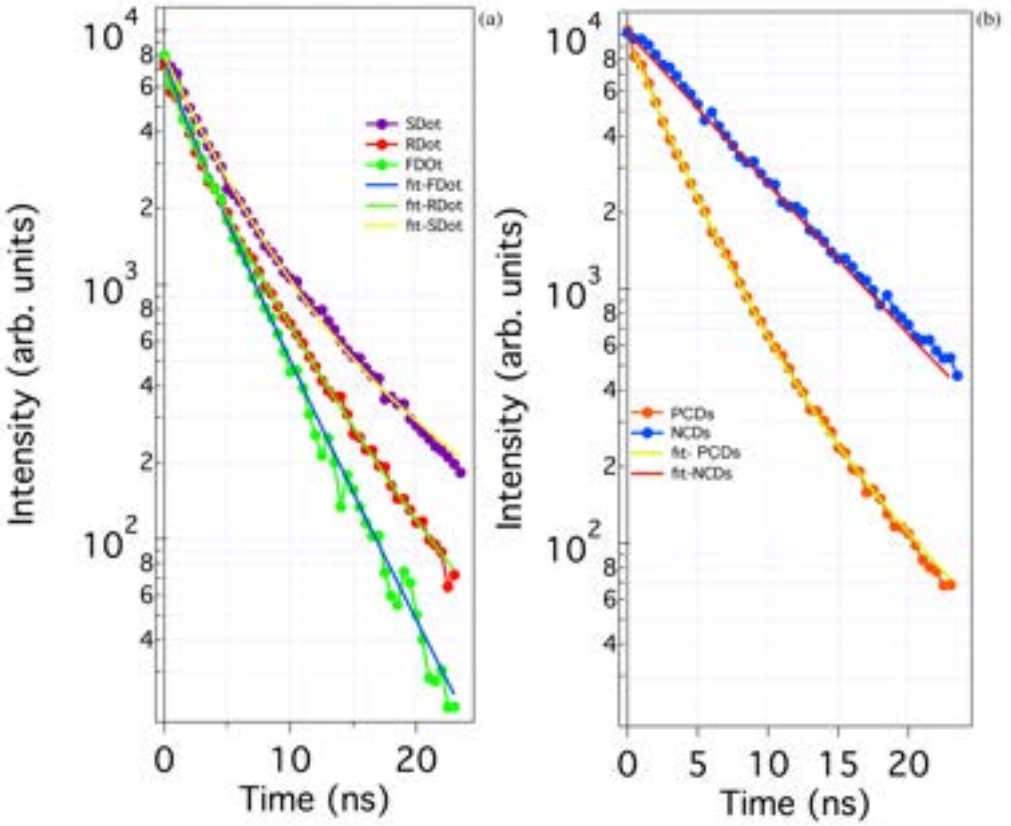

Figure 4.8: a) Fluorescence decay time analysis of solvothermal prepared samples SDot (purple), RDot (red) and FDot (green). The full lines represent the best-fit curves of experimental data using single or double exponential law, b) Fluorescence decay time analysis for reactor-prepared samples NCDs (blue) and PCDs (orange).

to create and adapt a selective chemosensor to the pollutants previously illustrated.

4.2 Synthesis by a Top down approach

The syntheses presented in this paragraph are carried out using a different approach to the previous one, i.e. a top-down approach. For this method of synthesis, extended precursors are used as the main carbon sources like graphite, graphene, carbon nanotubes and fullerene, but the synthesis carried out during this work was conducted with graphite extended precursor. This method of synthesis makes it possible to obtain a material with the structural properties of which are very similar to the precursors. The main syntheses that have been proposed in the literature are certainly chemical oxidation, laser ablation and chemical exfoliation, but in this thesis work only chemical oxidation is proposed. In addition to the chemical oxidation process of extended precursors, in this thesis work, functionalisations of the surface of the post-oxidation carbon nanodots are also carried out, in order to decorate the surface with different chemical groups that influence the optical properties and the interactions with pollutants [246]. The synthesis proposed is chemical oxidation as mentioned above, i.e. the extended precursor, in this case graphite, is added to a reaction flask (shown in Fig. 4.9) with a mixture of acids, in this case sulphuric and nitric acid in a ratio of 3:1, where the sulphuric acid has the task of splitting the C-C bonds of the carbonaceous network and the nitric acid of promoting the oxidation of the surface by creating terminations in the nanomaterial such as COOH and OH.

The synthesis of CQDs was conducted by adding 500 mg of carbon nanopowder (Sigma Aldrich-nanoparticles with a nominal average size <100 nm) to a reaction flask in a mixture of H_2SO_4 (Sigma Aldrich, 96%) and HNO_3 (Sigma Aldrich, 65%) in a 3:1 ratio (total volume 50 mL), under continuous stirring and maintaining the temperature at 140°C for 48 hours. The reaction pathway (figure 4.10) hypotized is precisely the one mentioned above, where the graphitic network is totally altered, in such a way that from an sp^2-type structure, we pass to an amorphous structure where both sp^2 and sp^3 hybridisation coexist, given the presence of functional groups on the surface.

After completing the synthesis, two aliquots of 10 mL of sample were taken and transferred to two different reaction flasks in order to functionalise the surface with small molecules. The small molecules used to functionalise the surface are in one case ethylenediamine, to increase nitrogen doping on the surface, and in the other case acetone to create highly oxygenated groups on the surface. Functionalisation, as well as increasing the heterogeneity of functional groups on the surface, also serves to increase the affinity towards certain chemical groups and compounds, which will be discussed in the following chapters.

The first functionalisation was carried out with acetone under acid catalysis, i.e. directly on CDs synthesised by chemical oxidation, a fraction of about 10 mL was taken

Figure 4.9: Top-down synthesis carried out at high temperature and reflux, mixing nitric acid and sulphuric acid with carbon nanopowder as extended precursor

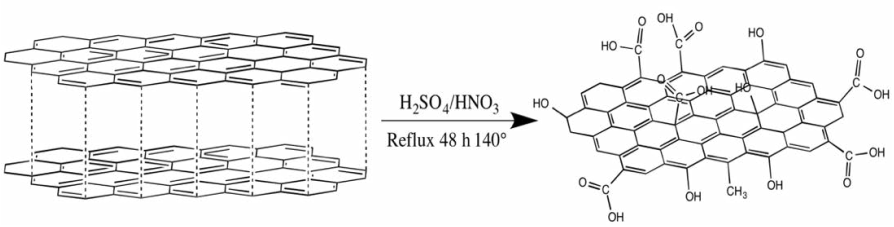

Figure 4.10: Reaction between graphite and acid mixture for the synthesis of CDs using the Top-Down method

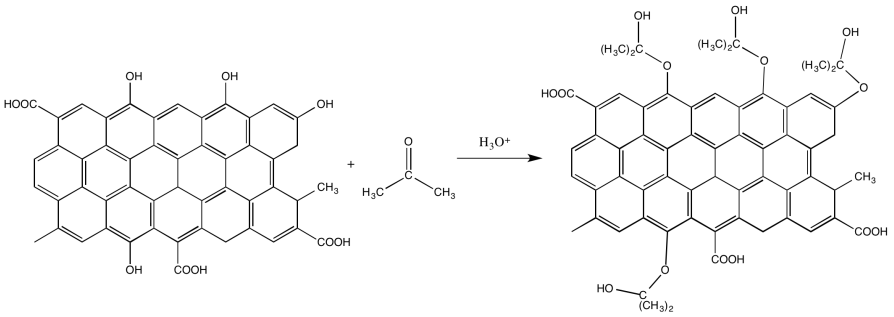

Figure 4.11: TDA, Possible reaction mechanism of surface functionalization with acetone molecules

and 10 mL of acetone was added in a still acidic environment in order to dope the surface with oxygen-rich groups, the sample obtained after this treatment was named TDA. The reaction mechanism hypothesised is that of the formation of acetals, given the possible formation of alcohol groups on the surface during acid oxidation. The reaction is also and above all favoured by the presence of the acid catalyst which favours the activation of the carbonyl group of the acetone.

As schematically shown in figure 4.11, hydroxyl groups on the surface of the CDs, in this case TDA, are replaced by acetal groups on the surface; this method of synthesis makes it possible to increase the amount of oxygen on the surface.

The second synthesis, on the other hand, made it possible to functionalise the surface of CDs with ethylenediamine, in order to dope with nitrogen and create new functional groups on the surface of CDs. The reason for choosing this molecule lies in its nucleophilic properties, especially in its interaction with carbonyl and carboxyl groups present on the dot. After bringing the native CDs solution to a pH of around 6, excess ethylenediamine was added. The reaction was then conducted at reflux under constant magnetic stirring for approximately 2 h. At the end of the reaction the solution changed from brownish to yellow and this is a first indication that the functionalisation was successful.The reaction pathway shown in figure 4.12 is assumed with an initial protonation of the OH group present in the acid after wich the amine acts as a nucleophile with the

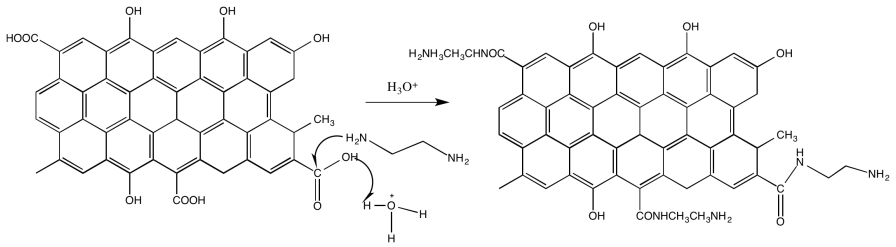

Figure 4.12: TDN, Possible reaction mechanism of surface functionalization with ethylenediamine molecules to increase nitrogen doping on the surface

final expulsion of a water molecule. Finally, all the compounds were purified in dialysis tubes with a cutoff of 0.5-1KD, and the best fractions were selected and optically characterised.

The optical characterisation of these materials was carried out under the same conditions as the bottom-up material, i.e. UV-Vis spectroscopy, fluorescence spectroscopy and time-resolved spectroscopy were used in order to understand the optical properties of these samples and distinguish them from previously synthesised bottom-up samples.

The normalized optical absorption spectra of TD, TDA and TDN samples are reported in Figure 4.13a, all spectra appear broad and structureless over the entire wavelength range suggesting a near continuum of absorption transitions and also a very similar carbon core of the nanoparticles. Small changes are present in the wavelength region around 300 nm, where the TDA features a small shoulder possibly due to n-π^* transitions associated to the surface changes that occurred with functionalization. Emission spectra recorded with excitation at 440 nm of TD, TDA and TDN samples feature a very broad band with a maximum emission efficiency in the green at about 524 nm as reported in Figure 4.13 b. The quantum yield (QY) of the samples at the excitation wavelength of 440 nm was estimated, taking fluorescein as a reference. The respective QYs is 6.1% for TD, 9.2% for TDA and 8.7% for TDN. Such relatively low QY values are known in the literature for carbon dots synthesised via Top-Down procedures.

Finally, the tunability of the samples prepared with the top-down approach was also studied in this case and as an example TD and TDA emissions are reported in figure 4.14. The fluorescence of TD and TDA is highly dependent on excitation energy, which is a typical feature observed in the photoluminescence of carbon nanodots. As shown in Figure 4.14a,b both samples show an identical trend; under excitation in a wide range of wavelengths, 410-620 nm, a significant emission shift ranging from cyan (480 nm) to red (650 nm) is found, thus maintaining a wide tunability. This is another evidence that functionalization does not significantly alter the emission properties of the studied CDs

While the steady state optical spectra do not give much information about the surface change due to functionalization, analysis using time-resolved spectroscopy allows us to highlight a quite appreciable difference in lifetimes. Typical PL time decay mea-

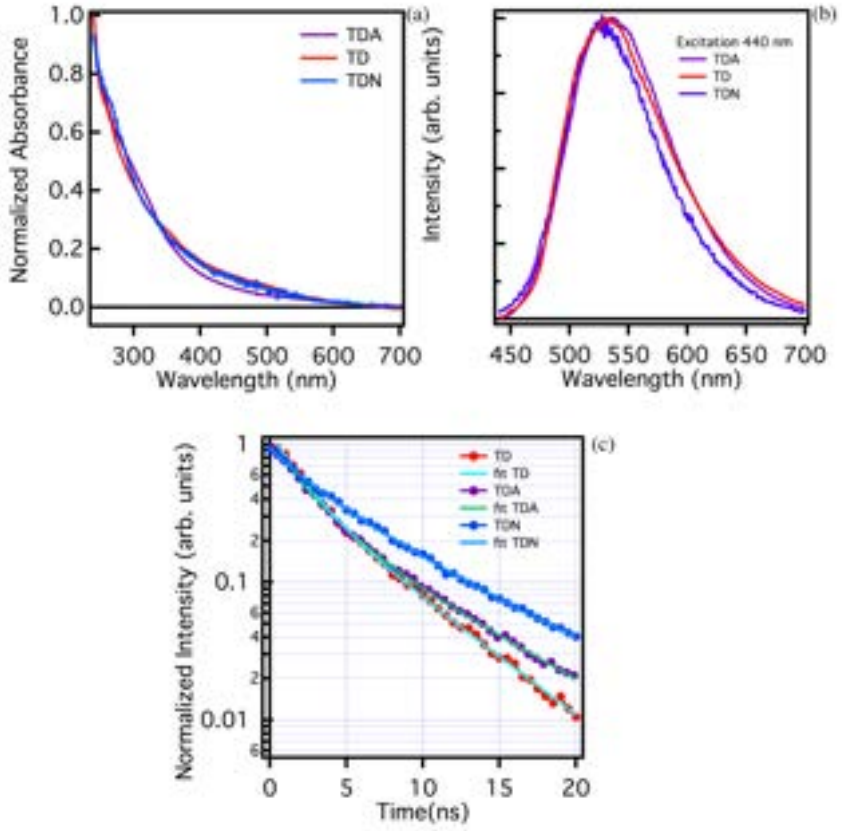

Figure 4.13: a) Absorption Spectra of TDA (purple line), TD (red line) and TDN (blu line) b) Emission spectra normalized to the maximum excited at the same wavelength of 440 nm. (c) Photoluminescence time decay at wavelength 520 nm, as collected by time-resolved fluorescence measurements on TDA (purple line), TD (red line) and TDN (blu line), excited at a wavelength of 440 nm

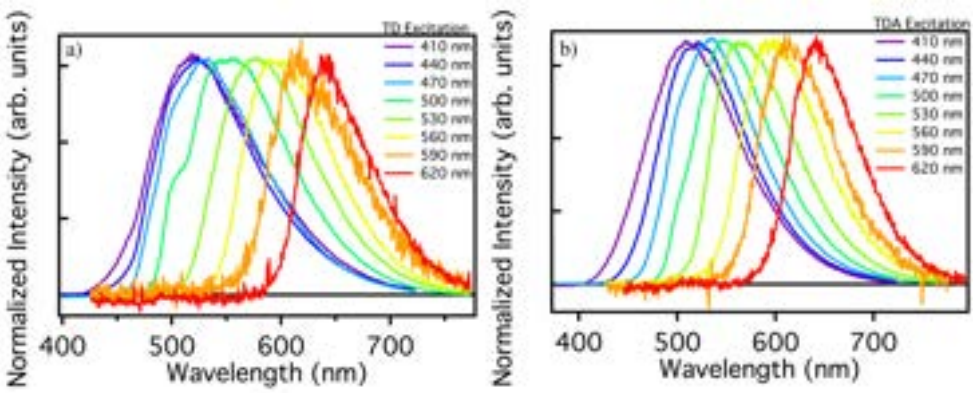

Figure 4.14: a) TD emission tunability normalized to the maximum as observed exciting the sample in the range 410-620 nm. (b) TDA emission tunability normalized to the maximum exciting the sample in the range 410-620 nm.

surements recorded at 520 nm are reported in fig. 4.13 c under pulsed excitation at 440 nm. A non-single-exponential decay is found for all samples. Although at the beginning of the decay the curves are very similar, it is possible to appreciate that the TD has then a faster decay than TDA, which becomes apparent at longer time delays. Analysing the decay curves with a double exponential fit $I(t) = A_1 e^{(-\frac{t-t_0}{\tau_1})} + A_2 e^{(-\frac{t-t_0}{\tau_2})}$ we found the lifetimes for TD, TDA and TDN. In particular, the final decay times are τ_1 =2.3 $\pm$ 0.2 ns and τ_2 =6.9 $\pm$ 0.2 ns for TDA, τ_1 =1.8 $\pm$ 0.2 ns and τ_2 =5.2 $\pm$ 0.4 ns for TD and τ_1 =1.9 $\pm$ 0.5 ns and τ_2 =6.4 $\pm$ 0.7 ns for TDN. The samples have a very similar initial decay rate and the first lifetime τ_1 is almost consistent within experimental uncertainty. However, we find that the second lifetime, τ_2 is appreciably shorter in TD. Evidently the chemical groups present on the surface after functionalization tend to reduce the effect of non-radiative relaxation in TDA and TDN samples, making their decay slower than TD. As far as the optical characterization of the three samples TD, TDA and TDN is concerned, it can be stated that their optical properties are very similar, i.e. all samples show very broad absorption spectra with an almost continuous structure, with some differences in the low wavelength region (300 nm). The emissive properties are also very similar, maintaining tunability over a large excitation range. This is a clear sign of a large structural disorder typical of fluorescent nanocarbons. A more appreciable change, possibly due to surface passivation, is found for the lifetime, which is slightly longer in TDA and TDN than in TD, which could mean that the functionalization process tends to switch off some radiative channels on the surface, creating new ones. Overall, passivation of the surface creates small changes in the optical properties, which can be appreciated in the absorption spectra and in the slight change in lifetime, so passivation creates small structural differences on the surface, without disrupting the emissive properties of the TDs.

4.3 Structure and Morphology

Structural and morphological measurements were carried out on CDs, so this section will consider both bottom-up and top-down synthesised nanoparticles. In-depth characterisation is motivated by the need to identify the presence of chemical groups on the surface of the carbon dots, so both FT-IR and ATR spectroscopy were used, which allowed us to compare and study the surfaces of the carbon dots and precisely identify the functional groups that cover them. In order to understand the structural properties, Raman spectroscopy was used to identify the structural difference of CDs, especially in terms of hybridisation, providing important information on the crystalline phase. In addition, atomic force microscopy (AFM) has enabled the size of carbon nanoparticles to be identified by means of intermittent contact measurements [216, 244, 246]. One of the main goals of our characterization is to carry out a side-to-side comparison between CDs synthesized through bottom-up (BU) and top-down (TD) methods. Typically, a dense surface functionalization of BU-NCDs automatically builds up during the synthesis, and their optical response is often very good without the need for further treatments.

The resulting data highlight both similarities and differences between BU and TD nanodots. Figure 4.15 a,b show the AFM images obtained from two representative samples, obtained by the two methods, after SEC or dialysis. While both images clearly show the presence of nanoparticles confirming the efficient production of CDs through both synthesis routes, their size distributions, plotted in Figure 4.15 c,d, are quite different. It can be seen that the BU nanoparticles featured an average size of about 2 nm, whereas the top-down nanoparticles showed a much larger average size, about 5 nm. The difference is justified by the different synthetic approaches. Indeed, BU synthesis proceeds through the carbonization of sub-nanometric molecular precursors, from which the reactive and growth processes only allow for the formation of relatively small carbon nanodots. In contrast, top-down synthesis begins from much larger precursors, in this case <100 nm graphite carbon nanoparticles, which are broken up into CDs by the reactive process, but only up to a certain extent. Both size distributions are quite broad, confirming a high structural inhomogeneity typical of most CDs, a property which seems to be independent of the synthesis route.

In Figure 4.16e, we report the Raman spectra of two representative samples, providing information about the core structure of the nanoparticles. The NCDs nanoparticles show the characteristic G band at 1598 $\pm$ 2 cm^{-1} and D band at 1356 $\pm$ 2 cm^{-1}, well-known as the typical Raman signals of carbonaceous nanomaterials, which thus confirmed the successful carbonization of the reactants into a well-defined nanoparticle. The intensity ratio I_D/I_G calculated to be 0.53, is consistent with a nanomaterial with a highly defective graphitic carbon core. This was confirmed by the displacement of the G and D bands from their usual positions for a carbon nanostructure with perfect sp^2 hybridization, that were at 1566 and 1364 cm^{-1}. Therefore, our nanoparticles displayed a carbon core with mixed sp^2 and sp^3 hybridization. The Raman spectrum of

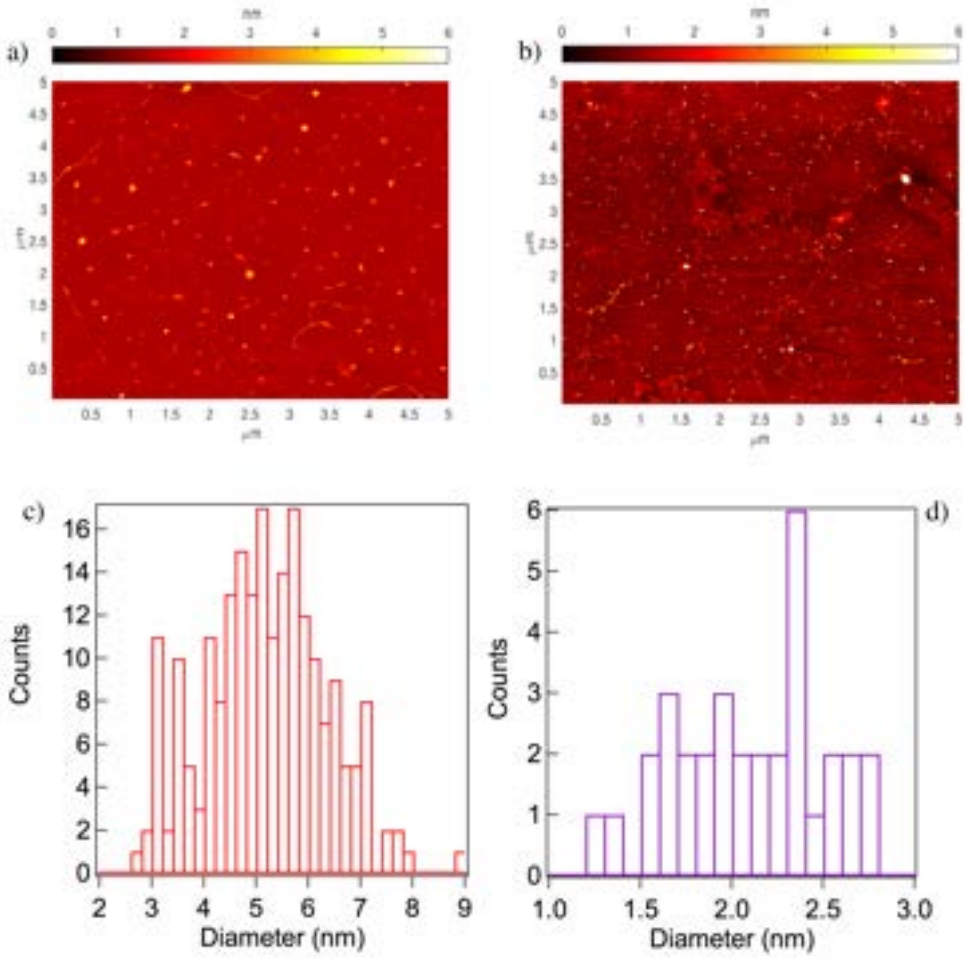

Figure 4.15: AFM images of representative (a) NCDs and (b) TD samples. Particle diameter distribution for the (c) NCDs and (d) TD samples.

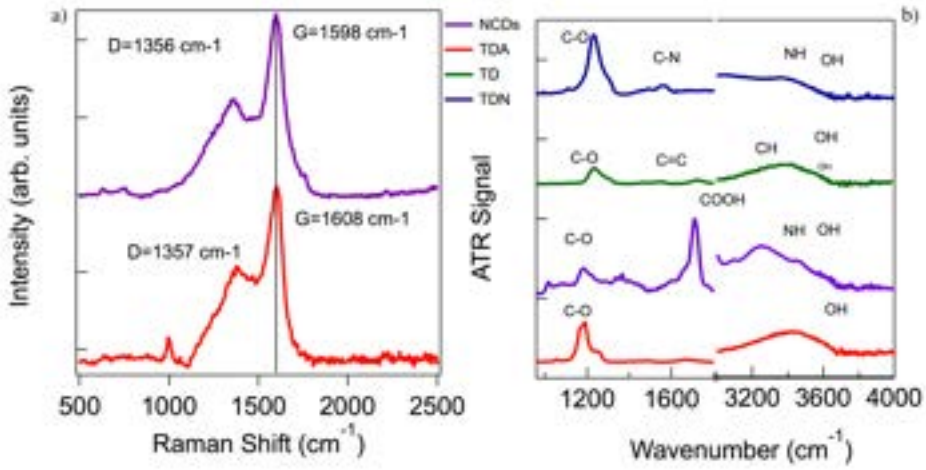

Figure 4.16: (a) Normalized Raman spectra of NCDs (purple line) and TDA (red line) samples and (b) normalized ATR spectra of NCDs (purple line), TD (green line), TDA (red line), and TDN (blue line) samples. In the latter two panels the spectra were arbitrarily vertically shifted for clarity.

the top-down CDs also contains the G and D bands, although their positions changed slightly with respect to NCDs (we found 1608 and 1357 cm^{-1}). Again, these shifts imply the presence of a nanocrystalline structure based on graphite, but with an amorphous component, possibly caused by the surface defects and surface passivation, which both contribute to a partial loss of the graphitic component. Notably, the TDA also showed a noticeable Raman band around 1000 cm^{-1}, probably related to the surface functionalization of these dots upon acetone addition. Furthermore, the I_D/I_G ratio, 0.55 in TDA, was very close to the NCDs. Therefore, apart from the size difference, the top-down and bottom-up cores were very similar. The nanodots were further analyzed by ATR spectroscopy, which made it possible to determine the functional surface groups present on the different CDs. ATR measurements were conducted on all the samples obtained by a top-down method, in order to assess the surface changes induced by functionalization with acetone and ethylenediamine, and repeated on one bottom-up sample only, that is NCD, for comparison purposes. As evidenced by Figure 4.16f, the sample that presented the most complex surface structure was the NCDs, based on the high number of different signals which can be discerned in the ATR spectrum. In particular, NCDs displayed broad bands at about 3500 and 3200 cm^{-1} that can be attributed to OH and NH stretching vibrations, respectively, a small band at 2990 cm^{-1} due to CH stretching, a very strong C=O stretching signal located at 1718 cm^{-1}, a C–N stretching vibration around 1400 cm^{-1}, a small signal around 1197 cm^{-1}, which can be attributed to C–O–C stretching, and several minor peaks of uncertain attribution. The C=O stretching signal most likely contains contributions from both amide carbonyl ($CONH_2$), already present in urea, and carboxylic acid (COOH), left as a residue of citric acid. The ATR spectra of the top-down CDs appeared much simpler than the NCDs, even after functionalization. The most prominent signals were found in the 1100–1200 cm^{-1} region, which can be attributed to C–O stretching vibrations. In particular, all the samples showed a prominent peak at 1120 $\pm$ 10 cm^{-1} due to C–OH surface groups vibrations. Only in the TDA did we detect an additional peak at 1193 cm^{-1}, which can be attributed to C–O–C stretching vibrations. Thus, the functionalization with acetone led to the formation of plentiful C–O–C bonds on the surface. Besides the C–O vibrations, all three TD nanoparticles also showed the broad band at about 3450 cm^{-1}, mostly due to OH stretching, and only the TDN showed significantly increased absorption in the region of N–H vibrations around 3200 cm^{-1}, confirming its successful functionalization with amine (likely NH_2) surface groups. Interestingly, no C=O stretching vibrations were visible in the infrared spectra of the TD samples.

Summarizing these results, both the bottom-up and top-down protocols lead to the successful production of CDs, defined as nanoparticles with a few nanometers diameter, a clear defective graphitic core, and a functionalized surface rich of oxygen. In this sense, the two types of CDs are very similar to each other. However, some key differences were highlighted as well in our study: the bottom-up NCDs are substantially

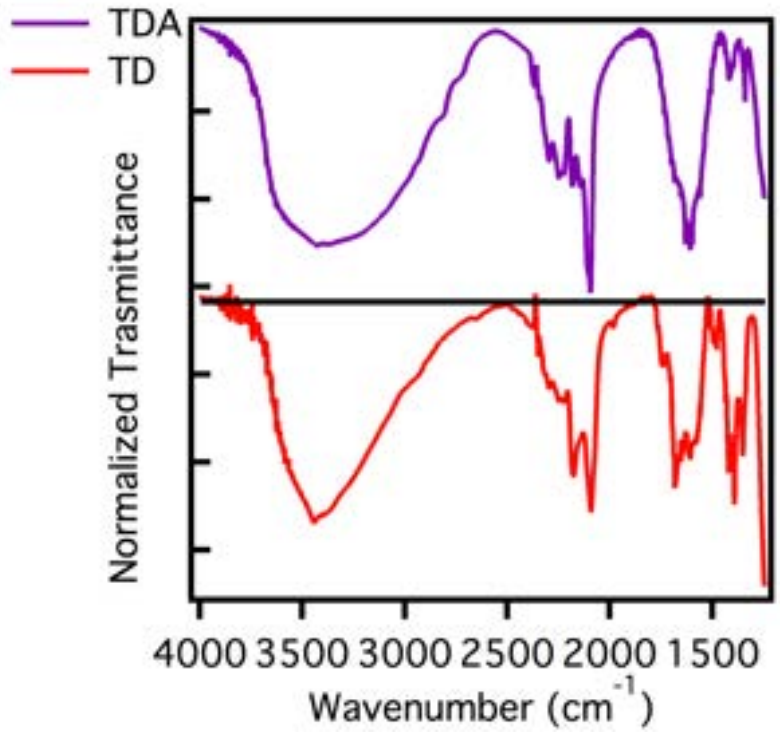

Figure 4.17: FT-IR spectra of TD (red line) and TDA (purple line) samples

smaller and display a complex and highly polyfunctional surface dominated by C=O moieties; in contrast, the TD samples are larger in size and display a much simpler surface structure. The main surface groups introduced by functionalization are C–O–C and NH_2 for TDA and TDN, respectively.

In order to gain a deeper understanding of the structural differences of the samples prepared by the Top-Down method, a comparison was made between two samples, TD and TDA. The characterisation process was therefore deepened using FT-IR spectroscopy to provide further information on the surface groups present on the carbon nanoparticle, which ATR spectroscopy had failed to capture. FT-IR spectra of TD and TDA samples are presented in figure 4.17. As can be seen, the two samples being prepared and purified under the same conditions show very similar characteristic signals.

As already reported (4.16) by ATR measurements in particular, there are very intense peaks around 1100 cm^{-1} for TD, which represent C-O stretching, especially in the presence of hydroxyls. As regards the TDA, again around 1100 cm^{-1}, the C-O signal is very intense, but the presence of a shoulder suggests the presence of the C-O-C bond, thus confirming the good functionalisation of the surface. FT-IR measurements reported in Figure 4.17, acquired in the spectral range 4000-1250 cm^{-1}, show a variety of signals due to different surface groups, with a few differences in the two samples. In both sam-

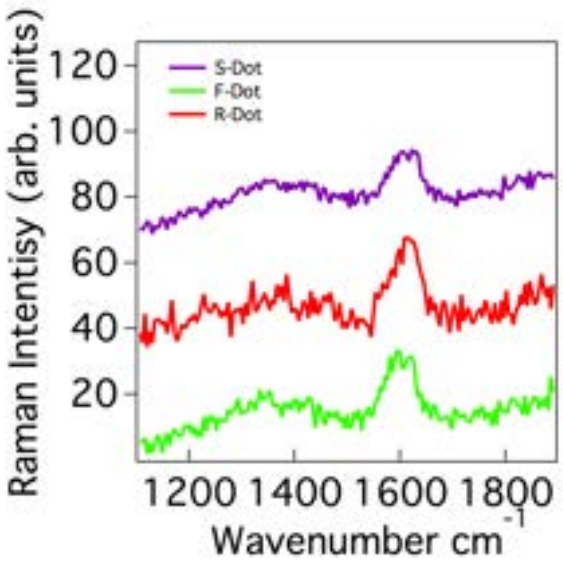

Figure 4.18: Normalized Raman spectra of SDot (purple line), RDot (red line) and FDot (green line)samples. Raman spectra have been arbitrarily vertically shifted for clarity.

ples a broad band around 3400 cm^{-1} is observed, it can be related to -OH stretching. It is worth to note that the shape of the band for TD and TDA is slightly different, thus suggesting the effect of surface interactions which can be related to functionalization. Both samples have bands peaking around 1600 cm^{-1}, more precisely located at 1656 cm^{-1} for TD and 1602 cm^{-1} for TDA, which are attributable to vibrational motions of the C=C bond. The spectra evidence a difference between TD and TDA in the peaks in the range 1440-1350 $cm\text{-}^{-1}$, which can be attributed to CH_2 bending. In fact, it is clear that the TD displays more pronounced peaks, unlike the TDA, which has almost no signals in this region. The near disappearance of CH_2 from the TDA can also be attributed to surface functionalization.

Finally, in regard to the xanthene samples prepared by the solvothermal route, their structural characterization is still incomplete. So far, the characterization was carried out by Raman spectroscopy. From a spectral point of view, Figure 4.18 does not allow the structures to be discriminated exactly, but although the signal is not very evident, clear the D and G band can be observed suggesting that all three samples show structures that tend to be amorphous, so there is a mixture of sp^2 and sp^3 hybridisation.

After a robust characterisation of the different types of CDs, sensing data with heavy metals and pesticides are presented in the next chapter, using fluorescence as an analytical technique to spectrally assess the interaction process between CDs and pollutants.

Chapter 5

Sensing test

In this chapter, the focus of this doctoral thesis, the sensing of certain pollutants in food, will be explored in detail. The measurements were carried out by carefully selecting different CDs with surface properties that could be exploited for the pollutants detection.The chapter will be divided into two sections, the first one considers the interaction between different CDs and heavy metals, observing by optical techniques the interaction process. The second section deals with the interaction between CDs and pesticides, again using fluorescence as a probe.

5.1 CDs: sensing with heavy metals

Heavy metals, as mentioned in the introduction, are important pollutants in food, often introduced due to human activities. This is why it is important to try to determine them precisely in order to safeguard consumer health. The metals taken into consideration during this thesis work include mercury, cadmium, cobalt and nickel, as well as other metals of environmental interest that merit some further investigation. The first to be analysed is mercury, which was made to interact with all types of CDs, i.e. NCDs for bottom up and TDs which proved to be excellent detectors for this metal.

5.1.1 Mercury Sensing

These sensing tests were performed on bottom-up NCDs and on the three types of top-down carbon dots (TD, TDA, TDN) samples by studying the changes of the fluorescence observed in the presence of increasing amounts of mercury (Hg^{2+}). Because the electrochemical potential for the reduction of mercury is very low (0.85 V vs. standard hydrogen electrode), one expects mercury to easily quench the CDs fluorescence by an electron transfer from the emissive chromophores of CDs to Hg ions, provided that the ion finds suitable interaction sites at CD surfaces. Thus, because the redox potential

should not be the limiting factor of fluorescence quenching, Hg^{2+}-induced quenching provides a convenient probe of the different interaction sites on the various types of CDs and their interplay with the emissive chromophores. As shown in Figure 5.1 , we found that samples NCDs and TDA both displayed a significant response to Hg^{2+}, with a decrease of the emission intensity clearly measurable upon the addition of even a few μM Hg^{2+} ions.

In contrast, we found that neither the non-functionalized TD sample, nor the amine-functionalized TDN sample were quenched by mercury ions within the experimental errors. Exciting the TDA sample at 440 nm and increasing the concentration of mercury (Figure 5.1), the sample presented a quenching already at the lowest tested concentration (1 μM). Successive additions led to a further reduction in the emission intensity, which leveled to about 60% of the initial value after the addition of 40 μ M ions. Here, quenching occurred with no significant changes of the emission band-shape [244]. The behavior of NCD, shown in Figure 5.1b, was very different. On the one hand, the extent of quenching was markedly higher, and the intensity of the emission decreased to about 40% after the addition of 40 μM mercury ions. Besides, in addition to the quenching, the fluorescence underwent a red shift, whereby the spectral maximum of the band moved from 522 nm to 534 nm when increasing the Hg^{2+} concentration. This change of shape is clearly most advantageous for sensing applications because it provides the emission peak position as an additional observable to monitor Hg^{2+}, along with fluorescence intensity. Stern–Volmer plots of the fluorescence data (Figure 5.1c) confirmed that the bottom- up and top-down samples responded differently to mercury ions. In TDA, after a very marked initial quenching already at low concentrations, the Stern–Volmer curve quickly reached a plateau. This suggests the complete saturation of a specific functional group on which mercury selectively, and very effectively, binds at the CD surface. The Stern–Volmer plot of the NCDs sample was very different and displayed two distinct trends with different slopes, one at low concentrations (from 0.5 to 5 μM) and one at higher concentrations (>5 μ M), the latter accounting for the majority of quenching. This suggests at least two different functional groups on the surface of the dot that may coordinate covalently with mercury, whereby interaction with the second group (at higher concentration) becomes appreciable only after saturation of the first. Generally speaking, the much stronger quenching exhibited by NCD is consistent with the highly functionalized surface, which certainly hosts abundant binding sites for Hg^{2+}. Besides, a certain heterogeneity of binding sites at the surface of NCD is to be expected considering the highly polyfunctional nature of their surfaces and may also explain the progressive red shift of the fluorescence (Figure 5.1b), if one assumes that the addition of Hg^{2+} selectively "turns off" a subset of the possible emission chromophores and progressively emphasizes the radiative channels responsible for a red-shifted emission. The strongest contribution to NCDs fluorescence quenching ($[Hg^{2+}] > 5$ μM) is most likely associated with the interaction of mercury ions and C=O groups, very abun-

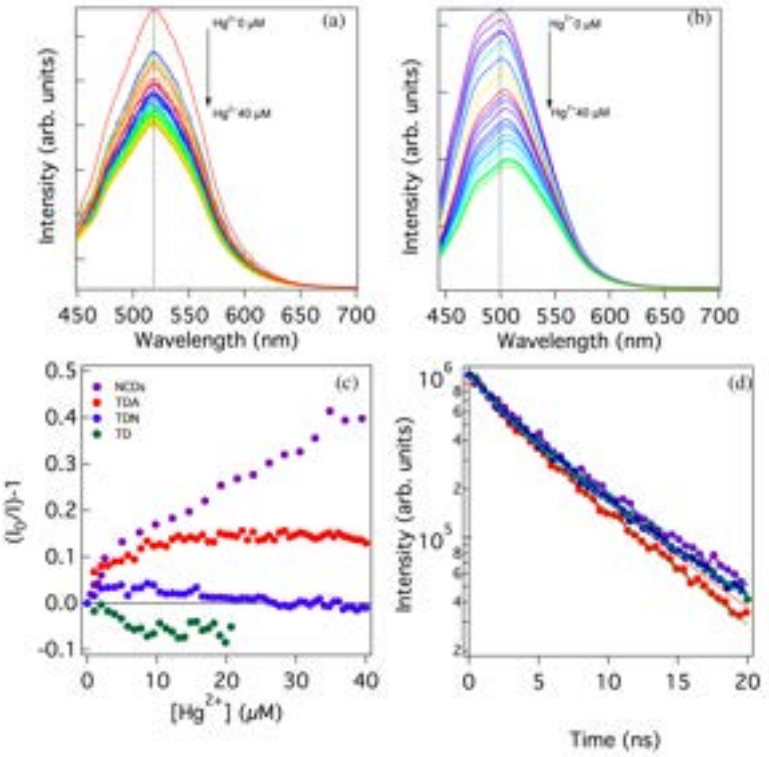

Figure 5.1: Emission spectra under excitation at 440 nm of the (a) TDA and (b) NCD samples in aqueous solution in the presence of increasing concentrations of Hg^{2+} ranging from 0 to 40 μM. (c) Stern–Volmer quenching plots of the integrated emission under excitation at 440 nm of NCD, TDA, TD, and TDN samples at different concentrations of Hg^{2+}; I_0 and I represent the emission intensity at zero and non-zero concentrations of Hg^{2+}, respectively. (d) Excited-state decay kinetics of the emission at the wavelength 520 nm under excitation wavelength of 440 nm of NCD, TDA, TD, and TDN samples in the presence of the same concentration of 40 μM mercury.

dant on the surface and closely involved in the emission mechanism of these dots. The initial smaller variation seen in the Stern–Volmer plot, observed at low concentrations, must be attributed to another surface moiety, being much less abundant than C=O, but strongly interacting with mercury ions. Besides C=O groups, NCDs samples also host a certain concentration of superficial C–O–C groups. Therefore, by analogy with TDA samples, we propose that the earliest trend observed in the Stern–Volmer plot of NCDs samples is associated with the interaction of Hg^{2+} with C–O–C sites.

Finally, the lifetime of the CDs taken into consideration was measured after the addition of a concentration 40 μM of mercury ions and no relevant change has been detected (see Figure 5.1 d). In general, lifetime analysis is a useful tool to discriminate static from dynamic quenching. Indeed, considering the very low concentration of Hg^{2+} ions at play, one suspects that the quenching mechanism here cannot be diffusional, but must be essentially static; that is, quenching occurs through the formation of a stable coordination compound of mercury with surface functional groups on CDs. From a practical point of view, these data demonstrate the need of oxygen-rich groups such as C=O and C–O–C, suggested here as the active binding sites on the surface of CDs, in order to get a significant response to quencher ions. Even after deliberate functionalization, which is crucial to activate a quenching response in TD samples, the abundance of binding sites on the latter remains relatively low as compared to NCDs, which are inherently very rich of C=O groups right after synthesis. For these reasons, NCDs samples behave much better as sensors, with the additional benefit of a progressive change of shape of the emission band with increasing Hg^{2+} ions, which can be seen as a side effect of their highly complex surface. On the other hand, the lack of sensitivity of TD and TDN surfaces might make them more appropriate for different applications, whenever ease of quenching is an undesired feature.

5.1.2 Cadmium Sensing

Another important pollutant in the food chain, as mentioned above, is cadmium, so it was studied with two different CDs, one of a bottom-up nature, NCDs, and one of a top-down nature, TDA, to understand the degree of interaction between this analyte and the different surface areas of the two CDs. The first sample examined was TDA, i.e. the acetone-functionalised sample, and the interaction process with an aqueous cadmium solution was studied. The analysis process consists of gradually increasing the concentration of cadmium in the range 0-75 μM, while keeping the concentration of TDA constant, which is 5 ppm. The analysis is aimed at assessing by fluorescence the type of interaction, i.e. whether fluorescence quenching is present as in the case of mercury. The TDA sample is excited at a wavelength of 440 nm and, as can be seen in figure 5.2, the interaction process indeed takes place. Fluorescence quenching occurs in two very different concentration ranges, the first ranging from 0-30 μM up to a plateau.

However, after small fluctuations, an additional, and very significant variation in

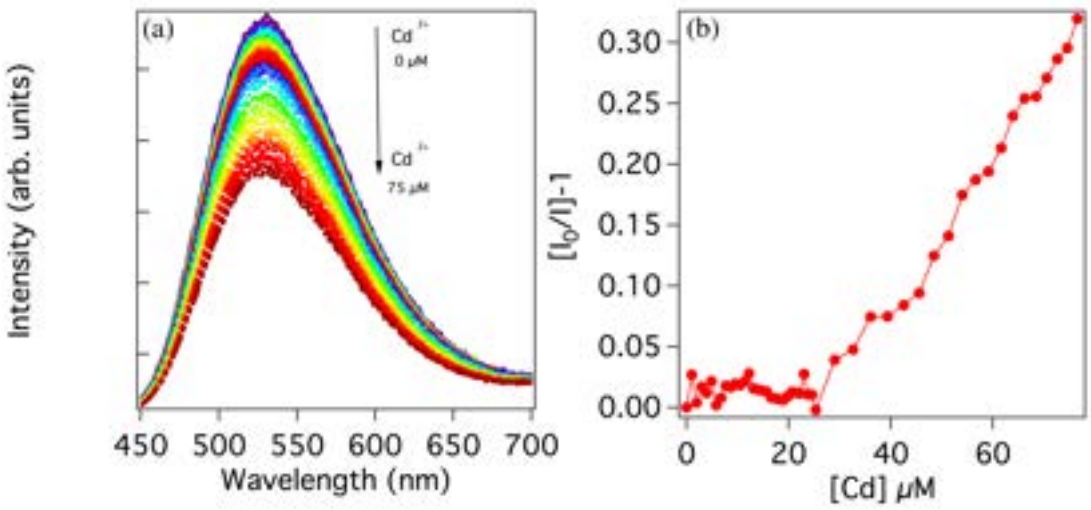

Figure 5.2: a) Emission spectrum under excitation at 440 nm of TDA sample in aqueous solution in the presence of increasing concentrations of Cd^{2+} ranging from 0 to 75 μM. (b) Stern–Volmer quenching plot of the integrated emission under excitation at 440 nm of TDA sample at different concentrations of Cd^{2+}; I_0 and I represent the emission intensity at zero and non-zero concentrations of Cd^{2+}, respectively.

luminescence intensity occurs from 30 μM onwards, where it is evident that, the carbon nanoparticle emission is quenched by the metal with a linear dependence of the intensity on the ion concentration. The possible sites of attack could be, as in the case of mercury, the oxygen groups present on the surface of the TDA, C-O-C and C-OH, given the high affinity between cadmium and oxygen.

However TDA appears not to be a good sensor for cadmium, as it selectively responds to concentrations that are too high and far outside the legal limits, thus not contributing to the sensing of this metal. The delayed onset of a significant quenching suggests that the chemical moieties that more strongly interact with Cd ions are not involved in the emission mechanism. Only after these groups are saturated by Cd, the emissive sites begin to interact with the ion giving rise to quenching. Stern-Volmer plot also shows a very low percentage of quenching at low concentrations of the metal, about 0.5%, but it is possible to appreciate a sizeable quenching of the fluorescence at high concentrations of cadmium up to 20% quenching. However, as mentioned above, TDA is not a good candidate to selectively determine Cd at low concentrations.

The same type of analysis was carried out using the NCDs sample as the fluorescent sensor, this time using the same range of concetrations as used for the TDA. The analysis carried out with NCDs and Cd also involves exciting the nanoparticle at 440 nm and evaluating the interaction process. As can be seen from the Stern-Volmer plot reported

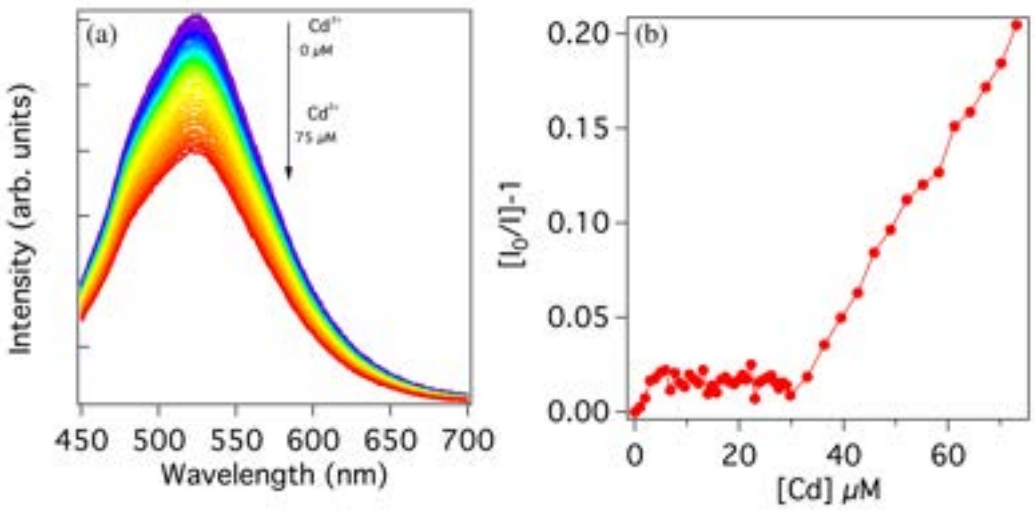

Figure 5.3: Emission spectrum under excitation at 440 nm of NCD sample in aqueous solution in the presence of increasing concentrations of Cd^{2+} ranging from 0 to 75 μM. (b) Stern–Volmer quenching plot of the integrated emission under excitation at 440 nm of TDA sample at different concentrations of Cd^{2+}; I_0 and I represent the emission intensity at zero and non-zero concentrations of Cd^{2+}, respectively.

in Figure 5.2 at high concentrations there is a gradual quenching of the fluorescence, so there is a switch-off of the radiative channels of the dot at high concentrations above 30 μM. The possible sites of attack are different chemical groups such as C=O, NH_2 and OH, given the variety present on the surface of the dot. Similarly to what observed in the top-down sample, also in this case it appears that the first surface sites that bind to Cd do not participate in the emissive activity of the nanoparticle.

Therefore, in an absolutely incredible way, even in this case, we see that the NCDs have a behaviour similar to TDA, so it is possible that the interactive process between the CDs and cadmium is prevented by a redox potential value that is too high (-0.41 eV) and therefore does not allow a correct electron transfer process

5.1.3 Other Metals Sensing

Besides the possiblity of using CD as sensors, evaluating their interactions with metal ions can also be used as a way to acquire information on the fundamental properties of the dot in itself. In other words, one possibility to discriminate and highlight optical and surface differences in TD and TDA is to evaluate their response to heavy metal ions in aqueous solution. In particular, the use of heavy metals of the first transition series (Fe, Co, Ni, Cu and Zn) as potential quenchers has been considered here. Sensing tests were

conducted on these two CDs, assessing by fluorescence and absorption spectroscopy any spectral changes in the presence of different aliquots of heavy metals. The first approach to determine and evaluate the interaction between transition metals and the samples under investigation was to use fluorescence spectroscopy. Figure (5.4) shows the emission of the two samples TD and TDA in the presence of increasing amounts of metal. In Figure 5.4 a, the interaction between Co^{2+} and TD is shown. It can be seen that as the amount of Co^{2+} increases, the emission intensity decreases steadily with each addition of metal, resulting in approximately 50% quenching of the fluorescence intensity at the maximum concentration 40 μM of metal ions. The same effect is found for the interaction between TDA and Co^{2+}. As reported in Figure 5.4 b, a decrease in emission intensity is observed as the amount of Co^{2+} increases and also in this case the quenching reaches 50 % for 40 μM of metal ions. The two fluorescence quenching processes appear to be very similar to each other, so the interaction process with Cobalt, a likely photoinduced electron transfer, is independent of surface functionalization. In Figure 5.4 c and 5.4 d, on the other hand, the interaction process between the two CDs and Zn^{2+}, is assessed. In this case the process is the reverse, i.e. the zinc causes an increase in fluorescence, and again both samples respond in the same way. This feature can be due to a screening effect by the Zn^{2+} ions that cover the surface of the CDs thus causing a consistent increase in emission intensity. Since similar results are found for TD and TDA it can be stated that the interaction process in this case too is independent of the functionalization of the surface.

To deepen the dependence on the metal ions concentration, the experiments were repeated also for other ions (Fe^{3+}, Cu^{2+}, Ni^{2+}) and a Stern-Volmer analysis has been performed. Figure (5.4e) and Figure (5.4f) show the concentration dependence of the emission in all considered cases. Different interaction processes between TD/TDA and metals ions under the same conditions can be guessed. As far as TD is concerned, the Stern-Volmer graphs show different trends for the different ions. The possible interaction process between Co^{2+} and TD, causes a clear fluorescence quenching with an important response over the whole concentration range. The possible interaction mechanisms is a formation of a coordination bond between Co^{2+} and OH groups [50] present in abundance on the TD surface. With regard to the other metals, Cu^{2+} induces an initial very pronounced fluorescence quenching of about 10%, but after the first few additions, the interaction process levels out until at high concentrations, the TD seems to be shielded by Cu and emission amplitude decreases. For the remaining metals, Ni, Fe and Zn, there does not seem to be a process of quenching of the fluorescence, but rather a process of intensity increase. It can be guessed that for these three metals there is an electronic screening of the surface from PL quenchers over the entire concentration range. Overall, from the above Stern-Volmer graphs it appears that TD has a remarkable selectivity and affinity towards the Co^{2+} ion over a wide range of concentrations, as it is the only metal that is able to significantly decrease the emission intensity of

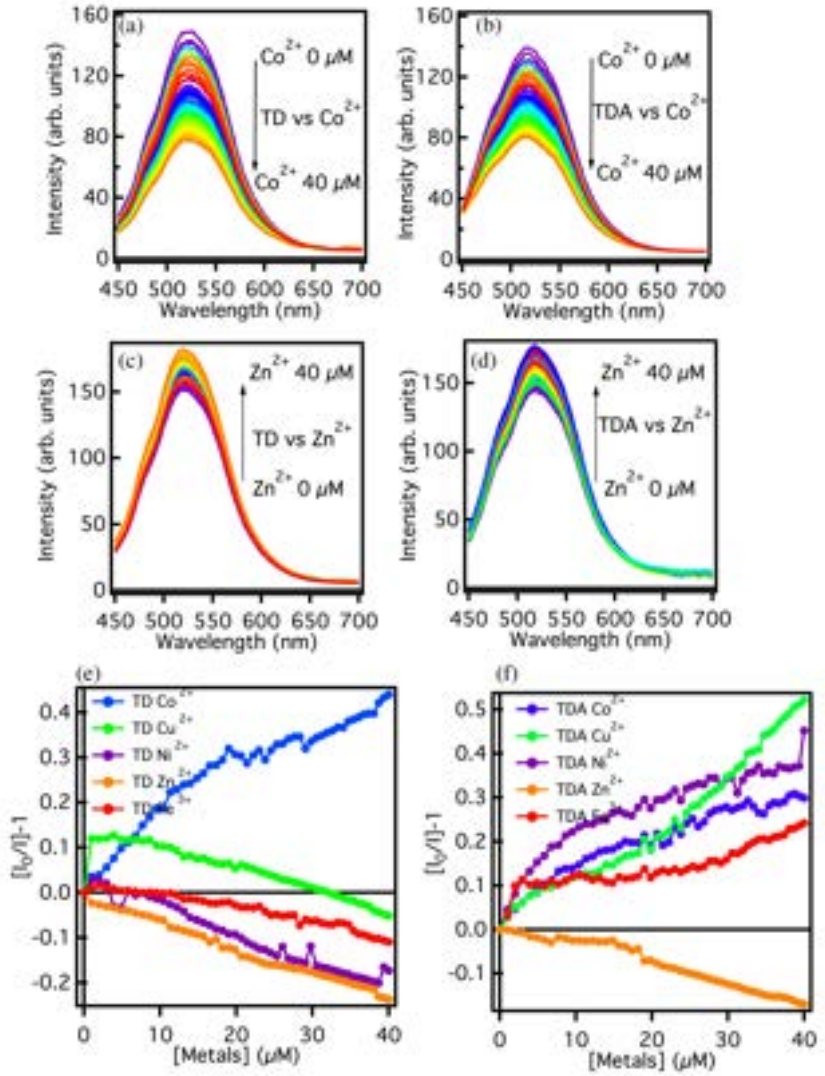

Figure 5.4: Emission spectra recorded with excitation wavelength at 440 nm for (a) TD and (b) TDA in aqueous solution with same concentration 5 mg/L, in the presence of Co^{2+} (0-40 μM), Emission spectra recorded with excitation wavelength at 440 nm for (c) TD and (d) TDA in aqueous solution in the presence of Zn^{2+} (0-40 μM). Stern-Volmer analysis at the emission wavelength 520 nm under excitation at 440 nm for (e) TD and (f) TDA in the presence of the metal ions Co^{2+} (blue line), Cu^{2+} (green line), Ni^{2+} (purple line), Zn^{2+} (orange line) and Fe^{2+} (red line).

TD, making this latter sample an ideal candidate for a sensing application towards this metal. By contrast the other metals, undergo a different interaction process with the TD surface causing essentially an increase of emission. TDA, on the other hand, shows a decidedly different trend in the Stern-Volmer plots: all the metals are able to reduce the intensity of emissions, and Co^{2+}, Fe^{3+}, Ni^{2+} and Cu^{2+}, in particular, seem to be excellent quenchers. Here, the ease of interaction between these metal ions and the surface of the TDA does not allow discrimination of the metals present in solution, and so in the case of these metals, the quenching selectivity of the carbon nanodots towards them is drastically reduced. However, TDA can be considered selective for Zn^{2+} ions, in that the interaction with this ion appears markedly different and in contrast to the pattern observed with the other metals. Zn^{2+} are in fact the only ions which cause an enhancement of TDA fluorescence intensity of about 15%. This effect could be due, as in the case of TD, to an electrostatic screening effect by the Zn^{2+} ions, which by attaching themselves to the surface can increase the PL intensity by limiting the geometric rearrangement of the surface groups. Among other things, the limit of detection (LOD) was calculated for Co^{2+} and Zn^{2+} respectively. For the LOD of Co^{2+} with TDA the value is 0.52 μM, for Zn^{2+} it is 0.84 μM. For TD-metal samples, on the other hand, the LOD values are 0.2 μM for Co^{2+} and 0.49 μM for Zn^{2+}, respectively. Finally, in order to distinguish the type of quenching and, to deepen, the type of interaction process between the samples examined, TD and TDA, and the heavy metals we carried out a study using time-resolved spectroscopy to assess the fluorescence decay kinetics, thus distinguishing whether the type of quenching could be static or dynamic. The study was carried out on both samples, using the maximum concentration of metals used in the previous experiment, i.e. 40 μM, and evaluating the PL time decay in the presence of heavy metals. The results of the experiments are reported in Figure 5.5. As far as TDA is concerned, Figure 5.5 b, despite the fact that the Stern-Volmer plots (Figure (5.4f)), shows an important PL quenching for metals such as Co^{2+}, Ni^{2+}, Fe^{3+}, Cu^{2+} and Zn^{2+}, it is clear that the decay kinetics in the presence and absence of metals remain completely unchanged within experimental uncertainty. This is the fingerprint of so-called static quenching, which is associated to the formation of entirely non-luminescent complexes between TDA and the quenchers, most likely quenched by extremely efficient (sub-nanosecond) photoinduced electron transfer. By analogy, this model can also be applied to the Zn^{2+} ion, where the increased fluorescence intensity in steady state measurements can be described as a static enhancement, occurring within stable TDA-Zn complexes [246].

As far as TD is concerned, exactly the same thing can be observed: although steady state measurements show a change in the emissive properties in the presence of the metal ions, the lifetime of TD in the presence of the ions does not change within the experimental repeatability, so here too the interaction process with the CDs can be defined as static, in the same sense explained above.

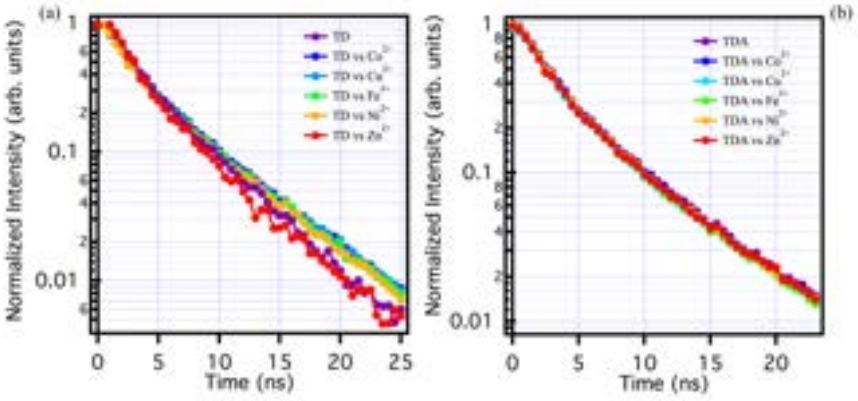

Figure 5.5: (a) Lifetime analysis for TD solutions with and without metals: pure TD (purple line), Co^{2+} (blue line), Cu^{2+} (light blue line), Fe^{3+} (green line), Ni^{2+} (orange line), Zn^{2+} (red line). (b) TDA lifetime analysis in solution with and without metals: pure TDA (purple line), Co^{2+} (blue line), Cu^{2+} (light blue line), Fe^{3+} (green line), Ni^{2+} (orange line), Zn^{2+} (red line). Lifetime has been always recorded at 520 nm under excitation at 440 nm.

Chapter 6

CDs: sensing test with pesticides

In this section, sensing with pesticides will be discussed. The challenge we have set ourselves is to analyse and determine small concentrations of pesticides of commercial interest and belonging to different classes already mentioned in the literature. Using carbon nanodots as a probe and fluorescence spectroscopy as a detector, CDs have been specially synthesised to study and evaluate the interaction process between these analytes of interest in regard to food contamination and this new class of CDs, which, as we will see in the following phases of this chapter, show different interaction capabilities compared to the CDs presented so far in this thesis. However, it is first necessary to present the analytes in question and what their physical and chemical properties are [115].

6.1 Pesticides

Three pesticides were chosen based on European standard regulations: Boscalid, Metolachlor and Oxadiazon. These three pesticides have distinctive chemical and physical properties, which cause major problems for human health. All the three compounds are small aromatic molecules, as shown in Figure 6.1.

Boscalid is a contact fungicide active substance with translaminar properties. It inhibits spore germination, germ tube elongation, mycelium growth and sporulation. Boscalid is absorbed by the leaf and migrates through the tissue to the opposite leaf. During this pathway, part of the active substance penetrates deep into the tissue and reaches the lymphatic circulation in an acropetal pattern until it reaches the apex and leaf margins. The quantities translocated are sufficient to ensure antifungal protection even in areas of the leaf which have not been directly treated. Metolachlor, also used in agriculture, is a synthetic product derived from aniline, and is used to prevent weed growth in fields. As can be seen in figure 6.1, similarly to, Boscalid, this molecule has aromatic groups that best perform its function as a herbicide. Finally, Oxadiazon is a

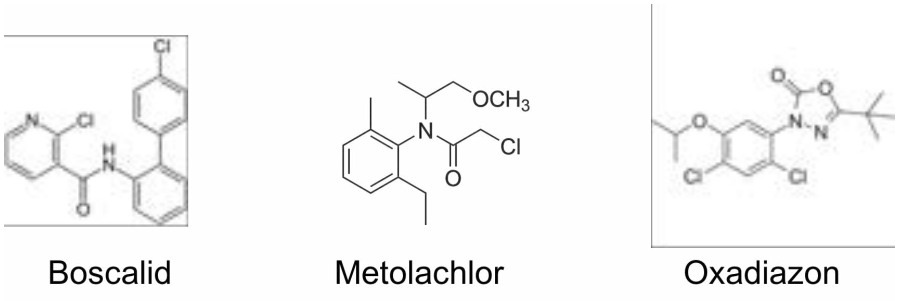

Figure 6.1: The three pesticides, from left to right, Boscalid, Metolachlor and Oxadiazon, selected for sensing tests with the different carbon nanodots.

herbicide used in many crops, such as peach and tobacco. It is applied to plants either directly by spraying the substance on the plant or by irrigating the soil and allowing the plant to absorb it. Here too, the chemical structure has aromatic rings to which various functional groups are linked, which protect the plant from pests. However, despite the fact that these molecules are necessary for crop protection, they have contraindications, i.e. they are particularly harmful to human health, both because many residues are directly in the food we eat and because they have a discrete persistence in agricultural soils. Therefore, in the following paragraphs, sensing tests will be carried out using the CDs that have been previously synthesised and characterised [122, 131].

6.1.1 Pesticides Sensing

For all pesticides, the sensing tests were conducted using steady state fluorescence spectroscopy. The most important part was to solubilise pesticides in an appropriate solvent, given its very poor solubility in water and its excellent solubility in water-immiscible organic solvents. However, after several attempts, the best measurement conditions were found by using a mixture of ethanol and water to solubilise about 1 mM of metabolite. This investigation was fundamental for the sensing study and thus to evaluate the interaction process between CDs (highly soluble in polar solvents) and different pesticides. The detection of pesticides was certainly a major challenge during this PhD, because the greatest difficulty was the lack of response of most of the CDs we considered to all three analytes. In fact for all TDs and NCDs we never observed any interaction processes that could help selectively determine analyte. For example, the effect of Oxadiazon on the fluorescence of TDA excited at 440 nm is shown in Figure 6.2 and in the Stern-Volmer plot, despite the quantities of Oxadiazon added to the CD sample are relatively large the emission band at 525 nm, shows no change despite the additions.

However, after several attempts with the different CDs synthesised and mentioned in the previous chapters, it seems that only one was able to interact with the different pesticides, SDot. This CDs, mentioned earlier in Chapter 4, was synthesised by py-

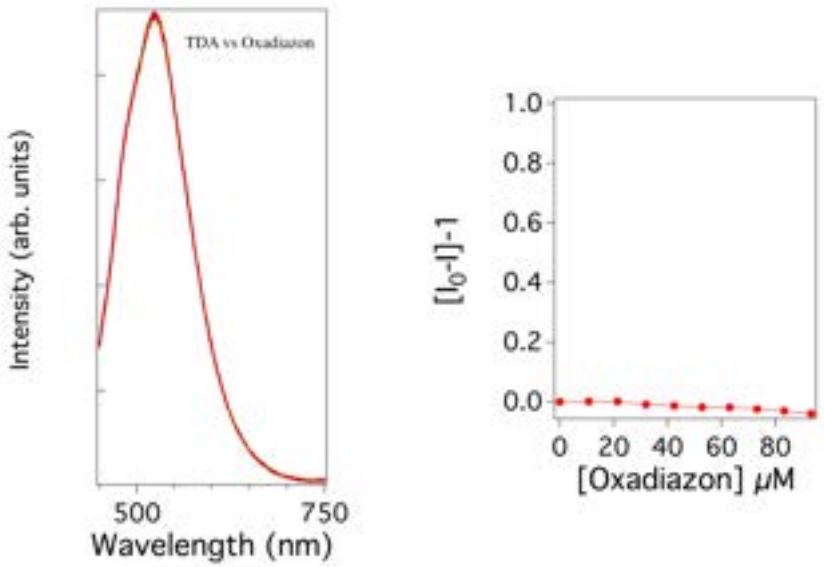

Figure 6.2: Emission spectra of the TDA with increasing Oxadiazon concentration in the range (0-90 μM) and the Stern-Volmer plot confirming the lack of interaction between nanoparticle and analyte.

rolysing two molecular precursors, safranin and citric acid in the same quantities. For pesticide sensing, a solution of SDot at a known concentration, i.e. 5 mg/L, was used as the analysis probe.

The first sensing test was carried out on Boscalid. To this purpose, a stock solution of the pesticide with a concentration of 1 mM was prepared, whereas SDot solution has a concentration of 5 mg/L, which was judged the best after multiple experiments at different concentrations. Then 2 mL of SDot solution at a known concentration was placed in a quartz cuvette of 1 cm optical path and all measurements were conducted using steady state fluorescence spectroscopy, exciting the sample of CDs at a fixed wavelength of 350 nm.

Increasing aliquots of Boscalid in the range 10-150 μM were added to the SDot sample, and, as can be seen in figure 6.3, already at the first addition of pesticide, 10 μM, there is an appreciable change in the emission spectrum of CDs, where the emission maximum undergoes a red-shift. Thereafter, continuing the titration we see that the shift of the emission maximum is constant until the end of the titration. The shift of the peak is quite evident going from 415 nm (SDot without the analyte) to 450 nm (maximum concentration of Boscalid). This extraordinary process of interaction between the pesticide and the dot can be seen as a sign that graphitic layers containing functionalities can interact distinctively with the molecular structure of Boscalid. The most likely interaction occurs between nitrogen- and oxygen-containing SDot groups and chemical

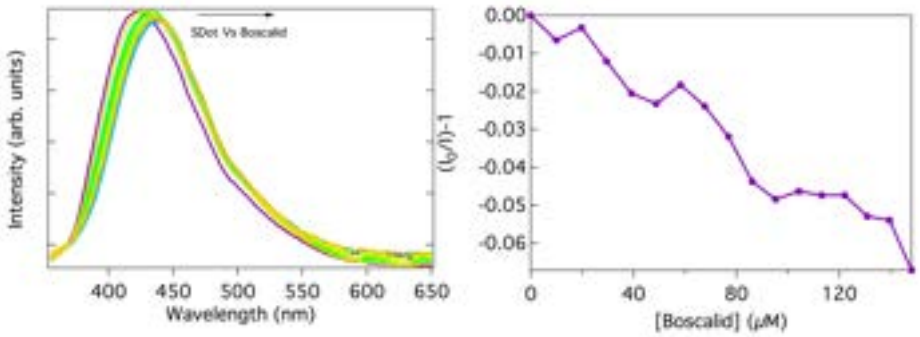

Figure 6.3: SDot emission spectra recorded at 350 nm of excitation, increasing the Boscalid concentration from 0-150 μM.

groups, such as chlorine and oxygen, with possible bonding between the pesticide and the carbon nanoparticle. The interaction of the dot with the aromatic chromophores on the pesticide is expected to alter the fundamental mechanism of the dot thus justifying the shift of the emission maximum to red. Another possible motivation leading to the band shift is the p-p stacking interaction, which leads to the weak interaction between the π orbitals of the pesticide and the sp^2-hybridised surface parts of the nanoparticle, thus involving an electronic transfer between the surface and the pesticide, thus changing the spectral position of the emission maximum.

Another sensing test, always using SDot as a sensitive nanomaterial, is that of Oxadiazon. Similarly to Boscalid, also in this case a solution of known concentration of Oxadiazon, 1 mM, was prepared and added in small aliquots to the SDot solution.

By exciting the SDot sample at 350 nm, the interaction with Oxadiazon was evaluated, adding small aliquots of pesticide, in the range 0-150 μM. Therefore it can be seen that, in Figure 6.4, as the pesticide concentration increases, the dot responds with the progressive quenching of the fluorescence, that is, a shutdown of the radiative channels of the dot nanoparticle.

As regards the Stern-Volmer plot, important information is also obtained on the percentage of fluorescence quenching which already at the first addition, 10 μM, is about 2%, up to a maximum of 8% at higher concentrations. The process of interaction between SDot and Oxadiazon is characterized by a small, but appreciable degree of fluorescence quenching. Thus our hypotesis is that the pesticide binds covalently to the surface of the dot, given the presence of chlorinated chemical groups, which are available to bind to the surface, thus switching off the radiative channels that allow the nanoparticle to emit.

Finally, the last pesticide analysed is Metolachlor. This pesticide was prepared in the same way as in the previous cases, i.e. a stock solution of the pesticide was prepared with a concentration of 1 mM. Again, the nanoparticle used for analysis is SDot,

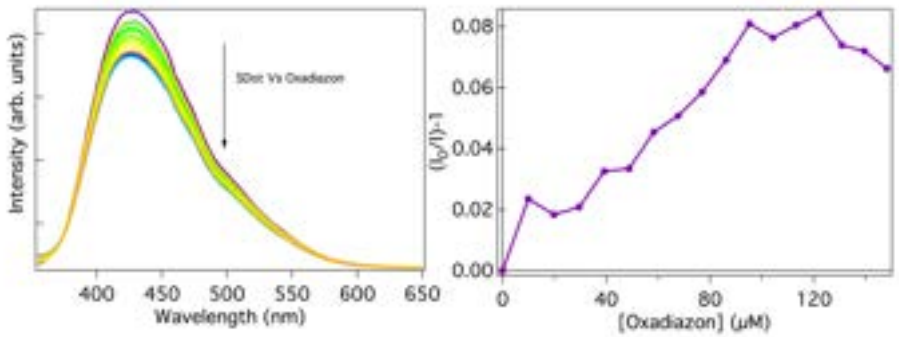

Figure 6.4: SDot emission spectra recorded at 350 nm of excitation, increasing the Oxadiazon concentration from 0-150 μM and the Stern-Volmer plot.

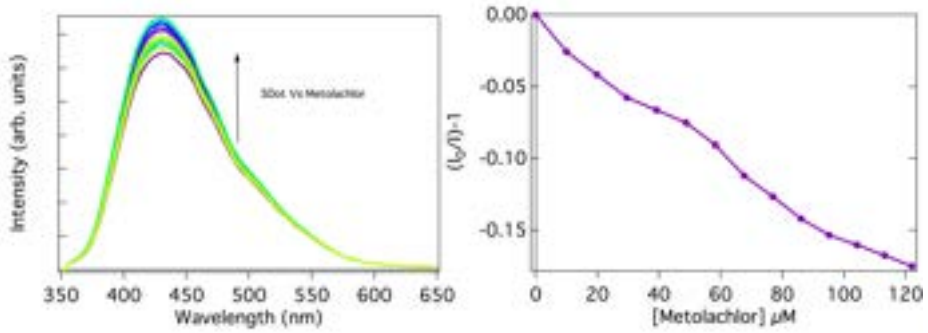

Figure 6.5: SDot emission spectra recorded at 350 nm of excitation, increasing the Metolachlor concentration from 0-120 μM and the Stern-Volmer plot.

prepared as in previous experiments. In this case too, the analysis proceeds by exciting the CDs at 350 nm, but as the concentration of the pesticide increases, unlike the other two pesticides, as shown in figure 6.5, the dot responds by showing an increase in fluorescence intensity [239].

From the very first addition, a slight increase in fluorescence is immediately apparent, later going up to 15% enanchement as can be seen from the Stern-Volmer plot. This enhancement can be tentatively attributed to an electrostatic screening effect by the pesticide, or another alternative is attaching themselves to the surface increasing the PL intensity by limiting the geometric rearrangement of the surface groups. In conclusion, it can be said that SDot is the only one of the synthesised CDs that responds appropriately to pesticides, given the different spectral responses. More precisely, the interaction with Boscalid causes a significant red-shift of the emission maximum, thus making this dot highly selective towards this analyte of absolute interest. The interaction process with Oxadiazon and Metolachlor is different, since in one case it causes a quenching of the fluorescence (Oxadiazon) and in the other case an enanchement of

the emission intensity (Metolachlor). However, although the data are very encouraging as SDot is the only one that responds with sensitivity and selectivity to pesticides, as a future perspective we will try to decrease the concentration to be determined.

After having done all the sensing tests with the reference analytes, the final goal is to build a sensor that can determine low concentrations of pesticides and heavy metals, therefore in the next chapter the construction of a chemosensor that uses CDs as fluorescent probes for the determination of the above mentioned analytes will be presented.

Chapter 7

Fluorescent Chemosensor

This chapter will describe the construction and engineering of the chemosensor that can be practically used for the determination and sensing of the analytes described in the previous chapters. Thanks to the collaboration with Infobiotech srl, active partner of this doctoral thesis, we have built a fluorescence sensor using real time fluorescence as a technology and CDs as an analytical probe, at least those that have turned out to be the best for sensing pollutants by the experiments described in the previous chapters. The aim of the research activities carried out at Infobiotech Srl is to verify the possibility of using Carbon Dots technology to create sensitive elements within diagnostic and/or analytical systems and devices. In particular, the focus will be on the detection of analytes whose presence is considered significant in the products and production processes of the agro-food chain. In order to achieve the objective, an optical transduction system compatible with the fluorescent characteristics of Carbon Dots and an electronic/informatics system for signal acquisition and processing have been designed.

7.1 Photodiodes, LED and filters

The construction of the chemosensor began with the selection of suitable precision optics and optoelectronics, i.e. filters to make the radiation monochromatic, LEDs for excitation and photodiodes for detection were evaluated. The photodiode remains the basic choice for photo detection among solid-state detectors. The process of selecting a sensor and designing an analogue front end can be reduced to seven steps:

- Describe the signal to be measured and the design goals.
- Select the right sensor and describe its electrical output.
- Identify an optimal amplifier and the preamplifier stage.
- Design the complete sensor and preamplifier gain block.

- Run a simulation.
- Take extra care when building hardware and validate.

All in all, commercial photodiodes from Hammamatsu were chosen for the sensor construction, with characteristics to match the excitation LEDs. Photodiodes are usually optimized during the design process for use in either "photovoltaic" mode or "photoconductive" mode. Responsivity, which is the ratio of the detector output to the detector input, is a key parameter of the photodiode. It's given in units of ampere/watt or volt/watt. The photodiode that was used has a spectral response in the visible range, which is suitable for the best possible fluorescence detection from the CDs that were previously synthesised. The photodiode that was chosen is a silicon one, because it contains a number of features, such as the wide spectral range 300-1100 nm, the short-circuit current and the dark current. The datasheet of the photodiode selected is reported in Figure 7.1, and evidences the best features of the chosen device, the LED was chosen to excite the CDs with a suitable wavelength.

Finally, filters were chosen with the appropriate characteristics, namely 9 mm filters monochromatize the light beam impinging into the sample, with a bandwidth centered at 440 nm to direct the light beam onto the sample and a dichroic mirror to remove stray wavelengths. The dichroic mirror allows an excitation wavelength of 410 nm to pass with a bandwidth of ± 3 nm, preventing the passage of wavelengths below 380 nm and wavelengths above 440 nm, however the collection of the signal and therefore of the reflected wavelength is centred at 520 nm.

7.2 CAD and 3D printing

One of the crucial parts of constructing the sensor was to use an appropriate CAD design program, in this case Fusion360, which enabled the optimisation of the optical geometries of the system and the construction of the sensor housing. The precision with which the optics, supports and final box were designed is of the order of a millimeter. The figure 7.2 reports the draft by CAD the design of the most appropriate optical geometry.In the figure 7.2 it can be seen in the top left the connections for the LED, connected to the board which allows the sample to be illuminated at a wavelength of 430 nm. This wavelength was chosen because it is ideal for exciting CDs. The samples is inserted inside a cuvette placed at the cenetr of the box. As shown in the bottom right part of fig.7.2 at 90 degrees with respect to the impinging light there is the photodiode which accumulates the signal on its board and then gives an electrical intensity value which is transformed into fluorescence emission intensity.

The CAD result was then 3D printed, and the result being shown in the Figure 7.3. Black PET was chosen as the material of choice to prevent light from entering from the

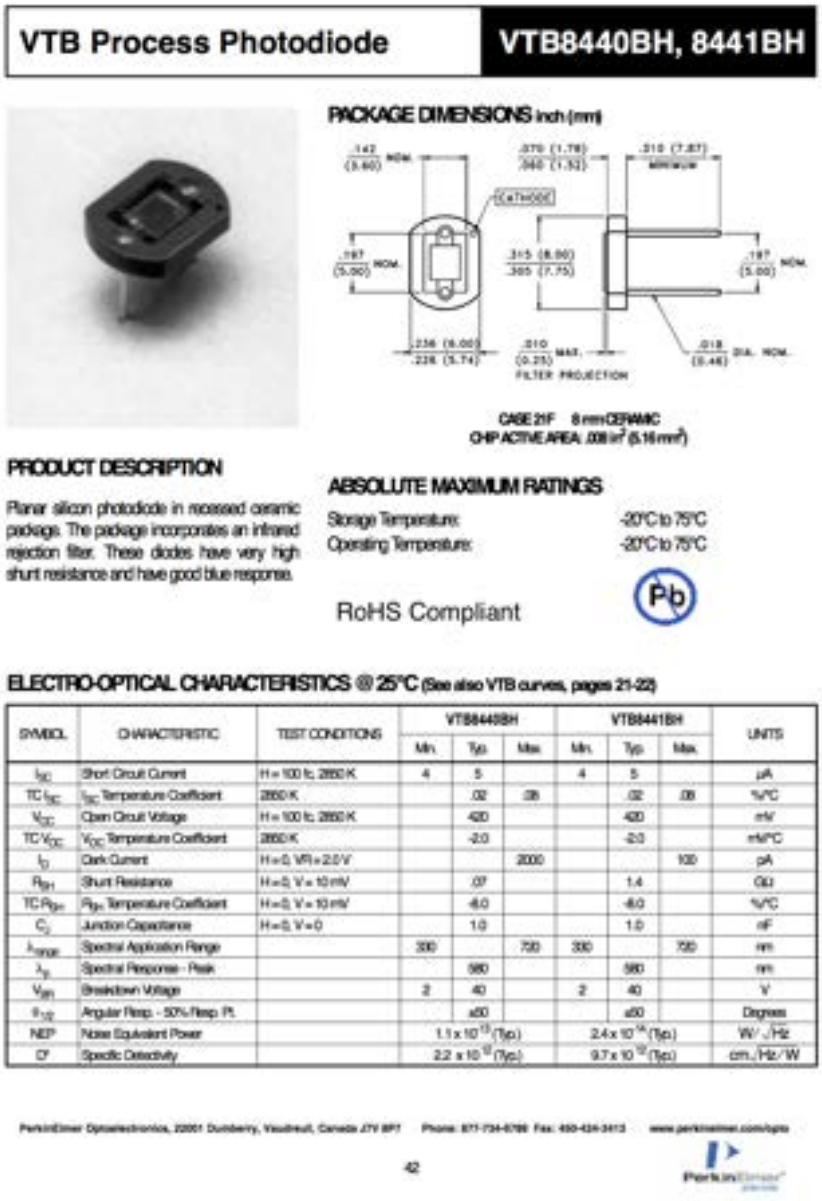

VTB Process Photodiode | **VTB8440BH, 8441BH**

PACKAGE DIMENSIONS inch (mm)

CASE 21F 6 mm CERAMIC
CHIP ACTIVE AREA: .008 in² (5.16 mm²)

PRODUCT DESCRIPTION

Planar silicon photodiode in recessed ceramic package. The package incorporates an infrared rejection filter. These diodes have very high shunt resistance and have good blue response.

ABSOLUTE MAXIMUM RATINGS

Storage Temperature:	-20°C to 75°C
Operating Temperature:	-20°C to 75°C

RoHS Compliant

ELECTRO-OPTICAL CHARACTERISTICS @ 25°C (See also VTB curves, pages 21-22)

SYMBOL	CHARACTERISTIC	TEST CONDITIONS	VTB8440BH			VTB8441BH			UNITS
			Min.	Typ.	Max.	Min.	Typ.	Max.	
I_{SC}	Short Circuit Current	H = 100 fc, 2850 K	4	5		4	5		µA
TC I_{SC}	I_{SC} Temperature Coefficient	2850 K		.02	.05		.02	.05	%/°C
V_{OC}	Open Circuit Voltage	H = 100 fc, 2850 K		420			420		mV
TC V_{OC}	V_{OC} Temperature Coefficient	2850 K		-2.0			-2.0		mV/°C
I_D	Dark Current	H = 0, VR = 2.0 V			2000			100	pA
R_{SH}	Shunt Resistance	H = 0, V = 10 mV		.07			1.4		GΩ
TC R_{SH}	R_{SH} Temperature Coefficient	H = 0, V = 10 mV		-6.0			-6.0		%/°C
C_J	Junction Capacitance	H = 0, V = 0		1.0			1.0		nF
λ_{range}	Spectral Application Range		300		700	300		700	nm
λ_p	Spectral Response - Peak			960			960		nm
V_{BR}	Breakdown Voltage		2	40		2	40		V
$\theta_{1/2}$	Angular Resp. - 50% Resp. Pt.			±50			±50		Degrees
NEP	Noise Equivalent Power			1.1×10^{-13} (Typ.)			2.4×10^{-14} (Typ.)		W/√Hz
D*	Specific Detectivity			2.2×10^{12} (Typ.)			9.7×10^{12} (Typ.)		cm√Hz/W

PerkinElmer Optoelectronics, 22001 Dumberry, Vaudreuil, Canada J7V 8P7 Phone: 877-734-6786 Fax: 450-424-3413 www.perkinelmer.com/opto

42

Figure 7.1: Datasheet of the photodiode used in the construction of the sensing device.

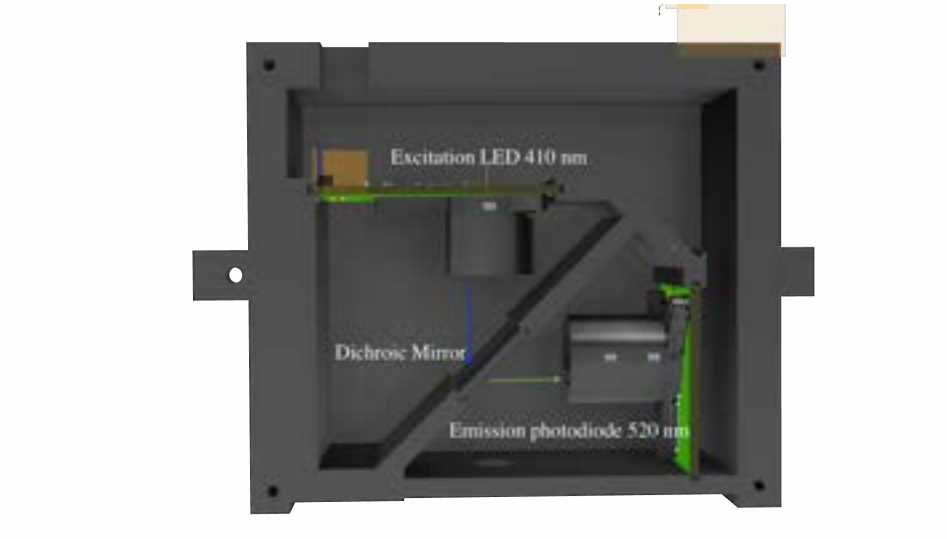

v21.png

Figure 7.2: CAD drawing of the optical geometry, which was printed in 3D. The blue arrow shows the emitted light direction from the sample placed below the excitation LED at 410 nm inside the cuvette holder, the green arrow shows the wave reflected by the dichroic mirror and collected by the photodiode placed in the bottom right.

outside and disturbing the light emitted by the LED and also to reduce any stray light in the visible range..

After designing the optical part, a box was built around it to prevent light from dissipating or stray light from entering from outside. Therefore the optics box was designed with the presence of the sample holder. The size of the sample holder is practically standard, because it corresponds to a cuvette with an optical path of 1 centimetre. In figure 7.4 you can see the sensor in all its parts.

Finally, a Bluetooth connection with an app, developed by the company's IT department, was made using ESP32 technology. The app works in a very simple way, the measurement is directly controlled by the app which turns on the excitation LED recording a fluorescence signal. First of all for each measurement the sensor is calibrated for any corrections to the instrument background by using distilled water instead of a CD solution. Tests with the samples were carried out at the time using two different CDs, namely NCDs and TDA, and the response to the analytes of interest was evaluated.

CDs samples are prepared at a known concentration, 5 mg/L, and inserted into the sensor. Therefore, after calibrating as mentioned above, the experiment consists of excitation of the CDs by the LED and a signal is collected in the photodiode which is equal to a luminescence intensity. At this point, known concentrations of three different metals were added to the CDs and the results are shown in the table 7.1.

From the data collected, as can be seen in the table, for both samples, TDA and

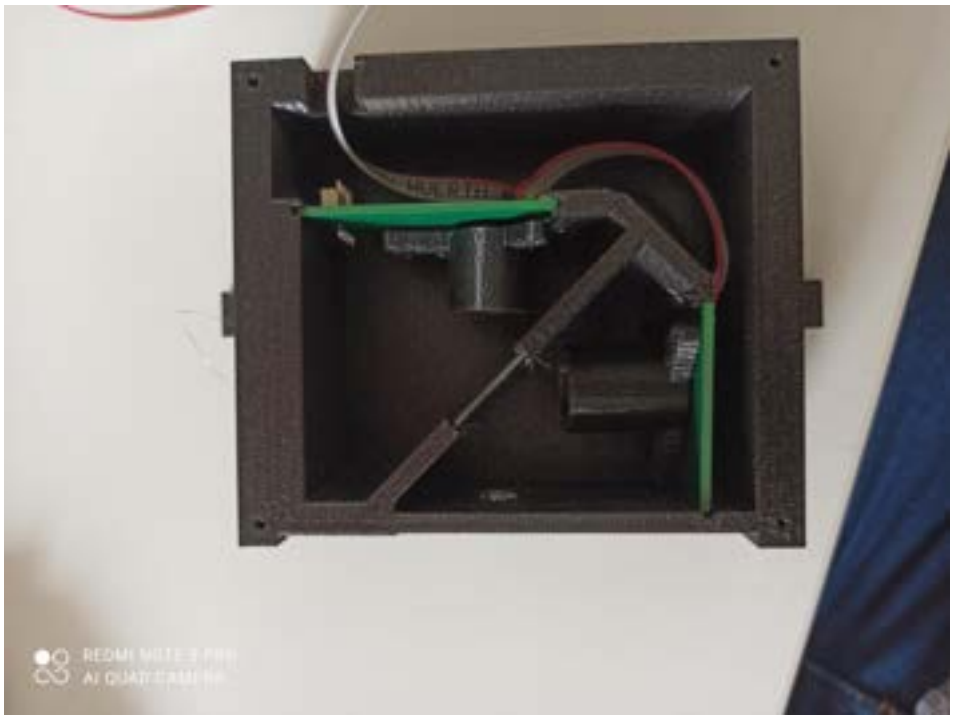

Figure 7.3: 3D printing with Prusa Slicer printer of CAD-designed geometry.

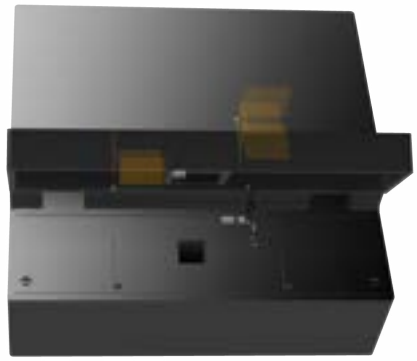

Figure 7.4: CAD drawing of the final device with adapted sample holder on 1 cm quartz cuvettes.

Table 7.1: Sensing tests collected using the device, metals analysed are Hg, Co and Cu, responses with respect to the two CDs (TDA and NCDs) are consistent with data recorded using other techniques

Analytes 10 μM	TDA	NCDs
NoMetals	2070.92 (PL Intensity)	2547.45 (PL Intensity)
$Hg2^{+}$	1863.83 (PL Intensity)	2166.02 (PL Intensity)
$Cu2^{+}$	1822.41 (PL Intensity)	2368.56 (PL Intensity)
$Co2^{+}$	1677.45 (PL Intensity)	2052.83 (PL Intensity)

NCDs, there are decreases in fluorescence intensity when there is an interaction with the reference analyte, values that are consistent with the analysis carried out in the laboratory using fluorescence spectroscopy.

In conclusion, the development of the sensor, thanks to the company's expertise, has provided some very interesting and important responses, and the choice of LED, photodiode and filters has been adapted to the specific needs of the CDs, furthermore, the measurements are reliable and aim at an efficient sensing using the optical properties of the CDs.

Chapter 8

Conclusion

The main goal of this work the was use of a new family of emerging materials, carbon nanodots (CDs) for sensing food pollutants, like heavy metals and pesticides. The idea of using fluorescent materials such as CDs stems from the fact that, in addition to exhibiting favourable optical properties, they are low-cost and easy to synthesise, so the project achieved its objective thanks to the collaboration with the Universidad de la Castilla-La Mancha and Infobiotech to build a fluorescence-based chemosensor implemented with CDs.

CDs were first synthesised at both UNIPA and UCLM, where different families of CDs were synthesised using the major techniques in use, namely bottom-up and top-down.

Bottom-up synthesis was carried out in Palermo, pyrolysing different molecular precursors, such as citric acid, urea, ortho-phenylenediamine, rhodamine, fluorescein and safranine, in order to have a plethora of carbon nanoparticles with different optical, morphological and structural properties. There are five samples resulting from these syntheses, namely NCDs (citric acid + urea), PCDs, (ortho-phenylenediamine + citric acid), SDot (Safranine + citric acid), RDot (Rhodamine + citric acid) and FDot (fluorescein + citric acid). The CDs resulting from the synthesis were purified using very precise and extensive purification methods, namely size-exclusion chromatography (SEC) and dialysis. These techniques made it possible to purify the carbon nanoparticles in the best possible way in order to obtain materials that were as pure as possible, i.e. without reaction by-products. After purification of the synthesised samples, the optical and structural properties of these samples were evaluated, as a preliminary step in view of sensing tests with food pollutants.

From an optical point of view, NCDs and PCDs were characterised using absorption spectroscopy, steady-state fluorescence spectroscopy and time-resolved spectroscopy. The optical absorption properties of the two samples are very different. However, the emission spectra recorded at 440 nm of excitation for both NCDs and PCDs show very broad and unstructured bands typical of carbon nanoparticles, with emission maxima

at 515 nm for NCDs and 530 nm for PCDs. Finally, the lifetime of these nanoparticles was also evaluated by time-resolved spectroscopy and the fluorescence decay times are quite different for both samples, therefore we can say that the samples from a surface point of view might be different, as they show chromophores with different optical properties. For the other bottom-up syntheses, i.e. those that used xanthene precursors, the optical characterisation shows that the samples differ significantly from each other. After careful purification of the samples, using the techniques mentioned above (SEC and dialysis), the samples were first characterised using absorption spectroscopy, where the spectral differences are clearly evident. The three samples, SDot, RDot and FDot, have very different absorption spectra, i.e. SDot has a band structured in the UV, around 350 nm, that extends into the near visible, RDot and FDot have similar spectra with a band that starts in the UV and ends in the near visible. Anyway, in none of the absorption spectra are the typical and characteristic bands of the molecular precursors present, which implies a successful pyrolysis. Also emission spectral SDot, RDot, FDot, recorded using an excitation wavelength of 350 nm show very broad characteristic bands, typical of carbon nanoparticles.

In the case of Top-Down CDs, the main synthesis was chemical oxidation of graphite with a concentrated acid mixture, which enabled the formation of carbon nanoparticles. Such "TD" samples were later functionalized with small molecules in order to dope the surface, in the case of this thesis work the functionalised agents were acetone, to increase the amount of oxygenated groups on the surface and with ethylenediamine, to increase nitrogen doping. These syntheses gave rise to three different samples TD, TDA and TDN. Also these samples were also optically characterised using absorption spectroscopy, fluorescence spectroscopy and time-resolved spectroscopy. The samples show almost identical absorption and emission spectra with resepct to the native ones, implying that functionalisation does not actively participate in the emissive properties of the CDs. The emission spectra were recorded by excitation of all samples at 440 nm, and in all three cases there are broad bands typical of nanoparticle material.

Another important aspect is the tunability, i.e. these samples have a large excitability range of the visible photoluminescence from 410 to 620 nm, always showing fairly bands, that continuously red shift following the change of excitation. Finally, the analysis of the lifetimes made it possible to identify the decay kinetics, which in all three cases are double exponential.

All samples, i.e. bottom-up and top-down, were characterised by structural and morphological techniques, such as Raman, ATR, FT-IR and AFM spectroscopy. The information given by Raman spectroscopy implies that all samples have tendentially amorphous crystal structures, which is confirmed by the I_D/I_G ratio, which gives important information on the type of hybridisation of the carbon atoms. As far as atomic force microscopy (AFM) is concerned, it is found that the samples have a different size distribution, i.e. the samples prepared by bottom-up approach, i.e. using molecular pre-

cursors, are smaller than those prepared by top-down approach which is to be expected given that the top-down samples are obtained from much larger starting materials.

Finally, surface characterisation was carried out using ATR and FT-IR, which made it possible to discriminate the functional groups present on the surface of CDs, especially for TD samples, which are optically and structurally very similar to each other.

After this lengthy and important characterisation process, the best CDs that could play an important role in sensing heavy metals and pestcides were evaluated. The heavy metal sensing tests involved four different CDs, namely NCDs, TD, TDA and TDN.

In the case of mercury sensing, NCDs seem to be the best compared to polyfunctional TDs, since mercury induces a fluorescence quenching process of about 40 %. The possible mechanism inhibiting the emission is the formation of a coordination compound, so that a static fluorescence quenching is assumed, another interesting point given by NCDs is that the quenching process is accompanied by a red-shift. NCDs is therefore a possible candidate for sensing low concentrations of mercury.

As far as cadmium is concerned, although for both samples presented, NCDs and TDA, fluorescence quenching occurs at very high concentrations, the latter are outside the proposed target range.

Interestingly, the sensing responses of TD and TDA to metal ions in solution are very different from each other. TD fluorescence shows a remarkable and selective quenching process in presence of Cobalt ions, about 50 % throughout the 0-40 μM concentration range. In contrast, the other transition metals only lead to an increase of the luminescence intensity. TDA, on the other hand, responds to all the metals taken into consideration, which are found to behave as excellent quenchers. However, an exception is represented by Zinc, which induces a continuous increase of the emission intensity in the whole range of explored concentrations (0-40 μM). Therefore, the optical response of TDA is selective to Zinc ions because of their unique behaviour in the interaction process.

Finally, the pesticide detection analysis was successful with another type of sample, SDot, which is able to interact selectively and differently with all three pesticides. Thus, excitation of a known amount of SDot at 350 nm causes a red-shift in the interaction process with Boscalid, a quenching of the luminescence intensity with oxadiazon and an increase in the luminescence intensity with metolachlor. However, the process of interaction between pesticides and SDot, which is the only considered carbon nanoparticles that detects these analytes, is unclear. Overall, we found that four typ of CDs are highly selective for specific analytes, specifically: NCDs for Hg, TD for Co, TDA for Zn and SDot for all pesticides.

Some of these dots were then tested within the chemosensor built with Inforbiotech srl. The chemosensor was built by assembling the necessary optical components (a LED, a photodiode, a filter and a dichroic mirror) into a case built with a 3D printer. An app for mobile phone was written and programmed that allows the sensor to communi-

cate the intensity of fluorescence. It can therefore be concluded that the synergistic work between universities (UNIPA and UCLM) and company (Infobiotech), has allowed the construction of a chemosensor that based on the final tests we conducted on the device, turns out show that uses the optical properties of CDs can be used for the detection of pollutants in food.

The future perspectives for this thesis work are to improve the sensitivity of CDs towards certain markers, so as to be able to further reduce the limit of detection of pollutants. Furthermore, as regards the chemosensor, being able to implement it with other optical properties and choice of the analytes on which to carry out the experimentation it could be adapted to detection of specific analytes of commercial interest for food companies.

Finally, I would like to say that no Carbon nanodots have been mistreated during this thesis work.

Bibliography

[1] Cornelius Oertel, Jörg Matschullat, Kamal Zurba, Frank Zimmermann, and Stefan Erasmi. Greenhouse gas emissions from soils—a review. *Geochemistry*, 76(3):327–352, 2016.

[2] Åsa Kasimir-Klemedtsson, L Klemedtsson, K Berglund, P Martikainen, J Silvola, and O Oenema. Greenhouse gas emissions from farmed organic soils: a review. *Soil use and management*, 13:245–250, 1997.

[3] Ram C Dalal and Diane E Allen. Greenhouse gas fluxes from natural ecosystems. *Australian Journal of Botany*, 56(5):369–407, 2008.

[4] Aranya Venkatesh, Paulina Jaramillo, W Michael Griffin, and H Scott Matthews. Uncertainty in life cycle greenhouse gas emissions from united states natural gas end-uses and its effects on policy. *Environmental science & technology*, 45(19):8182–8189, 2011.

[5] Daniel JG Crow, Paul Balcombe, Nigel Brandon, and Adam D Hawkes. Assessing the impact of future greenhouse gas emissions from natural gas production. *Science of the total environment*, 668:1242–1258, 2019.

[6] Robert W Howarth. A bridge to nowhere: methane emissions and the greenhouse gas footprint of natural gas. *Energy Science & Engineering*, 2(2):47–60, 2014.

[7] Daniel A Lashof and Dilip R Ahuja. Relative contributions of greenhouse gas emissions to global warming. *Nature*, 344(6266):529–531, 1990.

[8] Mohammad Songolzadeh, Mansooreh Soleimani, Maryam Takht Ravanchi, and Reza Songolzadeh. Carbon dioxide separation from flue gases: a technological review emphasizing reduction in greenhouse gas emissions. *The Scientific World Journal*, 2014, 2014.

[9] YUE Xi-Liu and GAO Qing-Xian. Contributions of natural systems and human activity to greenhouse gas emissions. *Advances in Climate Change Research*, 9(4):243–252, 2018.

[10] Ana Maria Roxana Petrescu, Glen P Peters, Greet Janssens-Maenhout, Philippe Ciais, Francesco N Tubiello, Giacomo Grassi, Gert-Jan Nabuurs, Adrian Leip, Gema Carmona-Garcia, Wilfried Winiwarter, et al. European anthropogenic afolu greenhouse gas emissions: a review and benchmark data. *Earth System Science Data*, 12(2):961–1001, 2020.

[11] Anu Ramaswami, Abel Chavez, Jennifer Ewing-Thiel, and Kara E Reeve. Two approaches to greenhouse gas emissions foot-printing at the city scale, 2011.

[12] Ruth DeFries, Frédéric Achard, Sandra Brown, Martin Herold, Daniel Murdiyarso, Bernhard Schlamadinger, and Carlos de Souza Jr. Earth observations for estimating greenhouse gas emissions from deforestation in developing countries. *Environmental science & policy*, 10(4):385–394, 2007.

[13] Steffen Lehmann. Low carbon construction systems using prefabricated engineered solid wood panels for urban infill to significantly reduce greenhouse gas emissions. *Sustainable Cities and Society*, 6:57–67, 2013.

[14] Lauri Linkosalmi, Roope Husgafvel, Anna Fomkin, Hilppa Junnikkala, Tiina Witikkala, Matti Kairi, and Olli Dahl. Main factors influencing greenhouse gas emissions of wood-based furniture industry in finland. *Journal of Cleaner Production*, 113:596–605, 2016.

[15] F-X Philippe and Baudouin Nicks. Review on greenhouse gas emissions from pig houses: Production of carbon dioxide, methane and nitrous oxide by animals and manure. *Agriculture, Ecosystems & Environment*, 199:10–25, 2015.

[16] Quantifying Methane Emissions from Livestock. Greenhouse gas emissions: Quantifying methane emissions from livestock. *Am. J. Engg. & Applied Sci*, 5(1):1–8, 2012.

[17] Robert W Howarth, Renee Santoro, and Anthony Ingraffea. Methane and the greenhouse-gas footprint of natural gas from shale formations. *Climatic change*, 106(4):679–690, 2011.

[18] Khagendra R Baral, Guillaume Jégo, Barbara Amon, Roland Bol, Martin H Chantigny, Jørgen E Olesen, and Søren O Petersen. Greenhouse gas emissions during storage of manure and digestates: Key role of methane for prediction and mitigation. *Agricultural systems*, 166:26–35, 2018.

[19] S Wulf, M Maeting, and J Clemens. Application technique and slurry cofermentation effects on ammonia, nitrous oxide, and methane emissions after spreading: Ii. greenhouse gas emissions. *Journal of environmental quality*, 31(6):1795–1801, 2002.

[20] Hannah Ritchie and Max Roser. CO_2 and greenhouse gas emissions. *Our world in data*, 2020.

[21] Mark D Staples, Robert Malina, and Steven RH Barrett. The limits of bioenergy for mitigating global life-cycle greenhouse gas emissions from fossil fuels. *Nature Energy*, 2(2):1–8, 2017.

[22] M Mercedes Maroto-Valer, Chunshan Song, and Yee Soong. *Environmental challenges and greenhouse gas control for fossil fuel utilization in the 21st century*. Springer Science & Business Media, 2002.

[23] Simon Caney. Justice and the distribution of greenhouse gas emissions. *Journal of global ethics*, 5(2):125–146, 2009.

[24] James R Whetstone. Significance of greenhouse gas measurement for carbon management technologies. *Advances in Carbon Management Technologies: Carbon Removal, Renewable and Nuclear Energy, Volume 1*, page 73, 2020.

[25] VM Kartavskaya and AV Kartavskaya. Reducing greenhouse gas emissions based on energy conservation. In *IOP Conference Series: Earth and Environmental Science*, volume 751, page 012009. IOP Publishing, 2021.

[26] Mohamed Rabie and Christian M Franck. Assessment of eco-friendly gases for electrical insulation to replace the most potent industrial greenhouse gas sf6. *Environmental science & technology*, 52(2):369–380, 2018.

[27] John G Owens. Greenhouse gas emission reductions through use of a sustainable alternative to sf 6. In *2016 IEEE Electrical Insulation Conference (EIC)*, pages 535–538. IEEE, 2016.

[28] JGJ Olivier and JAHW Peters. Trends in global co2 and total greenhouse gas emissions. *PBL Netherlands Environmental Assessment Agency: The Hague, The Netherlands*, 2020.

[29] Rattan Lal. Soil erosion and gaseous emissions. *Applied Sciences*, 10(8):2784, 2020.

[30] Kenneth R Olson, Alexander N Gennadiyev, Andrey P Zhidkin, and Maxim V Markelov. Impact of land use change and soil erosion in upper mississippi river valley on soil organic carbon retention and greenhouse gas emissions. *Soil Science*, 176(9):449–458, 2011.

[31] Pasquale Borrelli, David A Robinson, Panos Panagos, Emanuele Lugato, Jae E Yang, Christine Alewell, David Wuepper, Luca Montanarella, and Cristiano Ballabio. Land use and climate change impacts on global soil erosion by water

(2015-2070). *Proceedings of the National Academy of Sciences*, 117(36):21994–22001, 2020.

[32] S Fred Singer. Global effects of environmental pollution. *Eos, Transactions American Geophysical Union*, 51(5):476–478, 1970.

[33] Kevin Zahnle, Laura Schaefer, and Bruce Fegley. Earth's earliest atmospheres. *Cold Spring Harbor perspectives in biology*, 2(10):a004895, 2010.

[34] RW Gurry. Composition of atmospheres inert to heated carbon steel. *JOM*, 2(4):671–687, 1950.

[35] Serkan Gürlük. Economic growth, industrial pollution and human development in the mediterranean region. *Ecological Economics*, 68(8-9):2327–2335, 2009.

[36] Pablo Fernández-Navarro, Javier García-Pérez, Rebeca Ramis, Elena Boldo, and Gonzalo López-Abente. Industrial pollution and cancer in spain: An important public health issue. *Environmental research*, 159:555–563, 2017.

[37] Willemijn Tuinstra. Preparing for the european thematic strategy on air pollution: at the interface between science and policy. *Environmental Science & Policy*, 10(5):434–444, 2007.

[38] John R Goldsmith and Stephen A Landaw. Carbon monoxide and human health. *Science*, 162(3860):1352–1359, 1968.

[39] O Badr and SD Probert. Carbon monoxide concentration in the earth's atmosphere. *Applied Energy*, 49(2):99–143, 1994.

[40] Bernard Weinstock. Carbon monoxide: Residence time in the atmosphere. *Science*, 166(3902):224–225, 1969.

[41] Vahid Safarianzengir, Behrouz Sobhani, Mohammad Hasan Yazdani, and Mohammadkia Kianian. Monitoring, analysis and spatial and temporal zoning of air pollution (carbon monoxide) using sentinel-5 satellite data for health management in iran, located in the middle east. *Air Quality, Atmosphere & Health*, 13(6):709–719, 2020.

[42] J Aswin Giri, S Karthikeyan, and M Gokul Raj. Effect of ambient concentration of carbon monoxide (co) on the in-vehicle concentration of carbon monoxide in chennai, india. *Environ. Eng. Res*, 26:200165, 2020.

[43] Amanda O Fisher-Hubbard, Colin Appleford, Kilak Kesha, Carl J Schmidt, and Avneesh Gupta. Accidental carbon monoxide poisoning while driving: a case report with review of the literature. *The American Journal of Forensic Medicine and Pathology*, 39(3):270–272, 2018.

[44] Suzuki Syofian, Aji Setiawan, Rolan Siregar, and Muhamad Fathan. Detection and monitoring of carbon monoxide (co) toxic gases in old vehicle cabin (odometer> 300k km) and its relationship to vehicle density using fuzzy method. In *Conference on Broad Exposure to Science and Technology 2021 (BEST 2021)*, pages 142–145. Atlantis Press, 2022.

[45] Donald H Stedman. Automobile carbon monoxide emission. *Environmental Science & Technology*, 23(2):147–149, 1989.

[46] M El-Fadel and L Abi-Esber. In-vehicle exposure to carbon monoxide emissions from vehicular exhaust: A critical review. *Critical Reviews in Environmental Science and Technology*, 39(8):585–621, 2009.

[47] S Dey and G Chandra Dhal. Controlling carbon monoxide emissions from automobile vehicle exhaust using copper oxide catalysts in a catalytic converter. *Materials Today Chemistry*, 17:100282, 2020.

[48] Neil B Hampson and James R Holm. Suicidal carbon monoxide poisoning has decreased with controls on automobile emissions. *Undersea Hyperb Med*, 42(2):159–164, 2015.

[49] BD Dombek. Metal hydrides in homogeneous catalytic reduction of carbon monoxide. *Annals of the New York Academy of Sciences*, 415(1):176–190, 1983.

[50] Motoki Tsujimura, Takehiko Furusawa, and Daizo Kunii. Catalytic reduction of nitric oxide by carbon monoxide over calcined limestone. *Journal of Chemical Engineering of Japan*, 16(2):132–136, 1983.

[51] Qirui Zhong, Ye Huang, Huizhong Shen, Yilin Chen, Han Chen, Tianbo Huang, Eddy Y Zeng, and Shu Tao. Global estimates of carbon monoxide emissions from 1960 to 2013. *Environmental Science and Pollution Research*, 24(1):864–873, 2017.

[52] Mohit Dalvi, Gufran Beig, Uday Patil, Akshara Kaginalkar, C Sharma, and AP Mitra. A gis based methodology for gridding of large-scale emission inventories: application to carbon-monoxide emissions over indian region. *Atmospheric Environment*, 40(16):2995–3007, 2006.

[53] DA Grantz, JHB Garner, and DW Johnson. Ecological effects of particulate matter. *Environment international*, 29(2-3):213–239, 2003.

[54] Francesca Dominici, Michael Greenstone, and Cass R Sunstein. Particulate matter matters. *Science*, 344(6181):257–259, 2014.

[55] Michelle L Bell, Jonathan M Samet, and Francesca Dominici. Time-series studies of particulate matter. *Annu. Rev. Public Health*, 25:247–280, 2004.

[56] Renyi Zhang, Gehui Wang, Song Guo, Misti L Zamora, Qi Ying, Yun Lin, Weigang Wang, Min Hu, and Yuan Wang. Formation of urban fine particulate matter. *Chemical reviews*, 115(10):3803–3855, 2015.

[57] Roy M Harrison and Jianxin Yin. Particulate matter in the atmosphere: which particle properties are important for its effects on health? *Science of the total environment*, 249(1-3):85–101, 2000.

[58] F Mazzei, A D'alessandro, F Lucarelli, S Nava, P Prati, G Valli, and R Vecchi. Characterization of particulate matter sources in an urban environment. *Science of the Total Environment*, 401(1-3):81–89, 2008.

[59] Steven D Colome, Norman Y Kado, Peter Jaques, and Michael Kleinman. Indoor-outdoor air pollution relations: particulate matter less than 10 μm in aerodynamic diameter (pm10) in homes of asthmatics. *Atmospheric Environment. Part A. General Topics*, 26(12):2173–2178, 1992.

[60] Xiaoxu Xie, Yuanyuan Wang, Ying Yang, Jihong Xu, Ya Zhang, Wenbin Tang, Tongjun Guo, Qiaomei Wang, Haiping Shen, Yiping Zhang, et al. Long-term effects of ambient particulate matter (with an aerodynamic diameter $\leq$ 2.5 μm) on hypertension and blood pressure and attributable risk among reproductive-age adults in china. *Journal of the American Heart Association*, 7(9):e008553, 2018.

[61] Cristina Linares and Julio Diaz. [impact of particulate matter with diameter of less than 2.5 microns [pm2. 5] on daily hospital admissions in 0-10-year-olds in madrid. spain [2003-2005]]. *Gaceta Sanitaria*, 23(3):192–197, 2009.

[62] Ernesto Alfaro-Moreno, Tim S Nawrot, Abderrahim Nemmar, and Benoit Nemery. Particulate matter in the environment: pulmonary and cardiovascular effects. *Current opinion in pulmonary medicine*, 13(2):98–106, 2007.

[63] Stephan F van Eeden, Adam Yeung, Kevin Quinlam, and James C Hogg. Systemic response to ambient particulate matter: relevance to chronic obstructive pulmonary disease. *Proceedings of the American Thoracic Society*, 2(1):61–67, 2005.

[64] Sean H Ling and Stephan F van Eeden. Particulate matter air pollution exposure: role in the development and exacerbation of chronic obstructive pulmonary disease. *International journal of chronic obstructive pulmonary disease*, 4:233, 2009.

[65] Natalie R Couling, Marcie G Towell, and Kirk T Semple. Biodegradation of pahs in soil: influence of chemical structure, concentration and multiple amendment. *Environmental Pollution*, 158(11):3411–3420, 2010.

[66] Yosadara Ruiz-Morales. Homo- lumo gap as an index of molecular size and structure for polycyclic aromatic hydrocarbons (pahs) and asphaltenes: A theoretical study. i. *The Journal of Physical Chemistry A*, 106(46):11283–11308, 2002.

[67] Fuat Topuz and Tamer Uyar. Poly-cyclodextrin cryogels with aligned porous structure for removal of polycyclic aromatic hydrocarbons (pahs) from water. *Journal of hazardous materials*, 335:108–116, 2017.

[68] Sheshanath V Bhosale, Chintan H Jani, and Steven J Langford. Chemistry of naphthalene diimides. *Chemical Society Reviews*, 37(2):331–342, 2008.

[69] Ki-Hyun Kim, Shamin Ara Jahan, Ehsanul Kabir, and Richard JC Brown. A review of airborne polycyclic aromatic hydrocarbons (pahs) and their human health effects. *Environment international*, 60:71–80, 2013.

[70] J t Karle and H Hauptman. Application of statistical methods to the naphthalene structure. *Acta Crystallographica*, 6(6):473–476, 1953.

[71] Guijian Liu, Zhiyuan Niu, Daniel Van Niekerk, Jian Xue, and Liugen Zheng. Polycyclic aromatic hydrocarbons (pahs) from coal combustion: emissions, analysis, and toxicology. *Reviews of environmental contamination and toxicology*, pages 1–28, 2008.

[72] Guor-Cheng Fang, Kuan-Foo Chang, Chungsying Lu, and Hsunling Bai. Estimation of pahs dry deposition and bap toxic equivalency factors (tefs) study at urban, industry park and rural sampling sites in central taiwan, taichung. *Chemosphere*, 55(6):787–796, 2004.

[73] Gizem Eker and Melis Hatipoglu. Effect of uv wavelength, temperature and photocatalyst on the removal of pahs from industrial soil with photodegradation applications. *Environmental technology*, 2018.

[74] Kristin K Clark and Arturo A Keller. Investigation of two magnetic permanently confined micelle array sorbents using nonionic and cationic surfactants for the removal of pahs and pesticides from aqueous media. *Water, Air, & Soil Pollution*, 223(7):3647–3655, 2012.

[75] Sascha Usenko, Dixon H Landers, Peter G Appleby, and Staci L Simonich. Current and historical deposition of pbdes, pesticides, pcbs, and pahs to rocky mountain national park. *Environmental science & technology*, 41(21):7235–7241, 2007.

[76] Anne Motelay-Massei, Tom Harner, Mahiba Shoeib, Miriam Diamond, Gary Stern, and Bruno Rosenberg. Using passive air samplers to assess urban- rural trends for persistent organic pollutants and polycyclic aromatic hydrocarbons. 2. seasonal trends for pahs, pcbs, and organochlorine pesticides. *Environmental science & technology*, 39(15):5763–5773, 2005.

[77] David H Phillips. Fifty years of benzo (a) pyrene. *Nature*, 303(5917):468–472, 1983.

[78] Kimberly P Miller and Kenneth S Ramos. Impact of cellular metabolism on the biological effects of benzo [a] pyrene and related hydrocarbons. *Drug metabolism reviews*, 33(1):1–35, 2001.

[79] Nisha Verma, Mario Pink, Albert W Rettenmeier, and Simone Schmitz-Spanke. Review on proteomic analyses of benzo [a] pyrene toxicity. *Proteomics*, 12(11):1731–1755, 2012.

[80] Vasudha Bansal, Pawan Kumar, Eilhann E Kwon, and Ki-Hyun Kim. Review of the quantification techniques for polycyclic aromatic hydrocarbons (pahs) in food products. *Critical Reviews in Food Science and Nutrition*, 57(15):3297–3312, 2017.

[81] Thomas Wenzl, Rupert Simon, Elke Anklam, and Juliane Kleiner. Analytical methods for polycyclic aromatic hydrocarbons (pahs) in food and the environment needed for new food legislation in the european union. *TrAC Trends in Analytical Chemistry*, 25(7):716–725, 2006.

[82] Zuzana Zelinkova and Thomas Wenzl. The occurrence of 16 epa pahs in food–a review. *Polycyclic aromatic compounds*, 35(2-4):248–284, 2015.

[83] Charles A Menzie, Bonnie B Potocki, and Joseph Santodonato. Exposure to carcinogenic pahs in the environment. *Environmental science & technology*, 26(7):1278–1284, 1992.

[84] M Huang and TM Penning. Processing contaminants: polycyclic aromatic hydrocarbons (pahs), 2014.

[85] Ying Chen, Rongzhi Zhao, Jun Xue, and Jinhui Li. Generation and distribution of pahs in the process of medical waste incineration. *Waste management*, 33(5):1165–1173, 2013.

[86] Nana Peng, Zhengang Liu, Tingting Liu, and Chao Gai. Emissions of polycyclic aromatic hydrocarbons (pahs) during hydrothermally treated municipal solid waste combustion for energy generation. *Applied Energy*, 184:396–403, 2016.

[87] SK Verma, RE Masto, Shalini Gautam, DP Choudhury, LC Ram, SK Maiti, and Sudip Maity. Investigations on pahs and trace elements in coal and its combustion residues from a power plant. *Fuel*, 162:138–147, 2015.

[88] Mafumi Watanabe and Yukio Noma. Influence of combustion temperature on formation of nitro-pahs and decomposition and removal behaviors in pilot-scale waste incinerator. *Environmental science & technology*, 43(7):2512–2518, 2009.

[89] Jian-hua Yan, Xiao-fang You, Xiao-dong Li, Ming-jiang Ni, Xue-feng Yin, and Ke-fa Cen. Performance of pahs emission from bituminous coal combustion. *Journal of Zhejiang University-SCIENCE A*, 5(12):1554–1564, 2004.

[90] Nguyen-Duy Dat and Moo Been Chang. Review on characteristics of pahs in atmosphere, anthropogenic sources and control technologies. *Science of the total environment*, 609:682–693, 2017.

[91] Ángeles C Ochoa-Martínez, Tania Ruíz-Vera, Lucia G Pruneda-Álvarez, Ana K González-Palomo, Claudia I Almendarez-Reyna, Francisco J Pérez-Vázquez, and Iván N Pérez-Maldonado. Serum adipocyte-fatty acid binding protein (fabp4) levels in women from mexico exposed to polycyclic aromatic hydrocarbons (pahs). *Environmental Science and Pollution Research*, 24(2):1862–1870, 2017.

[92] Feidi Wang, Haijun Zhang, Ningbo Geng, Xiaoqian Ren, Baoqin Zhang, Yufeng Gong, and Jiping Chen. A metabolomics strategy to assess the combined toxicity of polycyclic aromatic hydrocarbons (pahs) and short-chain chlorinated paraffins (sccps). *Environmental pollution*, 234:572–580, 2018.

[93] Do-Yeong Kim, Boram Kim, and Han-Seung Shin. Reduction of polycyclic aromatic hydrocarbons (pahs) in sesame oil using cellulosic aerogel. *Foods*, 10(3):644, 2021.

[94] Dimosthenis A Sarigiannis, Spyros P Karakitsios, Dimitrios Zikopoulos, Spyridoula Nikolaki, and Marianthi Kermenidou. Lung cancer risk from pahs emitted from biomass combustion. *Environmental Research*, 137:147–156, 2015.

[95] Eunkyung Yoon, Kyungah Park, Hyomin Lee, Jae-Ho Yang, and Cherlho Lee. Estimation of excess cancer risk on time-weighted lifetime average daily intake of pahs from food ingestion. *Human and Ecological Risk Assessment*, 13(3):669–680, 2007.

[96] Rachel Stading, Grady Gastelum, Chun Chu, Weiwu Jiang, and Bhagavatula Moorthy. Molecular mechanisms of pulmonary carcinogenesis by polycyclic aromatic hydrocarbons (pahs): Implications for human lung cancer. In *Seminars in cancer biology*, volume 76, pages 3–16. Elsevier, 2021.

[97] Qianqi Yang, Zhiyuan Li, Xiaoning Lu, Qiannan Duan, Lei Huang, and Jun Bi. A review of soil heavy metal pollution from industrial and agricultural regions in china: Pollution and risk assessment. *Science of the total environment*, 642:690–700, 2018.

[98] Shuiping Cheng. Heavy metal pollution in china: origin, pattern and control. *Environmental science and pollution research*, 10(3):192–198, 2003.

[99] Thomas Sawidis, J Breuste, M Mitrovic, P Pavlovic, and K Tsigaridas. Trees as bioindicator of heavy metal pollution in three european cities. *Environmental pollution*, 159(12):3560–3570, 2011.

[100] Harry Harmens, Alan Buse, Patrick Büker, David Norris, Gina Mills, Bronwen Williams, Brian Reynolds, Trevor W Ashenden, Åke Rühling, and Eiliv Steinnes. Heavy metal concentrations in european mosses: 2000/2001 survey. *Journal of Atmospheric Chemistry*, 49(1):425–436, 2004.

[101] C Micó, L Recatalá, M Peris, and J Sánchez. Assessing heavy metal sources in agricultural soils of an european mediterranean area by multivariate analysis. *Chemosphere*, 65(5):863–872, 2006.

[102] Johannes Godt, Franziska Scheidig, Christian Grosse-Siestrup, Vera Esche, Paul Brandenburg, Andrea Reich, and David A Groneberg. The toxicity of cadmium and resulting hazards for human health. *Journal of occupational medicine and toxicology*, 1(1):1–6, 2006.

[103] Francois Putois. Market for nickel-cadmium batteries. *Journal of Power Sources*, 57(1-2):67–70, 1995.

[104] Andréa Moura Bernardes, D Crocce Romano Espinosa, and JA Soares Tenório. Recycling of batteries: a review of current processes and technologies. *Journal of Power sources*, 130(1-2):291–298, 2004.

[105] AJ Spencer. Dental amalgam and mercury in dentistry. *Australian Dental Journal*, 45(4):224–234, 2000.

[106] Dan C Langan, PL Fan, and Alice A Hoos. The use of mercury in dentistry: a critical review of the recent literature. *The Journal of the American Dental Association*, 115(6):867–880, 1987.

[107] Mahmood A Khwaja and Maryam Shabbir Abbasi. Mercury poisoning dentistry: high-level indoor air mercury contamination at selected dental sites. *Reviews on environmental health*, 29(1-2):29–31, 2014.

[108] L Gerhardsson and DK Brune. Mercury in dentistry. In *Occupational hazards in the health professions*, pages 307–321. CRC Press, 2020.

[109] Semra Ilhan, Macit Nurbaş Nourbakhsh, Serpil Kiliçarslan, and Huseyin Ozdag. Removal of chromium, lead and copper ions from industrial waste waters by staphylococcus saprophyticus. *Turkish Electronic Journal of Biotechnology*, 2(2):50–57, 2004.

[110] Xi Tian, Yu Gong, Yufeng Wu, Amma Agyeiwaa, and Tieyong Zuo. Management of used lead acid battery in china: Secondary lead industry progress, policies and problems. *Resources, conservation and recycling*, 93:75–84, 2014.

[111] Kewei Hou. Industry information diffusion and the lead-lag effect in stock returns. *The review of financial studies*, 20(4):1113–1138, 2007.

[112] Ramona Massoud, Mohammad Rasoul Hadiani, Pegah Hamzehlou, and Kianoush Khosravi-Darani. Bioremediation of heavy metals in food industry: Application of saccharomyces cerevisiae. *Electronic Journal of Biotechnology*, 37:56–60, 2019.

[113] Jing Jing Zhang and Hong Yang. Metabolism and detoxification of pesticides in plants. *Science of the Total Environment*, 790:148034, 2021.

[114] Otto Daniel, Matthias Samuel Meier, Josef Schlatter, and Peter Frischknecht. Selected phenolic compounds in cultivated plants: ecologic functions, health implications, and modulation by pesticides. *Environmental Health Perspectives*, 107(suppl 1):109–114, 1999.

[115] Marianne Köck-Schulmeyer, Marta Villagrasa, Miren López de Alda, Raquel Céspedes-Sánchez, Francesc Ventura, and Damià Barceló. Occurrence and behavior of pesticides in wastewater treatment plants and their environmental impact. *Science of the total environment*, 458:466–476, 2013.

[116] Tanha Talaviya, Dhara Shah, Nivedita Patel, Hiteshri Yagnik, and Manan Shah. Implementation of artificial intelligence in agriculture for optimisation of irrigation and application of pesticides and herbicides. *Artificial Intelligence in Agriculture*, 4:58–73, 2020.

[117] Aruna Sharma and TI Khan. Organochlorine pesticides in irrigation water of jaipur city (india). *Journal of Environmental Science & Engineering*, 51(3):175–178, 2009.

[118] RF Spalding, ME Burbach, and ME Exner. Pesticides in nebraska's ground water. *Groundwater Monitoring & Remediation*, 9(4):126–133, 1989.

[119] European Food Safety Authority (EFSA), Alba Brancato, Daniela Brocca, Laszlo Bura, Harry Byers, Arianna Chiusolo, Daniele Court Marques, Federica Crivellente, Chloé De Lentdecker, Marcella De Maglie, et al. Peer review of the pesticide risk assessment for the active substance metazachlor in light of confirmatory data submitted. *EFSA Journal*, 15(6):e04833, 2017.

[120] Jan Alexander, Diane Benford, Alan Boobis, Mari Eskola, Johanna Fink-Gremmels, Peter Fürst, Claudia Heppner, Josef Schlatter, and Rolaf van Leeuwen. Risk assessment of contaminants in food and feed. *EFSA Journal*, 10(10):s1004, 2012.

[121] European Food Safety Authority (EFSA), Jorge Borroto, Alba Brancato, Luis Carrasco Cabrera, Anna Federica Castoldi, Arianna Chiusolo, Angelo Colagiorgi, Mathilde Colas, Federica Crivellente, Chloe De Lentdecker, et al. Peer review of the pesticide risk assessment for the active substance penthiopyrad in light of confirmatory data submitted. *EFSA Journal*, 20(1):e07037, 2022.

[122] Iman A Al-Saleh. Pesticides: a review article. *Journal of environmental pathology, toxicology and oncology: official organ of the International Society for Environmental Toxicology and Cancer*, 13(3):151–161, 1994.

[123] Jan Dich, Shelia Hoar Zahm, Annika Hanberg, and Hans-Olov Adami. Pesticides and cancer. *Cancer causes & control*, 8(3):420–443, 1997.

[124] Christopher J Bosso. *Pesticides and politics*. University of Pittsburgh Pre, 1987.

[125] Isra Mahmood, Sameen Ruqia Imadi, Kanwal Shazadi, Alvina Gul, and Khalid Rehman Hakeem. Effects of pesticides on environment. In *Plant, soil and microbes*, pages 253–269. Springer, 2016.

[126] Roman Davydov, Michael Sokolov, William Hogland, Alexey Glinushkin, and Artem Markaryan. The application of pesticides and mineral fertilizers in agriculture. In *MATEC web of conferences*, volume 245, page 11003. EDP Sciences, 2018.

[127] Nayana Sharma and Ritu Singhvi. Effects of chemical fertilizers and pesticides on human health and environment: a review. *International journal of agriculture, environment and biotechnology*, 10(6):675–680, 2017.

[128] Pratibha Prashar and Shachi Shah. Impact of fertilizers and pesticides on soil microflora in agriculture. In *Sustainable agriculture reviews*, pages 331–361. Springer, 2016.

[129] Arun Lal Srivastav. Chemical fertilizers and pesticides: role in groundwater contamination. In *Agrochemicals detection, treatment and remediation*, pages 143–159. Elsevier, 2020.

[130] Jennifer E Fox, Jay Gulledge, Erika Engelhaupt, Matthew E Burow, and John A McLachlan. Pesticides reduce symbiotic efficiency of nitrogen-fixing rhizobia and host plants. *Proceedings of the National Academy of Sciences*, 104(24):10282–10287, 2007.

[131] ISAM Bashour, M Tolba, and N Saab. Pesticides, fertilizers and food safety. In *Arab Environment: Future Challenges. Tolba, M., and Saab, N.(Ed.), Report of the Arab Forum for Environment and Development (AFED) and Technical Publications, Beirut, Lebanon*, pages 137–145, 2008.

[132] Si-fan Cui, Yuan-zhou Fu, Bai-qin Zhou, Jin-xin Li, Wen-yan He, Ya-qi Yu, and Jin-yan Yang. Transfer characteristic of fluorine from atmospheric dry deposition, fertilizers, pesticides, and phosphogypsum into soil. *Chemosphere*, 278:130432, 2021.

[133] LI Ju-Ying, HAN Ai-Liang, WANG Hai-Yan, WANG Wei, and YE Qing-Fu. A review: radiolabeled synthesis of pesticides. *Journal of Nuclear Agricultural Sciences*, 24(2):415, 2010.

[134] Nisha Aggarwal, Rajesh Kumar, Chitra Srivastva, Prem Dureja, and JM Khurana. Synthesis of nalidixic acid based hydrazones as novel pesticides. *Journal of agricultural and food chemistry*, 58(5):3056–3061, 2010.

[135] NS Pawar, UR Kapadi, DG Hundiwale, and PP Kumbhar. Applications of polymer-supported reactions in the synthesis of pesticides i: Alkylation and acylation of n-hydroxy phthalimide. 2002.

[136] Agnes M Rimando and Stephen O Duke. Natural products for pest management. ACS Publications, 2006.

[137] Carl A Johansen. Pesticides and pollinators. *Annual review of entomology*, 22(1):177–192, 1977.

[138] Stéphane Kluser and Pascal Peduzzi. Global pollinator decline: a literature review. 2007.

[139] Tomasz Kiljanek, Alicja Niewiadowska, and Andrzej Posyniak. Pesticide poisoning of honeybees: a review of symptoms, incident classification, and causes of poisoning. *Journal of Apicultural Science*, 60(2):5–24, 2016.

[140] Walter M Jarman and Karlheinz Ballschmiter. From coal to ddt: the history of the development of the pesticide ddt from synthetic dyes till silent spring. *Endeavour*, 36(4):131–142, 2012.

[141] Ming Hung Wong, AOW Leung, JKY Chan, and MPK Choi. A review on the usage of pop pesticides in china, with emphasis on ddt loadings in human milk. *Chemosphere*, 60(6):740–752, 2005.

[142] D Bagchi, M Bagchi, EA Hassoun, and SJ Stohs. In vitro and in vivo generation of reactive oxygen species, dna damage and lactate dehydrogenase leakage by selected pesticides. *Toxicology*, 104(1-3):129–140, 1995.

[143] Karashdeep Kaur and Rupinder Kaur. Occupational pesticide exposure, impaired dna repair, and diseases. *Indian journal of occupational and environmental medicine*, 22(2):74, 2018.

[144] Lawrence J Blus. Organochlorine pesticides. In *Handbook of ecotoxicology*, pages 337–364. CRC Press, 2002.

[145] Ravindran Jayaraj, Pankajshan Megha, and Puthur Sreedev. Organochlorine pesticides, their toxic effects on living organisms and their fate in the environment. *Interdisciplinary toxicology*, 9(3-4):90, 2016.

[146] Poonam Kaushik and Geetanjali Kaushik. An assessment of structure and toxicity correlation in organochlorine pesticides. *Journal of Hazardous Materials*, 143(1-2):102–111, 2007.

[147] Mohsen Kazemi, Abdol Mansour Tahmasbi, Reza Valizadeh, Abbas Ali Naserian, and Ashish Soni. Organophosphate pesticides: A general review. *Agricultural science research journals*, 2, 2012.

[148] Tai C Kwong. Organophosphate pesticides: biochemistry and clinical toxicology. *Therapeutic drug monitoring*, 24(1):144–149, 2002.

[149] Gurpreet Kaur Sidhu, Simranjeet Singh, Vijay Kumar, Daljeet Singh Dhanjal, Shivika Datta, and Joginder Singh. Toxicity, monitoring and biodegradation of organophosphate pesticides: a review. *Critical reviews in environmental science and technology*, 49(13):1135–1187, 2019.

[150] Maliwan Boonsaner, Thamnoon Kaewumput, and Arthorn Boonsaner. Bioaccumulation of organophosphate pesticides in vetiver grass (vetiveria zizanioides nash.). *Science & Technology Asia*, pages 30–39, 2002.

[151] T Roy Fukuto. Mechanism of action of organophosphorus and carbamate insecticides. *Environmental health perspectives*, 87:245–254, 1990.

[152] Baljinder Singh. Review on microbial carboxylesterase: general properties and role in organophosphate pesticides degradation. *Biochem Mol Biol*, 2:1–6, 2014.

[153] K Vala Ragnarsdottir. Environmental fate and toxicology of organophosphate pesticides. *Journal of the Geological Society*, 157(4):859–876, 2000.

[154] Touraj Nasrabadi, Gholamreza Nabi Bidhendi, Abdolreza Karbassi, Peter Grathwohl, and Nasser Mehrdadi. Impact of major organophosphate pesticides used in agriculture to surface water and sediment quality (southern caspian sea basin, haraz river). *Environmental Earth Sciences*, 63(4):873–883, 2011.

[155] Kinga Ślósarczyk and Andrzej Jarosław Witkowski. Preliminary evaluation of the possible occurrence of pesticides in groundwater contaminated with nitrates—a case study from southern poland. *Water*, 13(21):3091, 2021.

[156] Alain Hildebrandt, Miriam Guillamón, Silvia Lacorte, Roma Tauler, and Damia Barceló. Impact of pesticides used in agriculture and vineyards to surface and groundwater quality (north spain). *Water research*, 42(13):3315–3326, 2008.

[157] Robert F Carsel, Russell L Jones, James L Hanse, Richard L Lamb, and Mary P Anderson. A simulation procedure for groundwater quality assessments of pesticides. *Journal of Contaminant Hydrology*, 2(2):125–138, 1988.

[158] Sudarshan Kurwadkar and Kartik Venkataraman. Reconnaissance of groundwater quality impact. *Water Environment Research*, 85(10):1700–1714, 2013.

[159] Shilpi Agarwal, Nima Sadeghi, Inderjeet Tyagi, Vinod Kumar Gupta, and Ali Fakhri. Adsorption of toxic carbamate pesticide oxamyl from liquid phase by newly synthesized and characterized graphene quantum dots nanomaterials. *Journal of colloid and interface science*, 478:430–438, 2016.

[160] Devdutt Chaturvedi, Nisha Mishra, and Virendra Mishra. Various approaches for the synthesis of organic carbamates. *Current Organic Synthesis*, 4(3):308–320, 2007.

[161] Saad R El-Zemity. Synthesis and molluscicidal activity of novel n-methyl carbamate derivatives based on naturally occurring monoterpenoids. *J. Appl. Sci. Res*, 2(2):86–90, 2006.

[162] LUCIA GUILHERMINO, PIEDADE BARROS, MC Silva, and AMADEU MVM SOARES. Short communication should the use of inhibition of cholinesterases as a specific biomarker for organophosphate and carbamate pesticides be questioned. *Biomarkers*, 3(2):157–163, 1998.

[163] Mohamed A Hassaan and Ahmed El Nemr. Pesticides pollution: Classifications, human health impact, extraction and treatment techniques. *The Egyptian Journal of Aquatic Research*, 46(3):207–220, 2020.

[164] Mahfouz H Zaki, Dennis Moran, and David Harris. Pesticides in groundwater: the aldicarb story in suffolk county, ny. *American Journal of Public Health*, 72(12):1391–1395, 1982.

[165] EFSA Panel on Contaminants in the Food Chain (CONTAM). Scientific opinion on the risks to animal and public health and the environment related to the presence of nickel in feed. *EFSA Journal*, 13(4):4074, 2015.

[166] EFSA Panel on Contaminants in the Food Chain (CONTAM). Scientific opinion on the risks to public health related to the presence of chromium in food and drinking water. *EFSA Journal*, 12(3):3595, 2014.

[167] EFSA Panel on Contaminants in the Food Chain (CONTAM). Statement on tolerable weekly intake for cadmium. *EFSA Journal*, 9(2):1975.

[168] European Food Safety Authority (EFSA). Cadmium in food - scientific opinion of the panel on contaminants in the food chain. *EFSA Journal*, 7(3):980, 2009.

[169] EFSA Panel on Contaminants in the Food Chain (CONTAM). Scientific opinion on lead in food. *EFSA Journal*, 8(4):1570.

[170] European Food Safety Authority (EFSA). Opinion of the scientific panel on contaminants in the food chain [contam] related to mercury and methylmercury in food. *EFSA Journal*, 2(3):34, 2004.

[171] EFSA Panel on Contaminants in the Food Chain (CONTAM). Scientific opinion on the risk for public health related to the presence of mercury and methylmercury in food. *EFSA Journal*, 10(12):2985, 2012.

[172] Jukka T Salonen, Kari Seppänen, Timo A Lakka, Riitta Salonen, and George A Kaplan. Mercury accumulation and accelerated progression of carotid atherosclerosis: a population-based prospective 4-year follow-up study in men in eastern finland. *Atherosclerosis*, 148(2):265–273, 2000.

[173] Shirlee W Tan, Jesse C Meiller, and Kathryn R Mahaffey. The endocrine effects of mercury in humans and wildlife. *Critical reviews in toxicology*, 39(3):228–269, 2009.

[174] David W Eggleston and Magnus Nylander. Correlation of dental amalgam with mercury in brain tissue. *The Journal of prosthetic dentistry*, 58(6):704–707, 1987.

[175] M Fujiki and S Tajima. The pollution of minamata bay by mercury. *Water Science and Technology*, 25(11):133–140, 1992.

[176] KUNIHIKO Nakamura, Mineshi Sakamoto, Hiroo Uchiyama, and Osami Yagi. Organomercurial-volatilizing bacteria in the mercury-polluted sediment of minamata bay, japan. *Applied and environmental microbiology*, 56(1):304–305, 1990.

[177] Mikio Kumagai and Hajime Nishimura. Mercury distribution in seawater in minamata bay and the origin of particulate mercury. *Journal of the Oceanographical Society of Japan*, 34(2):50–56, 1978.

[178] Shigeo Ekino, Mari Susa, Tadashi Ninomiya, Keiko Imamura, and Toshinori Kitamura. Minamata disease revisited: an update on the acute and chronic manifestations of methyl mercury poisoning. *Journal of the neurological sciences*, 262(1-2):131–144, 2007.

[179] J Gardiner. The chemistry of cadmium in natural water—ii. the adsorption of cadmium on river muds and naturally occurring solids. *Water Research*, 8(3):157–164, 1974.

[180] Xiuying Zhang, Dongmei Chen, Taiyang Zhong, Xiaomin Zhang, Min Cheng, and Xinhui Li. Assessment of cadmium (cd) concentration in arable soil in china. *Environmental Science and Pollution Research*, 22(7):4932–4941, 2015.

[181] HCH Hahne and W Kroontje. Significance of ph and chloride concentration on behavior of heavy metal pollutants: mercury (ii), cadmium (ii), zinc (ii), and lead (ii). Technical report, Wiley Online Library, 1973.

[182] PD Moskowitz, VM Fthenakis, and K Zweibel. Health, safety and environmental issues relating to cadmium usage in photovoltaic energy systems. Technical report, Solar Energy Research Inst., Golden, CO (USA), 1990.

[183] WJ Rühl. Cadmium in polymers—product control in the automobile industry. *Fresenius' Zeitschrift für analytische Chemie*, 322(7):710–712, 1985.

[184] H Sakabe, K Ushio, et al. Acute cadmium soap poisoning in industry. *Bull. natn. Inst. Ind. Health*, (3):56–60, 1960.

[185] Dan Murphy, Aishwarya Mathew, Benjamin James, and David Hutchinson. Could the inhalation of cadmium and other metals in addition to textile dust inhalation account for the observed increased risk of rheumatoid arthritis in textile workers? *Annals of the Rheumatic Diseases*, 75(5):e30–e30, 2016.

[186] Coline Druart, Renaud Scheifler, and Annette De Vaufleury. Towards the development of an embryotoxicity bioassay with terrestrial snails: Screening approach for cadmium and pesticides. *Journal of Hazardous Materials*, 184(1-3):26–33, 2010.

[187] KV Sastry and PK Gupta. The effect of cadmium on the digestive system of the teleost fish, heteropneustes fossilis. *Environmental research*, 19(2):221–230, 1979.

[188] O Olgun, AO Yildiz, and A Şahin. Evaluation of dietary presence or use of cadmium in poultry. *World's Poultry Science Journal*, 76(1):64–73, 2020.

[189] CJ Van Leeuwen, WJ Luttmer, and PS Griffioen. The use of cohorts and populations in chronic toxicity studies with daphnia magna: a cadmium example. *Ecotoxicology and Environmental Safety*, 9(1):26–39, 1985.

[190] JF Postma, MC Buckert-de Jong, N Staats, and C Davids. Chronic toxicity of cadmium to chironomus riparius (diptera: Chironomidae) at different food levels. *Archives of Environmental Contamination and Toxicology*, 26(2):143–148, 1994.

[191] Masahiko Satoh, Hiroshi Koyama, Toshiyuki Kaji, Hideaki Kito, and Chiharu Tohyama. Perspectives on cadmium toxicity research. *The Tohoku journal of experimental medicine*, 196(1):23–32, 2002.

[192] AM Hidalgo, MD Murcia, M Gomez, E Gomez, C García-Izquierdo, and C Solano. Possible uses for sludge from drinking water treatment plants. *Journal of Environmental Engineering*, 143(3):04016088, 2017.

[193] Enrico Dinelli, Annamaria Lima, Stefano Albanese, Manfred Birke, Domenico Cicchella, Lucia Giaccio, Paolo Valera, and Benedetto De Vivo. Comparative study between bottled mineral and tap water in italy. *Journal of Geochemical Exploration*, 112:368–389, 2012.

[194] EFSA Panel on Contaminants in the Food Chain (CONTAM). Scientific opinion on lead in food. *EFSA Journal*, 8(4):1570, 2010.

[195] Esben Budtz Jørgensen. An international pooled analysis for obtaining a benchmark dose for environmental lead exposure in children. *EFSA Supporting Publications*, 7(4):47E, 2010.

[196] Anjum Ara, Jawed Ahmad Usmani, et al. Lead toxicity: a review. *Interdisciplinary toxicology*, 8(2):55–64, 2015.

[197] DA Gidlow. Lead toxicity. *Occupational medicine*, 54(2):76–81, 2004.

[198] M Anthony Verity. Comparative observations on inorganic and organic lead neurotoxicity. *Environmental health perspectives*, 89:43–48, 1990.

[199] Ole Andersen and Philippe Grandjean. Effects of inorganic and organic lead compounds on chromosomal length in human lymphocytes. *Applied organometallic chemistry*, 1(1):15–19, 1987.

[200] Kimberlie A Graeme and Charles V Pollack Jr. Heavy metal toxicity, part ii: lead and metal fume fever. *The Journal of emergency medicine*, 16(2):171–177, 1998.

[201] T Nielsen, KA Jensen, and P Grandjean. Organic lead in normal human brains. *Nature*, 274(5671):602–603, 1978.

[202] Y Motarjemi, F Käferstein, G Moy, S Miyagawa, and K Miyagishima. Importance of haccp for public health and development the role of the world health organization. *Food Control*, 7(2):77–85, 1996.

[203] Francesca Latronico, Sandra Correia, Teresa da Silva Felicio, Michaela Hempen, Winy Messens, Angel Ortiz-Pelaez, Pietro Stella, Ernesto Liebana, and Marta Hugas. Challenges and prospects of the european food safety authority biological hazards risk assessments for food safety. *Current Opinion in Food Science*, 18:50–55, 2017.

[204] Rosa Draisci, Alberto Renzoni, and Luca Lucentini. The istituto superiore di sanità, the organization responsible for the evaluation and accreditation of food product testing laboratories. *Annali Dell'istituto Superiore di Sanita*, 38(1):63–67, 2002.

[205] EFSA Scientific Committee. Statement on the benefits of fish/seafood consumption compared to the risks of methylmercury in fish/seafood. *EFSA Journal*, 13(1):3982, 2015.

[206] European Food Safety Authority (EFSA). Mercury as undesirable substance in animal feed - scientific opinion of the panel on contaminants in the food chain. *EFSA Journal*, 6(4):654, 2008.

[207] Yasemin Şahan, Fikri Basoglu, and Seref Gücer. Icp-ms analysis of a series of metals (namely: Mg, cr, co, ni, fe, cu, zn, sn, cd and pb) in black and green olive samples from bursa, turkey. *Food Chemistry*, 105(1):395–399, 2007.

[208] Andrea Hercegová, Milena Dömötörová, and Eva Matisova. Sample preparation methods in the analysis of pesticide residues in baby food with subsequent chromatographic determination. *Journal of Chromatography A*, 1153(1-2):54–73, 2007.

[209] Clara Naccari, Andrea Macaluso, Giuseppe Giangrosso, Francesco Naccari, Vincenzo Ferrantelli, et al. Risk assessment of heavy metals and pesticides in honey from sicily (italy). *Journal of food Research*, 3(2):107, 2014.

[210] Ali Bashiri Dezfouli, Jamileh Salar-Amoli, Tahereh Ali-Esfahani, Hedayat Hosseini, and Kiandokht Ghanati. Evaluating total mercury and methyl mercury contents in canned tuna fish of the persian gulf. *Iranian journal of pharmaceutical research: IJPR*, 17(2):585, 2018.

[211] Lok Nath Neupane, Eun-Taex Oh, Heon Joo Park, and Keun-Hyeung Lee. Selective and sensitive detection of heavy metal ions in 100% aqueous solution and cells with a fluorescence chemosensor based on peptide using aggregation-induced emission. *Analytical chemistry*, 88(6):3333–3340, 2016.

[212] Jeffrey Morton, Nathaniel Havens, Amos Mugweru, and Adam K Wanekaya. Detection of trace heavy metal ions using carbon nanotube-modified electrodes. *Electroanalysis: An International Journal Devoted to Fundamental and Practical Aspects of Electroanalysis*, 21(14):1597–1603, 2009.

[213] Qingfeng Yang, Jing Wang, Xinyu Chen, Weixia Yang, Hanna Pei, Na Hu, Zhonghong Li, Yourui Suo, Tao Li, and Jianlong Wang. The simultaneous detection and removal of organophosphorus pesticides by a novel zr-mof based smart adsorbent. *Journal of Materials Chemistry A*, 6(5):2184–2192, 2018.

[214] Mitchell Bacon, Siobhan J Bradley, and Thomas Nann. Graphene quantum dots. *Particle & Particle Systems Characterization*, 31(4):415–428, 2014.

[215] Susana Campuzano, Paloma Yáñez-Sedeño, and José M Pingarrón. Carbon dots and graphene quantum dots in electrochemical biosensing. *Nanomaterials*, 9(4):634, 2019.

[216] Alice Sciortino, Andrea Cannizzo, and Fabrizio Messina. Carbon nanodots: a review—from the current understanding of the fundamental photophysics to the full control of the optical response. *C*, 4(4):67, 2018.

[217] P Tian, L Tang, KS Teng, and SP Lau. Graphene quantum dots from chemistry to applications. *Materials today chemistry*, 10:221–258, 2018.

[218] Yan Du and Shaojun Guo. Chemically doped fluorescent carbon and graphene quantum dots for bioimaging, sensor, catalytic and photoelectronic applications. *Nanoscale*, 8(5):2532–2543, 2016.

[219] Zhaofeng Wang, Huidan Zeng, and Luyi Sun. Graphene quantum dots: versatile photoluminescence for energy, biomedical, and environmental applications. *Journal of Materials Chemistry C*, 3(6):1157–1165, 2015.

[220] Shengliang Hu, Jun Liu, Jinlong Yang, Yanzhong Wang, and Shirui Cao. Laser synthesis and size tailor of carbon quantum dots. *Journal of Nanoparticle Research*, 13(12):7247–7252, 2011.

[221] Helena Gonçalves, Pedro AS Jorge, JRA Fernandes, and Joaquim CG Esteves da Silva. Hg (ii) sensing based on functionalized carbon dots obtained by direct laser ablation. *Sensors and Actuators B: Chemical*, 145(2):702–707, 2010.

[222] Francesca Arcudi and Maurizio Prato. Design, synthesis, and functionalization strategies of tailored carbon nanodots. *Accounts of chemical research*, 52(8):2070–2079, 2019.

[223] Haitao Li, Xiaodie He, Zhenhui Kang, Hui Huang, Yang Liu, Jinglin Liu, Suoyuan Lian, Chi Him A Tsang, Xiaobao Yang, and Shuit-Tong Lee. Water-soluble fluorescent carbon quantum dots and photocatalyst design. *Angewandte Chemie International Edition*, 49(26):4430–4434, 2010.

[224] Yuan Xiong, Julian Schneider, Elena V Ushakova, and Andrey L Rogach. Influence of molecular fluorophores on the research field of chemically synthesized carbon dots. *Nano Today*, 23:124–139, 2018.

[225] Woosung Kwon, Sungan Do, Ji-Hee Kim, Mun Seok Jeong, and Shi-Woo Rhee. Control of photoluminescence of carbon nanodots via surface functionalization using para-substituted anilines. *Scientific reports*, 5(1):1–10, 2015.

[226] W Wang, Bingzhe Wang, Heidemarie Embrechts, Cornelia Damm, Alejandro Cadranel, Volker Strauß, Monica Distaso, Vanessa Hinterberger, Dirk M Guldi, and Wolfgang Peukert. Shedding light on the effective fluorophore structure of high fluorescence quantum yield carbon nanodots. *RSC advances*, 7(40):24771–24780, 2017.

[227] Wen Shi, Xiaohua Li, and Huimin Ma. A tunable ratiometric ph sensor based on carbon nanodots for the quantitative measurement of the intracellular ph of whole cells. *Angewandte Chemie International Edition*, 51(26):6432–6435, 2012.

[228] Ruquan Ye, Changsheng Xiang, Jian Lin, Zhiwei Peng, Kewei Huang, Zheng Yan, Nathan P Cook, Errol LG Samuel, Chih-Chau Hwang, Gedeng Ruan, et al. Coal as an abundant source of graphene quantum dots. *Nature communications*, 4(1):1–7, 2013.

[229] Somes K Das, Yiyang Liu, Sinhea Yeom, Doo Young Kim, and Christopher I Richards. Single-particle fluorescence intensity fluctuations of carbon nanodots. *Nano letters*, 14(2):620–625, 2014.

[230] Nikolaos Papaioannou, Adam Marinovic, Noriko Yoshizawa, Angela E Goode, Michael Fay, Andrei Khlobystov, Maria-Magdalena Titirici, and Andrei Sapelkin. Structure and solvents effects on the optical properties of sugar-derived carbon nanodots. *Scientific reports*, 8(1):1–10, 2018.

[231] Kofi Oti Boakye-Yiadom, Samuel Kesse, Yaw Opoku-Damoah, Mensura Sied Filli, Md Aquib, Mily Maviah Bazezy Joelle, Muhammad Asim Farooq, Rukhshona Mavlyanova, Faisal Raza, Rohit Bavi, et al. Carbon dots: Applications in bioimaging and theranostics. *International journal of pharmaceutics*, 564:308–317, 2019.

[232] Bisang Chen, Feiming Li, Shunxing Li, Wen Weng, Hongxu Guo, Tao Guo, Xiaoyang Zhang, Yabin Chen, Tingting Huang, Xiaolin Hong, et al. Large scale synthesis of photoluminescent carbon nanodots and their application for bioimaging. *Nanoscale*, 5(5):1967–1971, 2013.

[233] Jing Tang, Biao Kong, Hao Wu, Ming Xu, Yongcheng Wang, Yanli Wang, Dongyuan Zhao, and Gengfeng Zheng. Carbon nanodots featuring efficient fret for real-time monitoring of drug delivery and two-photon imaging. *Advanced materials*, 25(45):6569–6574, 2013.

[234] Haodong Ji, Wen Liu, Fengbin Sun, Taobo Huang, Long Chen, Yue Liu, Juanjuan Qi, Chenghan Xie, and Dongye Zhao. Experimental evidences and theoretical calculations on phenanthrene degradation in a solar-light-driven photocatalysis system using silica aerogel supported tio2 nanoparticles: Insights into reactive sites and energy evolution. *Chemical Engineering Journal*, 419:129605, 2021.

[235] Bo Song, Qiao Wang, Li Wang, Jing Lin, Xin Wei, Vignesh Murugadoss, Shide Wu, Zhanhu Guo, Tao Ding, and Suying Wei. Carbon nitride nanoplatelet photocatalysts heterostructured with b-doped carbon nanodots for enhanced photodegradation of organic pollutants. *Journal of colloid and interface science*, 559:124–133, 2020.

[236] Madeeha Batool, Hafiz Muhammad Junaid, Sobia Tabassum, Farah Kanwal, Kamran Abid, Zara Fatima, and Asma Tufail Shah. Metal ion detection by carbon dots—a review. *Critical Reviews in Analytical Chemistry*, pages 1–12, 2020.

[237] Lei Wang, Baoqiang Li, Feng Xu, Xinyao Shi, Demeng Feng, Daqing Wei, Ying Li, Yujie Feng, Yaming Wang, Dechang Jia, et al. High-yield synthesis of strong photoluminescent n-doped carbon nanodots derived from hydrosoluble chitosan for mercury ion sensing via smartphone app. *Biosensors and Bioelectronics*, 79:1–8, 2016.

[238] Vallerie A Muckoya, Azeez O Idris, Philiswa N Nomngongo, and Jane C Ngila. Synthesized carbon nanodots for simultaneous extraction of personal care products and organophosphorus pesticides in wastewater samples prior to lc-ms/ms determination. *Analytical and bioanalytical chemistry*, 411(23):6173–6187, 2019.

[239] Hongxia Li, Xu Yan, Geyu Lu, and Xingguang Su. Carbon dot-based bioplatform for dual colorimetric and fluorometric sensing of organophosphate pesticides. *Sensors and Actuators B: Chemical*, 260:563–570, 2018.

[240] Bernard Valeur and Mário Nuno Berberan-Santos. *Molecular fluorescence: principles and applications*. John Wiley & Sons, 2012.

[241] Cassini Monge. Molecular fluorescence: Principles and applications. bernard valeur> 2001 wiley-vch verlag gmbh isbns: 3-527-29919-x (hardcover); 3-527-60024-8 (electronic). *Molecular Fluorescence*.

[242] Christiane Albrecht. Joseph r. lakowicz: Principles of fluorescence spectroscopy, 2008.

[243] Ashutosh Sharma and Stephen Gregory Schulman. *Introduction to fluorescence spectroscopy*, volume 13. Wiley New York, 1999.

[244] Federico Bruno, Alice Sciortino, Gianpiero Buscarino, Maria Laura Soriano, Ángel Ríos, Marco Cannas, Franco Gelardi, Fabrizio Messina, and Simonpietro Agnello. A comparative study of top-down and bottom-up carbon nanodots and their interaction with mercury ions. *Nanomaterials*, 11(5):1265, 2021.

[245] Mani Vedamalai, Arun Prakash Periasamy, Chia-Wei Wang, Yu-Ting Tseng, Lin-Chen Ho, Chung-Chien Shih, and Huan-Tsung Chang. Carbon nanodots prepared from o-phenylenediamine for sensing of cu 2+ ions in cells. *Nanoscale*, 6(21):13119–13125, 2014.

[246] Federico Bruno, Alice Sciortino, Gianpiero Buscarino, Marco Cannas, Franco Mario Gelardi, Fabrizio Messina, and Simonpietro Agnello. Sensing of transition metals by top-down carbon dots. *Applied Sciences*, 11(21):10360, 2021.